master thesis

From Simplicity to Complexity

the reciprocal relationship of linear motion and spatial form of bending active, splayed plates

Micha Schneider

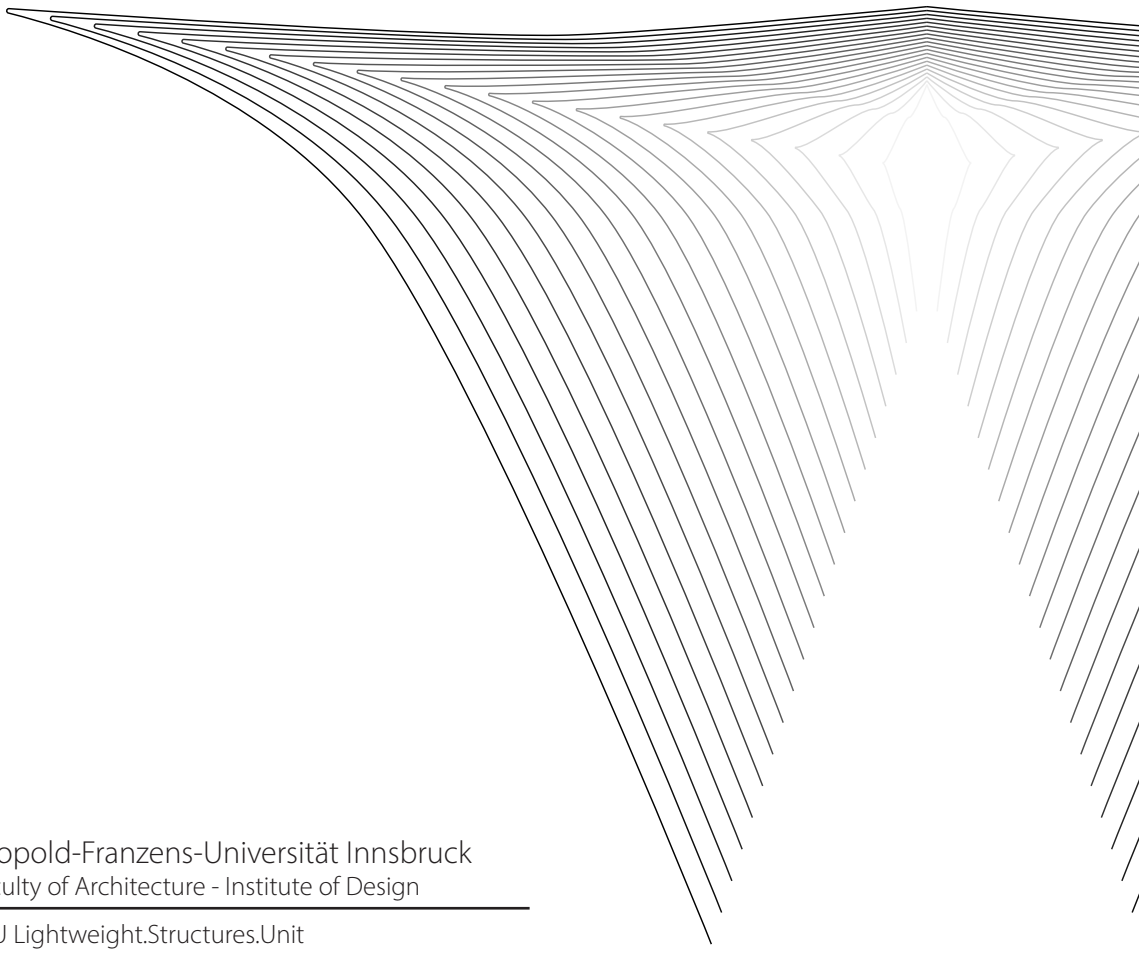

Leopold-Franzens-Universität Innsbruck
Faculty of Architecture - Institute of Design

LSU Lightweight.Structures.Unit

Micha Schneider, Bachelor of Arts

From Simplicity to Complexity

the reciprocal relationship of linear motion and spatial form
of bending active, splayed plates

master thesis
submitted to the

Leopold-Franzens-Universität Innsbruck
Faculty of Architecture

to obtain the academic degree of
Diploma engineer

Supervisor:
Dipl.Ing. Dr.techn. M.Eng.Univ. Professor, Günther Filz

Institute of Design
LSU Lightweight.Structures.Unit
Innsbruck, 07/24

Acknowledgment

This thesis was developed between 2023 and 2024 in the university of Innsbruck, Institute of Design, LSU Lightweight.Structures.Unit

I would like to express my deepest gratitude to professor Günther Filz for his inspiring ideas and the trust he has placed in me and my work. Thanks to M.A. Fereshteh Khojastehmehr and M.A. Mohammad Hassan Saleh Tabari for their great help.

I would like to express my deepest gratitude to my mother, father, sister and brothers who have supported me in every step I have ever taken.

My deepest gratitude goes to my partner Klara, for her love and unwavering support during this time and our journey.

Finally i want to express special thanks to Moria, Simon, Beam and Herold for their inspiring and moral input.

This work is dedicated to Maria, R.I.P

Abstract

This thesis aims to contribute to relatively young field of bending-active plate systems by focusing on the manipulation of planar plates to achieve large-scale elastic deformations, resulting in spatial accentuated geometries. The research explores the impact of various geometric and physical boundary conditions on its deflective behavior. Inspired by recent advances in computational methods, this study examines techniques using form-finding as a design strategy

Bending-active systems exploit the elastic properties of initially flat elements to create curved, lightweight structures. In contrast to traditional engineering, which typically avoids bending moments to prevent material failure, the bending-active approach is utilizing the stress to develop structural and spatial efficient systems.

By exploring the geometrical and structural properties of bending-active plate systems which are being deformed by the controlled in plane displacement of points, leading to an elastic deformation of a initial flat plate, I want to contribute to the field of bending-active plate systems. This is being achieved by analyzing the impact on shape given boundary conditions, its controlled manipulation and its material properties.

Table of Content

Abstract iv

Introduction 12
Bending-active systems 14
Bending-active structures 16
Form-Finding 17

Focused Literature Review 26
Bending-Active Plates 28
Linearity 30
Plates and shells 32

Methodology and Approach 34
Concept 36
Boundary conditions 38
Physical testing 40
Computational Method 44
3-d Scan 46
Validation 48

Behavior 54
Concept 55
Mechanical behavior 56
Structural behavior 58
Curvature/Stress 62

Workflow 64

Evaluation 66
Polygon 4 74
Circular 94
Diamond 110

Application 120

Showcases 152

Data 190

Appendix 198

Motivation

The work of visionaries such as Buckminster Fuller and Frei Otto, along with my own work over the past few years, have focused my attention in the area of bending-active structures. Bending-active systems are characterized by using the inherent flexibility of materials to create functional and aesthetically pleasing structures. While bending is usually avoided in classical engineering, bending-active systems utilize the elastic properties of initially flat elements to create curved, lightweight structures, to their advantage. This makes it possible to create structures that are not only efficient, but also resilient, adaptable and aesthetically pleasing.

While working mostly with rod and cable systems, I have been fascinated by the developments in recent years, especially the bending-active plate systems. In this thesis, I deal with the behavior of originally flat elements that are deformed by targeted manipulation in the plane of the plate leading to an elastic deformation. For this purpose, digital and physical methods have been developed to study the deflective behavior, in terms of its structural characteristics and spatial behavior. This method is applied to various input geometries, which are manipulated, based on the gathered insights and data.

My goal is to demonstrate how bending-active plate systems can be effectively utilized to create sustainable and innovative systems for architectural applications. Through this research, I aim to contribute to the advancement of lightweight and adaptive structures, inspiring future research and practical applications in the architectural field.

Overview

This thesis deals with the form finding and its structural and spatial characteristics of bending-active plates. The knowledge gained from this work serves as a foundation for understanding the mechanic and spatial behavior of initially manipulated, flat planes that are buckled out of plane by a controlled in-plane displacement of two points.

The first chapter describes the basic concept of active bending systems, as well as the most important terminology. It is giving a brief overview of the different types of bending-active systems, its different type of approaches and its historical development.

The second chapter deals with selected works that extend the understanding of bending-active plates and its mechanical properties while being bent. In addition to its basic deformation states, it deals with its specific behavior while being under stress, regarding its mechanical and geometrical properties.

The third chapter deals with the basic behavior of the deformed plates and its unique characteristics. Furthermore it describes the method how the boundary conditions are determined, to apply them into a physical and digital test environment. Both the physical and digital model are being calibrated to validate the correctness of the digital environment. This lays the foundation to investigate the specific behavior and characteristics of the initial planar sheets being deformed and manipulated based on the data gathered from the digital model.

The fourth chapter describes the specific behavior of the initial plates and its variants to be deformed. Based on the ground work in the third chapter, the initial flat plates are studied in terms of its mechanical, structural and geometrical behavior and characteristics.The data obtained, is then used to optimize the input geometry, by creating strategically placed cutouts to prevent early material failure.

A workflow is then applied using the knowledge gained. In the fourth chapter, this is applied to the evaluation of different input geometries, which are then evaluated with reference to their spatial and geometric behavior and different basic input geometries and their variants.

The fifth chapter deals with the concept of functional beauty and its dynamic transformation between simplicity and complexity. This creates a duality of form and function that serves to emphasize the innovative character of the design. In these designs, aesthetics and technical principles merge seamlessly.

Introduction

Background

Bending-active systems

Bending-active systems are typically described as structural processes that employ large-scale deformations to achieve form-giving and self-stabilizing strategies. These systems leverage the dynamic relationship between material properties and forming processes to create structures that are both visually appealing and functional.

In engineering, the focus is on minimizing deformation and bending, as it often is associated with material failure. Traditional engineering solutions are therefore based on rigid, non-deformable components that can withstand bending and deformations. Over the past few decades, the field of active bending has become more accessible to a wider audience as a result of significant advances in material science and computational methods.

The basic principle of active bending is to subject the geometry or material to loads in strategically selected areas without causing material damage, which results in elastic deformation. This method, unlike conventional ones, is characterized by creating structures that are lightweight, material-efficient and eventually capable of adapting to eventually changing environmental conditions.

In the last few decades, and in particular from the turn of the last century to the present day, three different approaches have emerged over time starting with the behavior-based approach, in which bending is employed in an intuitive manner. The geometry and structural behavior of the system are empirically studied, and material limitations are subjected to physical testing.

A geometry-based approach is employed, whereby the system's geometry is predefined based on analytical geometry or experimental form-finding techniques. The constraints imposed by the material are evaluated through an analysis that considers the relationship between momentum and curvature.

The last approach has been emerged mostly in the last decades because of advances in computational and material technology .The elastic bending deformation is analyzed through numerical form finding, which enables full control of material behavior based geometry. Material characteristics and limitations are included in the numerical analysis model.

Bending-active structures

While conventional lightweight systems try to reduce the amount of bending in structures, bending-active systems follow the idea of taking advantage of the internal strain in the material, leading to an elastic deformation of the structure . By exploiting the structures flexibility and being able to understand the parameters, designers are able developing form-giving and self-stabilizing or elastic kinetic structures.

Since bending-Active structures in general do not describe a specific structural type, but rather an approach. Thus structures in general are not described by a specific load bearing behavior or geometrical definition, but as a formation process while they are elastically bent[1]

Within this general characterization of bending-active structures , some types of structures can be identified:[2]

- Elastic Gridshells
- Bending Plate structures
- Textile Hybrids
- Elastic kinetic structures

Form-Finding

Form-finding is generally known as a process of generating a structure based on its natural mechanical behavior.[3] In contrast to conventional design processes, form-finding is a deterministic process resulting in a single solution constrained by material and physical boundary conditions It is commonly associated with tensile membrane structures, centenary arches, and shells.[4]

In bending-active structures, the geometry must be form-found, meaning that stresses and mechanical behavior are integral parts of the solution. While these properties are included in the process, they are not the only boundary conditions to be considered.[5] Form-finding in bending-active structures includes other variables such as geometric variation, coupling and internal constraints. Despite the constraints ruling the design, there usually is not one exclusive solution, allowing enough creativity and freedom in design.

Approach

The design approach of bending-active structures can be categorized in behaviour-based, geometry-based, or integrated-based approach.[6]

Behavior-based approach
Bending is initially used intuitively; the system's geometry and structural behaviour is studied empirically.

Geometry-based approach
The system's geometry is predefined based on analytical geometry or experimental form-finding methods, both of which are used as a controlled means to approximate the actual bending geometry. Material limitations are considered analytically based on momentum curvature relation.

Integral-approach
The elastic bending deformation is analyzed through numerical form finding, which enables full control of material behvior based geometry. Material characteristics and limitations are included in the numerical analysis model.

Fig.1 Historical development of bending-active structures

Behavior based approach

While the behavior based approach relies on the building material been used and its bending behavior to gain insights to form a structure. Tension arc systems, described in the encyclopedia of vernacular architecture, are in use since over 5000 years ago, on every continent. Known as vernacular architecture, various cultures have been making use of the elastic behavior of their building materials. Different construction techniques found in vernacular architecture capitalize on the flexible properties of their building materials, resulting in identifiable construction styles prevalent in specific cultures and applications.

Mudhif cane huts in Ma'dan, south Iraq, are one of the early examples of early elastically formed arc and shell structures construction methods based, on the elasticity of their building materials. These permanent structures using vertically fixed, in a circular array positioned reed bundles, that are connected on their tops towards the center of the circular shape to build a elastically formed arc.

Another bending construction system which still is in use until today are mobile shelter systems. Tents of nomadic tribes are common examples taking advantage of using active bending systems.

Even today, bending-active structures that follow the behaviour based approach are being built like the Vo Trong Nghia's, large bamboo structures, or small pavilion structures like "The Loop" (Howeler and Yoon, 2013) and the "elastic habitat" (Santini and Taddei, 2006)

Fig.2 Yamut, Iran

Fig.3 Mudhif Houses, Iraq

Fig.4 The Loop" (Howeler ,Yoon, 2013), "elastic habitat" (Santini,Taddei, 2006)

Geometry based approach

The extensive exploration of lightweight structures, initiated in the mid-twentieth century, sparked a heightened fascination with double curved surfaces and grid-shells. Since the computational methods at this time were not able to simulate large deformations, the prevailing method, which is known as geometry based approach for form-finding, was the hanging model and elastica curve[1], which was applicable to both experimental and analytical approaches.

Buckminster Fuller presented an innovative method for crafting surface shells, which emerged in his exploration of geodesic domes. In 1957, he devised the plydome structures as part of his research efforts. These structures, depicted (Figure 7) are characterized by a spherical form. Fuller employed initially flat plywood panels primarily curved along a single axis and linked them at the topological vertices of the geodesic dome.

In the early 60', Frei Ottos experimental research on large deflections, led to large span grid-shell structures. By using hanging-chain models he was able to predict the final shape of structures without the use of computational power. After a few prototype structures he was able to build his first large-scale grid-shell structure. The wooden laths from the initially flat grid were shaped into the desired configuration, guided by the suspended model (Figure 5,6).

Fig.5 Hanging model multihalle mannheim

Fig.6 Multihalle Mannheim

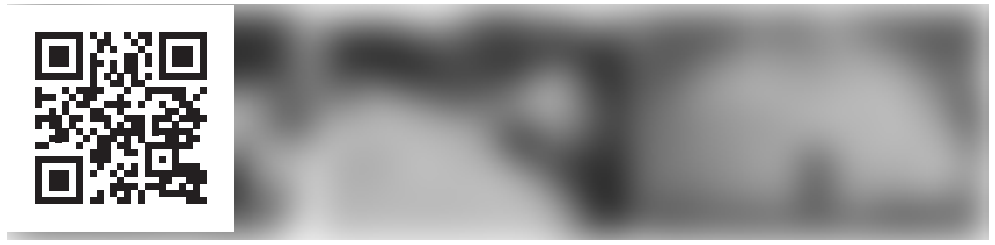

Fig.7 Plydome, Buckminster Fuller in 1959

Integral approach

Advances in computational simulation techniques now enable the form-finding and analysis of structures whose intricate curved shapes are solely determined by their elastic deformation during the erection process.

The integrative design approach for bending-active systems provides more flexibility in terms of computational automating of designs.

The characteristics of an integrative approach require intensive laboratory testing to understand the material characteristics and its limitations. The insights gained are utilized as boundary conditions for computational design tools to fine-tune the FEM software. By synchronizing both, physical and digital studies, designers can accurately characterize material behavior during the form-finding process, leading to enhanced feedback on the resulting structure's geometry's.

Projects like the 2010 ICD/ITKE Research Pavilion take advantage of the concept of the integrative design. This structure, constructed entirely from thin, elastically-bent plywood strips, challenges traditional approaches to digital design by directly integrating physical behavior and material characteristics into the computational generation of form. Through thoroughly experimentation and parametric modeling, the pavilion's design capitalizes of the elastic bending properties of birch plywood to create a lightweight yet robust system. The computational design process, supported by Finite Element Method (FEM) simulations, accurately predicts the structural performance of the pavilion, including its response to external forces such as wind and snow loads. By seamlessly combining computational design with materialization, the pavilion exemplifies a successful integration of theory and practice in architecture.

Fig.8 ICD research pavilion, 2010

Fig.9 Bending stress test

Fig.10 Computational Model

Focused Literature Review

Bending-Active Plates

Form and Structure, Riccardo La Magna, Simon Schleicher, and Jan Knippers, (September 2016), pp:170-186

The focus of the paper is to apply the top-down rather than the bottom-up method, in which the initial conditions are a predefined shape for which the geometrical and structural properties of the plates to be bent, must be developed. It describes the limited formability and the complexity of maintaining the structural integrity of a bending-active plate, while applying it onto a doubly curved shape. It suggests a strategy to overcome the problem by removing material thus freeing the material from stiffening constraints.

To overcome the principal limit of material formability, which results in irreversible, plastic deformation or ultimate failure, it is essential to understand the geometric and mechanical properties of the plates to be bent.

The work identifies two basic deformation states: membrane and bending-action. While in membrane deformation the load is applied over the entire cross-section of the element, in bending-dominated(pure-bending) deformation it roughly preserves the mid-surfaces fiber length, resulting in a flexible element. Pure bending deformations are referred to as inextensional deformations, as the neutral surface is completely free from longitudinal tension or compression. Therefore it suggests that isometric transformations of a plane always result in cones and cylinders. In shell structures, membrane deformation is generally preferred as the cross section is completely utilized to improve the shell's load-bearing behavior. Bending-active structures undergo primarily in-extensional deformations, which are defined as pure bending deformations.

Fig.11 Computational workflow

Fig.12 Bend9 case study

Linearity

Bending-Active Plates Strategies for the Induction of Curvature through the Means of Elastic Bending of Plate-based Structures. Riccardo La Magna, October 2017, pp:41-43

In this chapter the author discusses the mechanical behavior of plate and shell structures under bending stress, and the significance of nonlinearity in the elastic theory. Emphasizing sources of nonlinearity which include geometric, material, force boundary condition and displacement boundary conditions. While geometric nonlinearity occurs due to non-neglectable changes in geometry under load, which is relevant for slender elements and tensile structures. Material nonlinearity depends on current and the history of its deformation state e.g. modeling effects like plasticity and viscoelasticity. Force and displacement boundary condition nonlinearities emerge from deformation-dependent applied forces or boundary conditions.
He categorizes the possible states in which a structure finds itself while maintaining bending-active deformation:
Materially-non-linear-only: large displacement ,large rotations with small strains, stress strain relationship is nonlinear (until the yield point has reached it is linear).
Large displacements, large rotations but small strains, the stress strain relation are either linear or non-linear.

Large displacements, large rotations, large strains, the stress strain relation is mostly linear. He focus on the small strain approximation where the elastic response is linear but large displacements and rotations are allowed.

With the elastic constitutive law and the geometrical non-linearity, he identified two sources of non-linearity in the theory of elasticity. While the first one responses to the intrinsic response of the material, the other one is tightly connected to the geometry.

This framework is pertinent for bending-active structures, with thin cross-sections to exploit its deformation capabilities. With the focus on the immediate structural response during form-finding and final shape, by observing the geometrical non-linearity.

Plates and shells

Bending-Active Plates Strategies for the Induction of Curvature through the Means of Elastic Bending of Plate-based Structures. Riccardo La Magna, October 2017, pp:44-45

This chapter addresses the differences between shells and plates and their structural behavior and mechanical response. While shells already present curvature in their stress free configuration, in which the type of curvature has a "major effect on the mechanical response on of the structure", plates are initially flat. From a geometric point of view both are defined as 2d elements and by their center surface and local thickness .

The structural behavior of shells is defined as a membrane deformation, which involves the strain of the center surface. While bending dominated deformation roughly preserve the length of the mid surface fibers and can be loaded by forces acting in plane or perpendicular to the plane, a flat plate subjected to forces, which are acting in plane, leads to in-plane actions and a membrane stress state, known as plane stress.

A flat plate loaded by in-plane forces induces membrane stress, also known as plane stress. This stress state is described by three components: normal stresses and shear stress per unit length.

If forces perpendicular to the center surface are applied to the plate, it will experience bending and torsion. The bending moments are oriented perpendicular to the x-z and y-z planes, respectively. Twisting moments are directed along the x and y axes. For equilibrium, these moments are balanced by shear forces, perpendicular to the center surface. Together with membrane theory, bending theory completes the mechanical behavior description of plate structures.

A shell or plate which is subjected to ***pure bending*** experiences a bending stress state without longitudinal extension or compression, also known as ***inextensional*** or ***isometric deformation***. These terms highlight different mechanical or mathematical aspects and refer to deformations preserving lengths, while membrane action is mostly preferred for structural applications. Structures, which are subjected to ***inextensional deformation*** (pure bending) are useful for deployable applications, since they allow significant shape changes without exceeding its state of critical stress. Because of their thin crossection compared to its length and width, this type of deformation is significant for bending-active structures.

Methodology and Approach

Concept

Starting from an initially flat geometry, there are various strategies for creating a spatial geometry. Depending on the materials elastic properties, the most common approaches are bending or folding the element. For bending, at least two points on the edges are typically moved within the geometry's boundaries by pulling them together, resulting in a three-dimensional object.[7] [8]

Starting with an originally flat surface, the process typically involves manipulating the material to merge specific points. For example in an initial flat circular shape a cutout is made, from the center to the edges. The resulting void is being pulled together, transforming into a three dimensional shape, resulting in a Cone. [9]

For this work, a different approach was taken. A cut is made from the edge toward the center of the geometry. The resulting points on the edges of the cut serve as attachment points that are displaced along the geometry's plane. By displacing its points of attachment in a counter directional manner apart, the applied force is then translated throughout the geometry's cross section, forcing the element to undergo a large transformation, in which the geometry buckles out of plane, resulting in a three-dimensional shape.

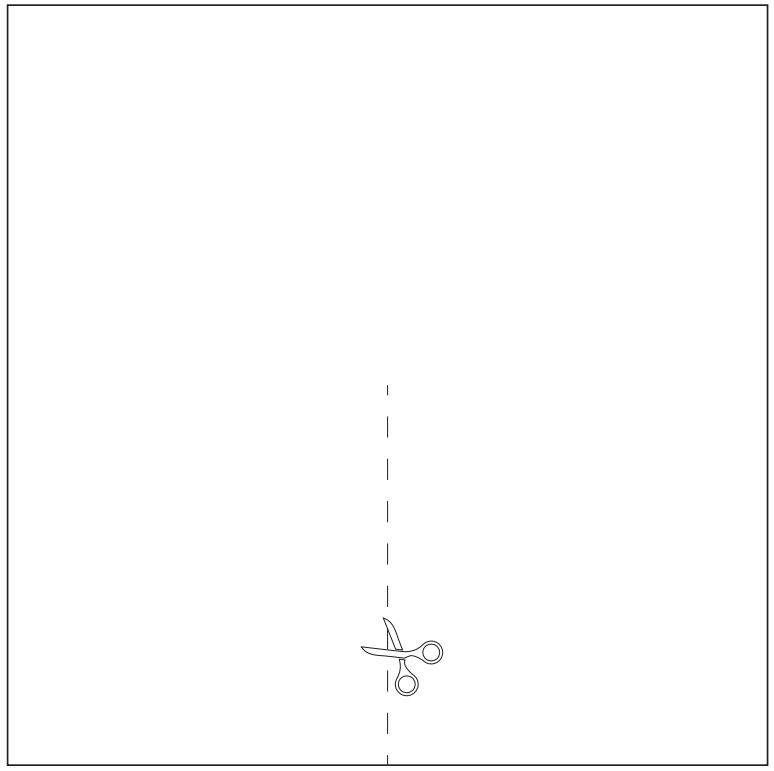

Fig.13 Initial shape

Boundary conditions

The in-plane displacement of the newly created points of attachment (x), (x'), introduces stress in the material, resulting in the elastic bending deformation of the object. To achieve this, certain boundary conditions must be defined. In the physical and digital model, the points, at which the surface is attached are allowed to rotate around their axes. In addition, it is essential to restrict the attachment points, which are displaced in the plane of the geometry, to the axis of the displacement. To ensure a controlled deformation out of the plane, it is also necessary to ensure that the edges can freely move except at the point of attachment. For the investigations, a maximum displacement of x to 25% of the geometry width has been defined as shown in Figure 14.

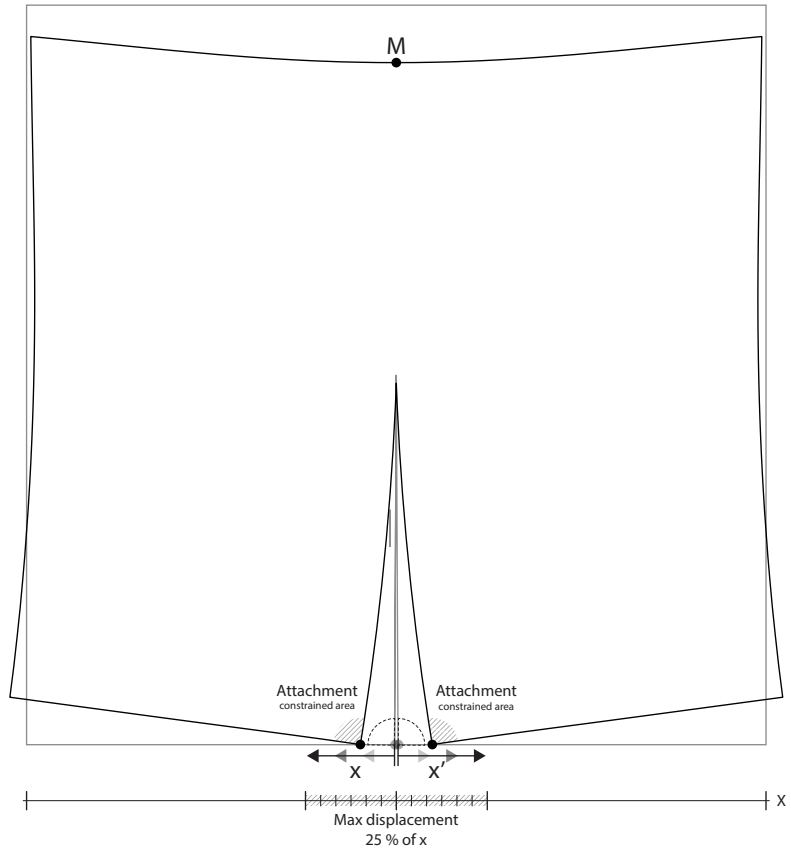

Fig.14 Boundary conditions

Physical testing

A basic prerequisite to achieve elastic deformation is, that the material needs to have flexibility and shear properties. At the same time, the applied forces should not exceed the material's elastic limits.

Initial physical tests with paper models demonstrated that controlling and manipulating the shape requires constraining the displaced points along their in-plane axis of movement. Small deviations perpendicular to this axis result in an uneven, flipped geometry (Figure 15). The stress applied into the material cross section is distributed unevenly over the surface. The geometry snaps perpendicular to the in-plane movement of the displaced points x/x' (Figure 17). This could be easily observed by displacing the geometry freely by hand (Figure 16). Because of this, it is almost impossible to keep the movement of its points on a constrained axis.

Since paper was used in the first tests, it showed that its anisotropic material properties meaning, one directional fiber alignment are not suitable for testing. This caused the geometry to flip or deform unpredictably. Therefore the selected material for further tests is a co-polyester called Vivak. This material, falls into the category of isotropic materials, it is very well suited for geometric deformations. Its flexibility properties, allowing it to bend and flex without cracking or breaking.

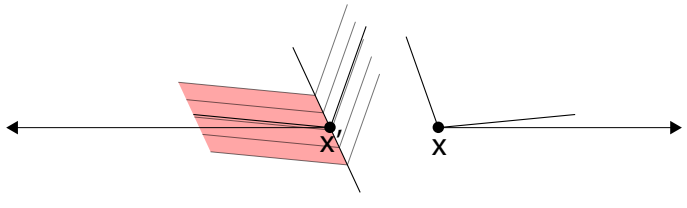

Fig.15 point x misalignment

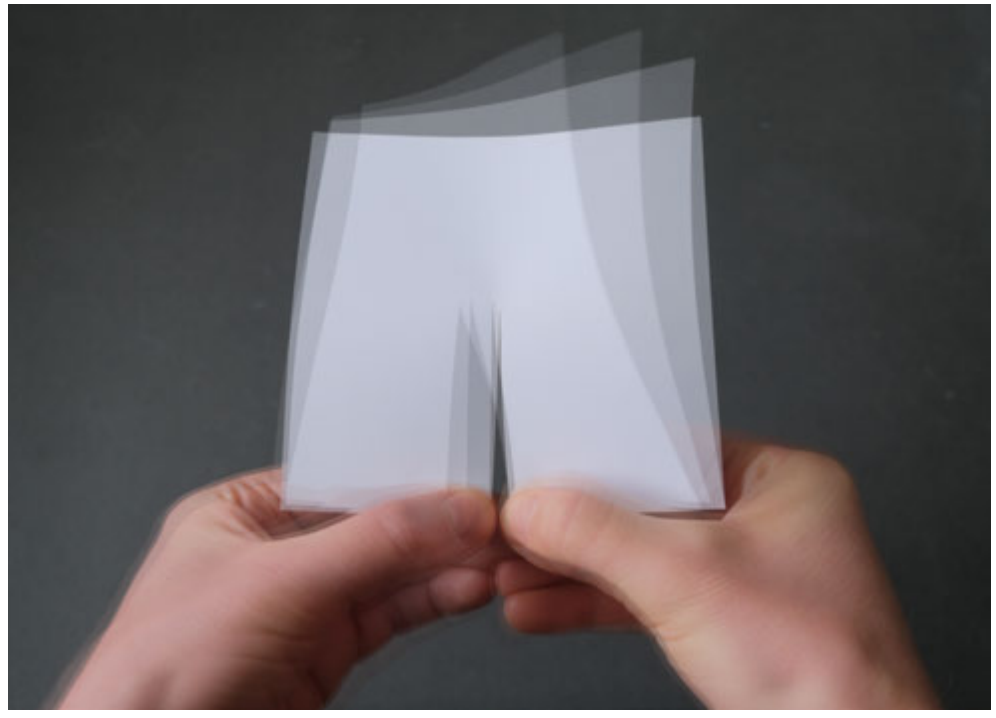

Fig.16 Physical test

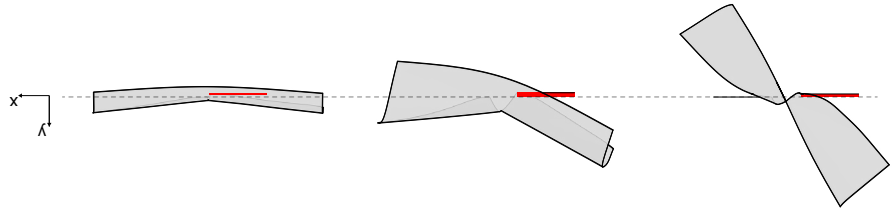

Fig.17 Deform instability

To better understand the bending behavior of the geometry, a test environment that provides reproducible results is crucial. In order to fulfill the conditions mentioned earlier, a physical and digital test environment must be created. A test apparatus that meets the aforementioned boundary conditions has been built. This enables us to study every step of the process and the special features and to draw initial conclusions about the deflective properties regarding its spatial and structural behavior.

With the sheet attached at two points (x,x'), the test setup is capable of precisely controlling the in-plane displacement and maintaining a consistent degree of opening. The ability to precisely control the in-plane displacement and maintain a uniform degree of opening is particularly important for studying the behavior of the sheet under constant test conditions, repeatedly, in different configurations (Figure 18).

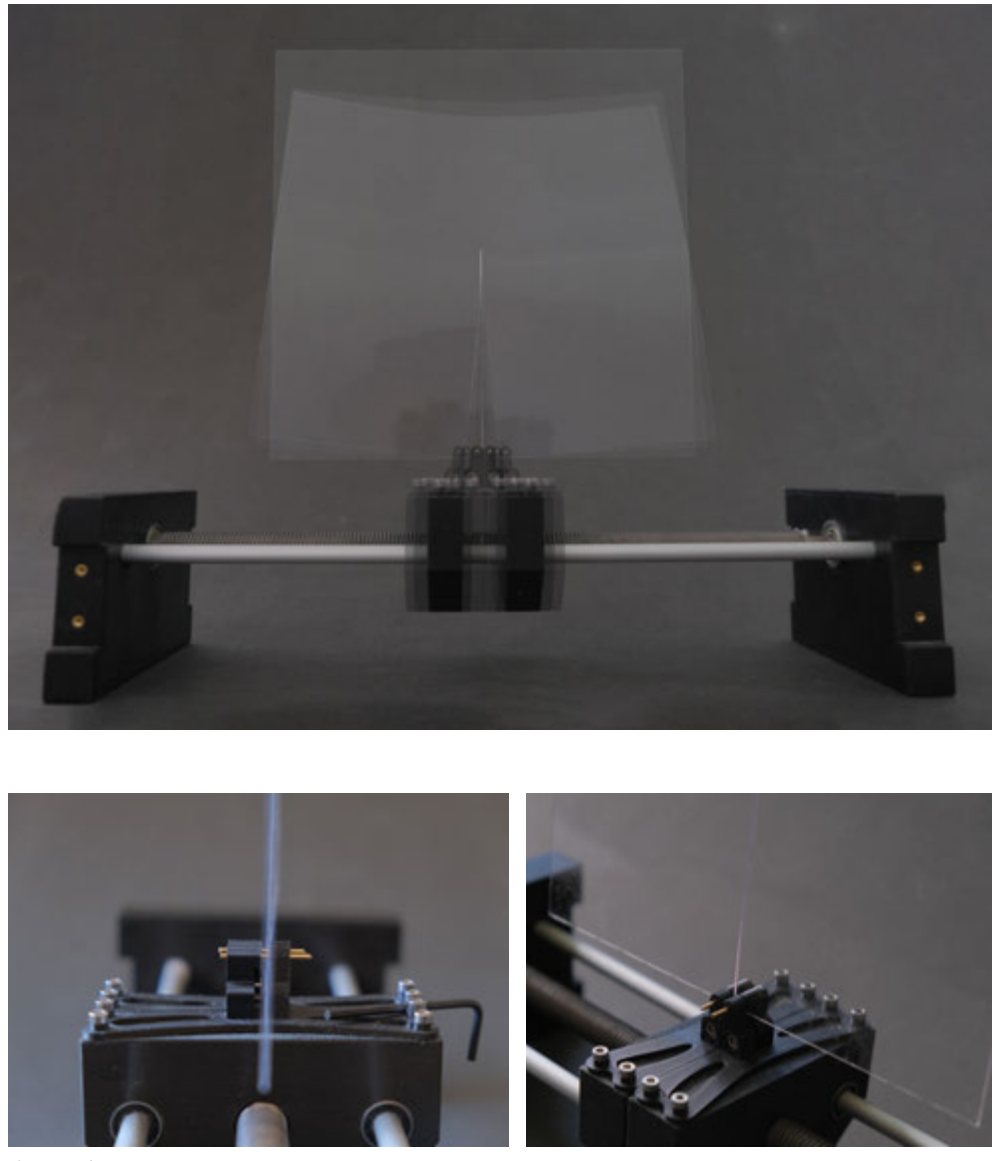

Fig.18 Test device

Computational Method

While physical experiments allow a superficial analysis of the deformation, some parameters remain hidden. A qualitative measurement of the extent to which the surface is deformed in space can only be roughly determined and is difficult to understand. Information such as the stress in the material remains hidden. By observing these parameters, it is possible to react to structural properties and draw conclusions about the elastic deformation and its spatial quality.

This is achieved by using Kiwi3d[10], an FEM tool for Rhino/Grasshopper[11]. Unlike many other tools, Kiwi3d is able to calculate large deformations.

By establishing a digital test environment, defining boundary conditions identified through physical experiments, and applying material properties in Kiwi3d, it is possible to gain a deeper understanding of the structural and geometric behavior of the plate's elastic deformation.

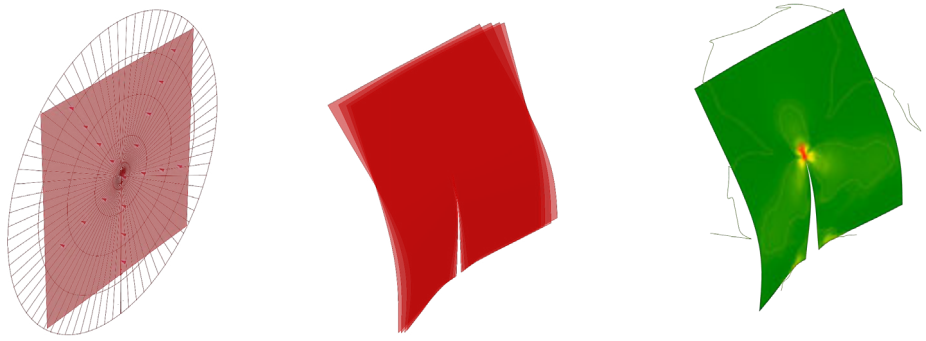

Fig.19 Computational method

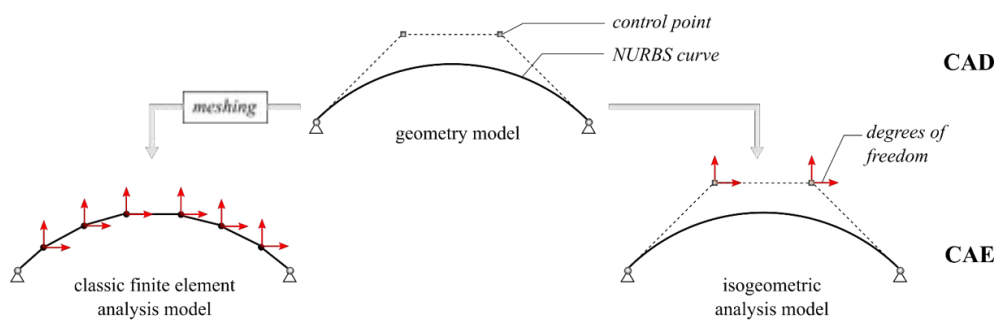

Fig.20 Kiwi3d isogeometric concept

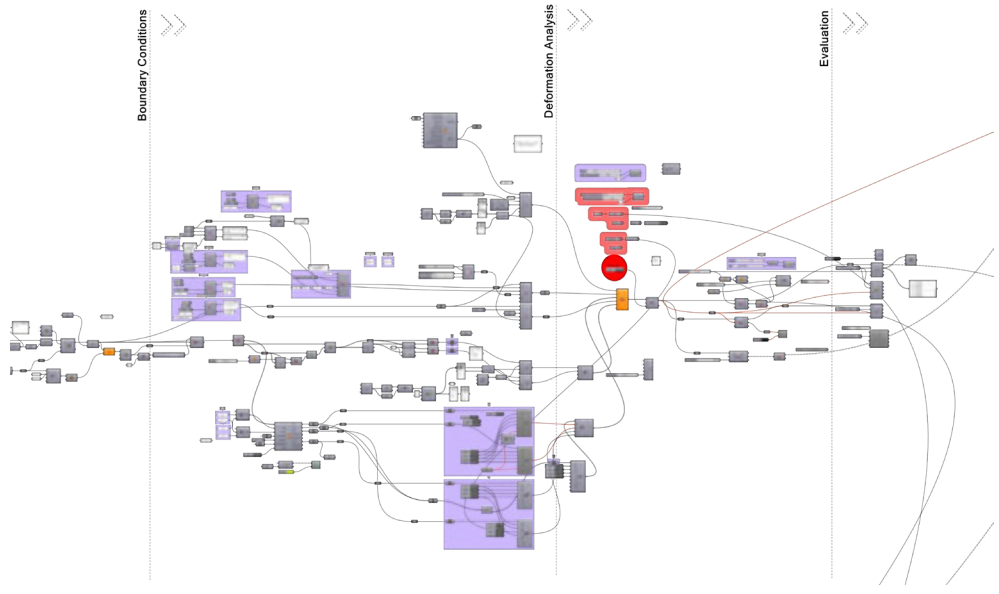

Fig.21 Grasshopper definition

3-d Scan

To calibrate the digital simulation, a 3D scan of the physically deformed plates are used as references. The scans are created using an advanced photogrammetry process. This is based on the so-called Neural Radiance Fields (NeRF) method. Similar to conventional photogrammetry, which creates a geometry using overlapping 2D images and its feature points, this procedure uses machine learning to create an accurate geometry based on 3D coordinates, color and density.

In order to generate a 3d-Scan NeRF-Studio[12], an open-source software, was used. By taking a video of the object the software extracted depending on the input settings 150 - 300 pictures from the recording. The algorithm matched overlapping pictures based on color, density.

Despite the high accuracy of the technology, the generated point-cloud of the scanned object has a thickness on average between 1.5 and 2.0 mm. This is mostly because of the resolution of the camera and of the real material thickness of 0.5 mm. Numerous improvements in a higher amount of images and adjustments within the cameras exposure and white balance settings provided detailed scans. Further, on the material itself, which is a highly reflective material, has to be coated with a chalk layer to improve the results of the scans.

The generated point-cloud then is translated within Rhinoceros into a 3d-mesh, which already shows a detailed geometry. In order to compare the FEM-simulation with the scanned mesh, the mesh with its material thickness of around 1.5 - 2.0 mm, needs to be translated in a 2d surface.

High-Density Pointcloud
> 10.000.000 points

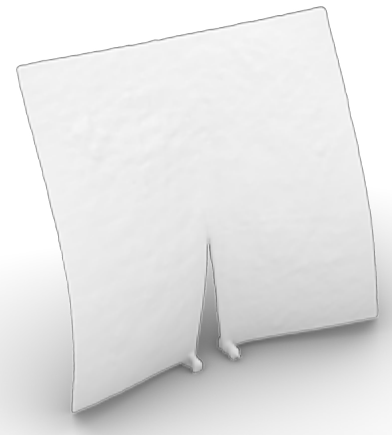

Meshed point-cloud

Fig.22 3D-scan NeRF workflow

Validation

The validation is achieved by approximate the scanned object. The surface is generated by a custom developed method realized with Grasshopper for Rhinoceros.

By generating a matrix (Figure 23a) with a resolution of 128 cells, in which each center point of the matrix cell is projected onto the front and back of the scanned geometry (Figure 23b). Points, representing the thickness of the object, then are connected with a line. By using the midpoint of each generated line inside the scanned geometry, a surface can be interpolated suitable to compare it to the simulated surface (Figure 24).

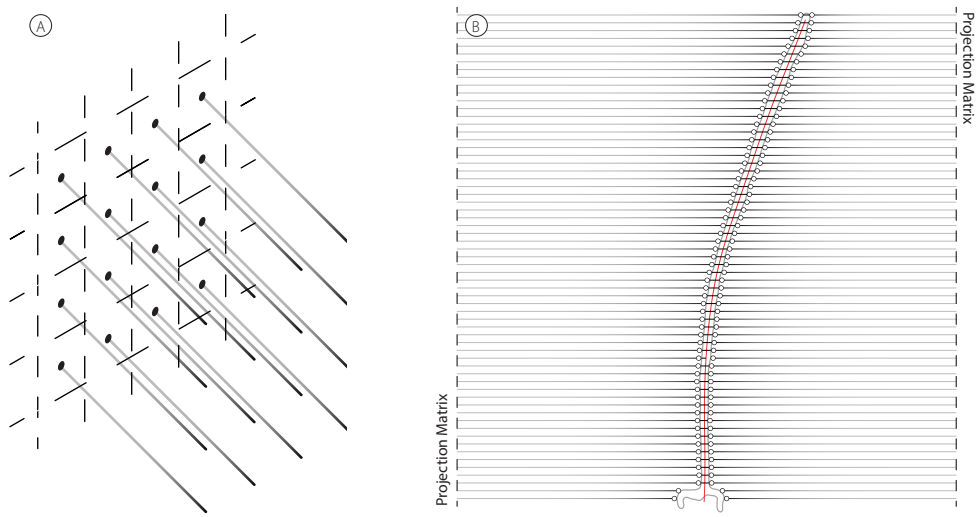

Fig.23 Matrix

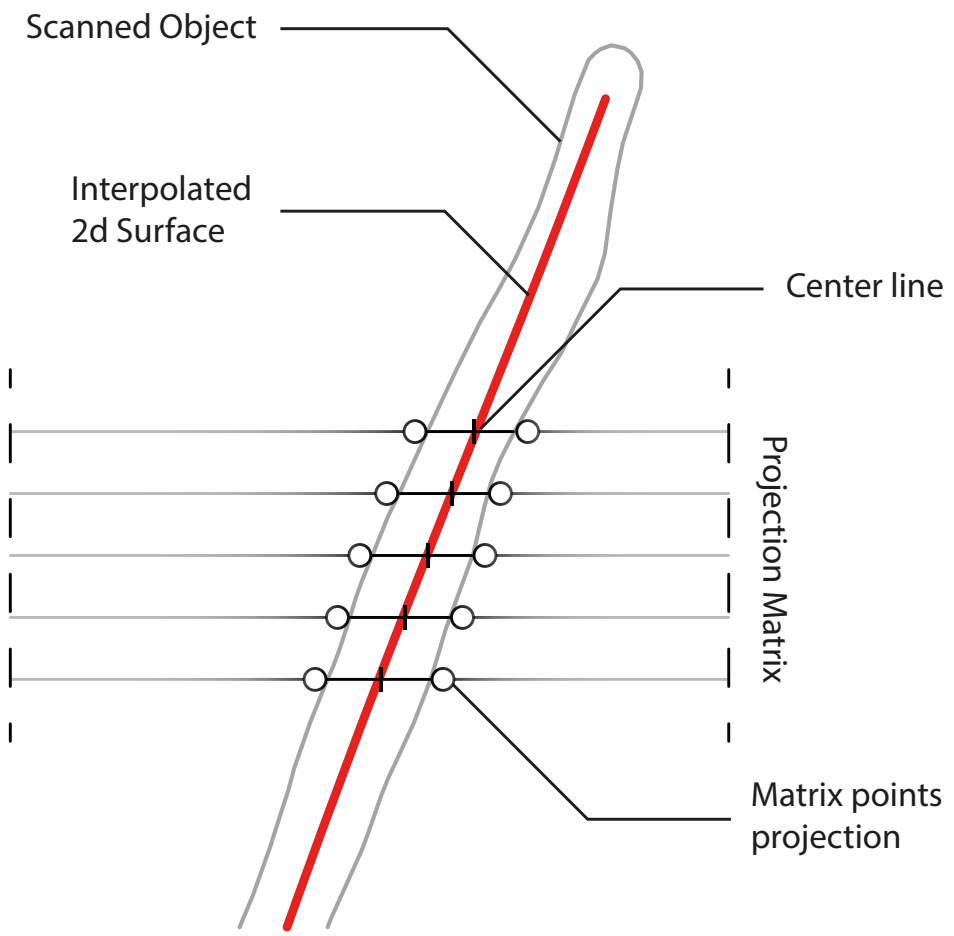

Fig.24 Interpolation

By comparing the simulated and scanned objects, an average deviation of 1.64 mm can be identified. Considering that the sheet size of 200 x 200 x 0.5 mm and the tolerances of the physical experiment, the deviation between the simulation and the scan is considered accurate enough to prove the correctness of the simulation (Figure 25).

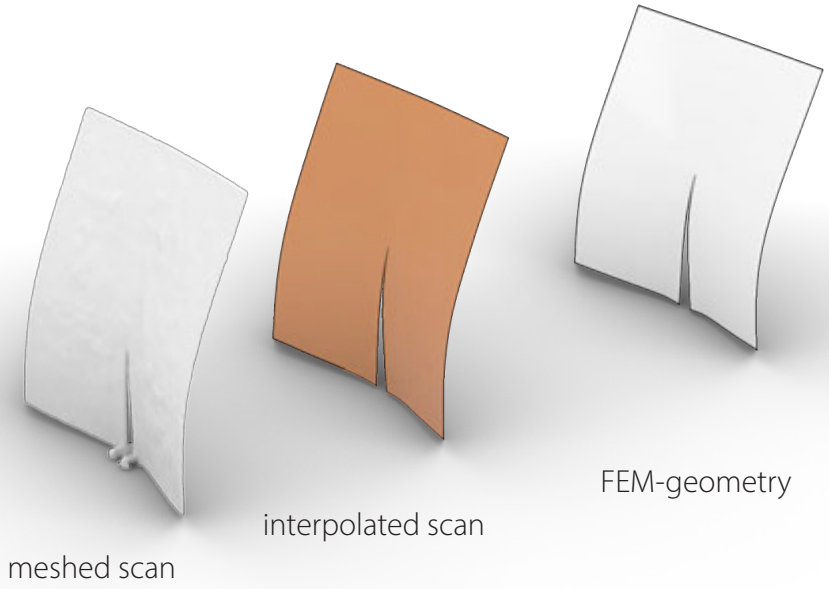

Fig.25 Scan Workflow

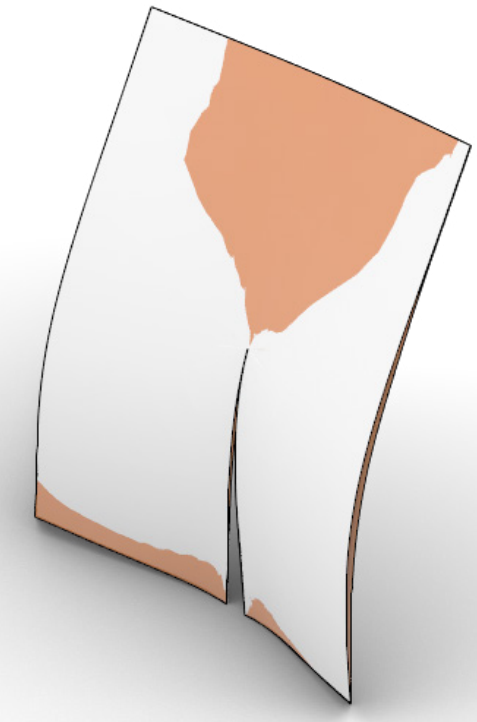

Fig.26 Scan/FEM comparison overlay of the scanned (brown) and simulated (white).

The preceding FEM simulation is used to optimize surface areas subjected to excessive stress, while minimizing the impact on deformation behavior.

The stress data obtained from the simulations are analyzed to identify regions of high stress concentration, which indicate potential areas of structural vulnerability. To mitigate this vulnerability, strategic cutouts are introduced on the surface based on the stress analysis results. The objective is to redistribute stress and minimize the risk of structural failure, while maintaining control over surface deformation.

For this purpose, the yield criterion was determined, using an ultimate tensile strength test. The test object was tensioned, using a spring balance, until it starts to tear. The value obtained at the breaking point is used as a reference to identify the area in the material where the stress exceeds the values obtained.

Fig.27 Tensile strength test

Behavior

Concept

Initial investigations and comparisons between observations of the physical model and the simulation provide insights into the geometric and structural behavior of the elastic bending of the plate. This makes it possible to describe the processes in more detail and draw conclusions about the bending behavior in relation to its shape and the manipulations, to which it is subjected. It is important to understand which influences determine the non-linear behavior and how optimizations based on FEM data effects its deflective behavior.

Mechanical behavior

To simulate the deformation, the gained insights from the physical tests serve as a basis for the boundary conditions to be set in grasshopper for Rhino[13]. It enables to simulate the spatial and structural impact on the applied load through the displacement of x,x'

The points of attachment (x,x') need to be constrained on the x-axis while these points are is placed in a counter directional in plane movement. The points of attachment acting as a pinned support allowing them to rotate freely around the axis perpendicular to the plane of displacement.

The applied forces are translated into shear forces that cause the upper and lower parts of the surface to experience a slight difference in length (compression, stretching), while the neutral surface remains free of longitudinal changes.

Shear forces are applied perpendicular to the neutral surface, causing the plane to experience bending and torsion. The axes of the bending moments are perpendicular to the zy and xy planes, while the torsional moments are in the z-axis and similarly in the x-axis.

The applied forces are translated into bending and torsion, and ultimately cause the plate to buckle out of its initial plane. The bending can be described as pure bending deformation since the neutral surface is free from longitudinal extension or compression. Only the fibers away from neutral surface are subjected to compression or tension[14].

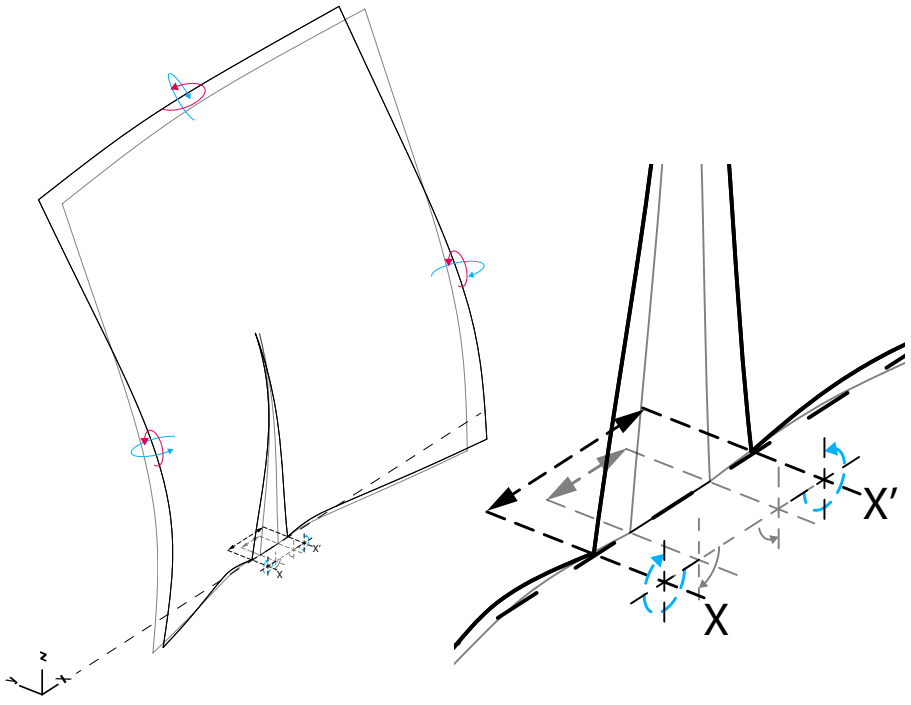

Fig.28 Geometrical behavior

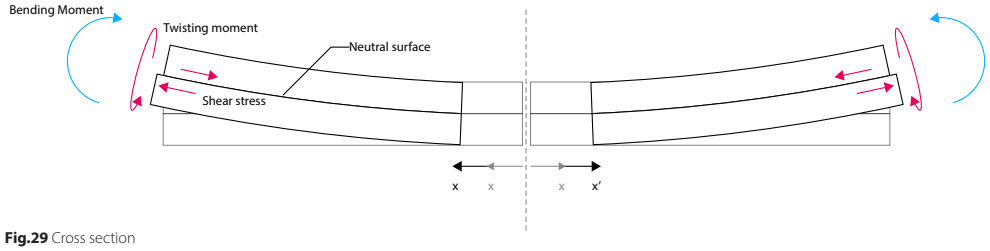

Fig.29 Cross section

Structural behavior

Bending-active plate structures are depending the equilibrium of in plane shear forces in the sheet material.[15]

The FEM simulation provides insight into the stress distribution within the material. In order to understand the geometric deformation and its spatial dynamics, it is essential to analyze the structural response as the initially flat plane bends out of plane.

When looking at the von Mises stress lines, it becomes clear how the stress spreads out from the center of the area uniformly in three main directions. The center of the highest stress is at the tip of the incision, from which the stress spreads out to the edges in a cloverleaf-like distribution (Figure 30,31).

During deformation, it can be observed how the stress peak, which spreads in the direction (M), remains almost in the same position, while the values continue to increase with a gradual displacement of x. The leaves that are oriented diagonally to the lower corners are rotating most likely because of the rotational movement of the points of attachment. It can be observed at the same time, with an increasing displacement of x, there is a concentration of stress towards the tip of the incision.

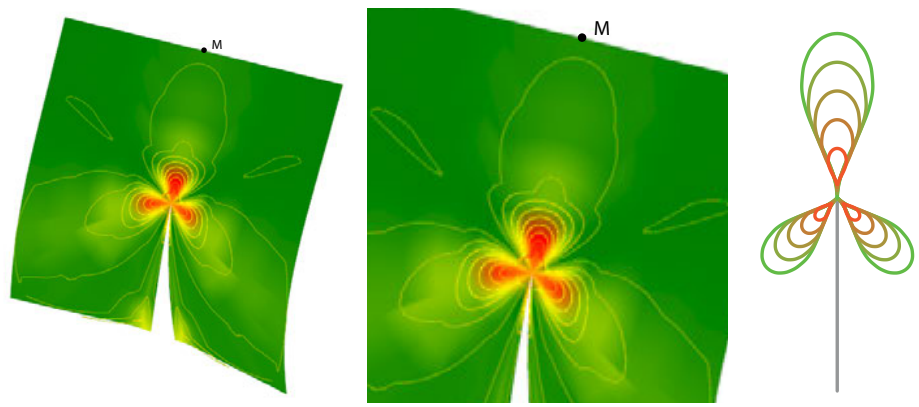

Fig.30 Stress bloom

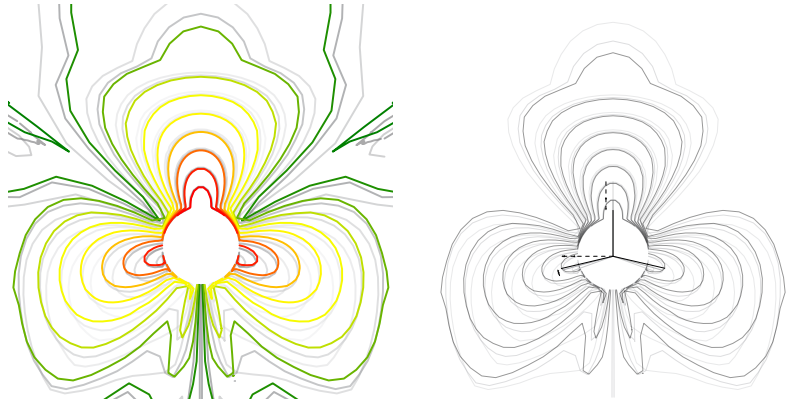

Fig.31 Stress distribution in relation to x displacement

By utilizing the data gathered from the FEM-analysis, we were able to identify the area, in which the yield criterion was exceed first. For all simulated geometries, a loop at the tip of the incision was found. This is most likely, because of the characteristics of the deformation. While the bottom part (area of attachment), is displaced the point tip of the incision at the geometries can be seen as a hinge, which transfers most of the stress at the top part of the plate (Figure 33).

Each new section is based on the data of the previous variant. Thus, a section is created for the first level of FEM simulation values. The first variant (c1) is based on the initial sheet. For the second variant (c2), as for the first, the previous variant (c1) is used. This is done up to the 3rd level because the complexity of the section and also the accuracy decreases with each new level due to the difficulty of creating complex sections with untrimmed NURBS surfaces. (Figure 34)

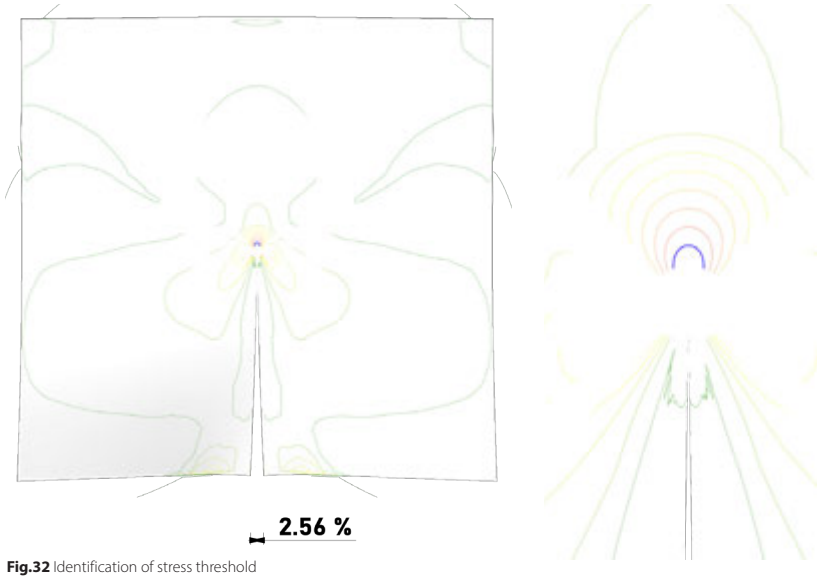

Fig.32 Identification of stress threshold

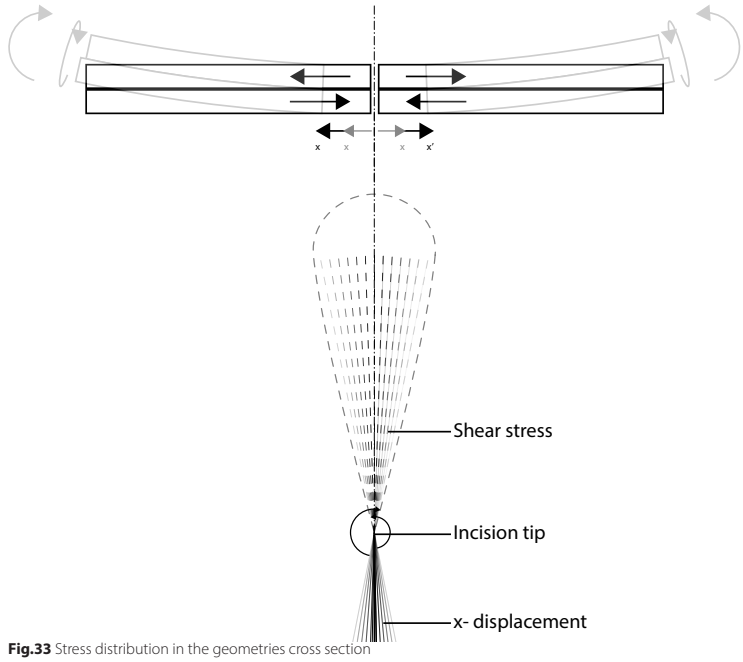

Fig.33 Stress distribution in the geometries cross section

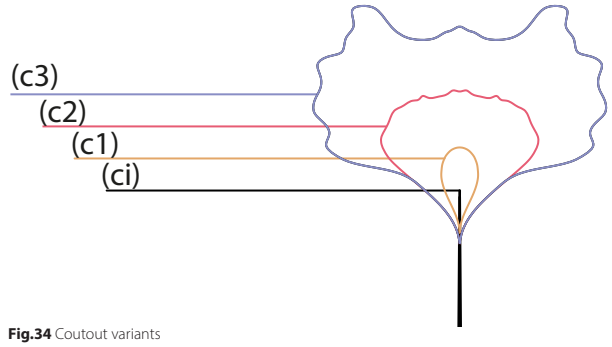

Fig.34 Coutout variants

Curvature/Stress

Since deployable bending-active structures benefit from bending-dominated transitions, inextensional deformations serve as the principal mechanism for achieving large-scale deformations without reaching the critical stress state in the material. This means, that the material is bent without stretching the neutral surface, also referred to as isometric deformations since the only surfaces that correspond to an isometric transformation are developable surfaces, i.e., cones and cylinders.[16]

When considering the curvature of the deformed geometry, it can be observed that it actually corresponds to the previously mentioned criteria. Specifically, it is mainly subjected to pure bending (inextensional bending).

The curvature of the surface is predominantly characterized by a monoclastic geometry, despite minor parts exhibiting anticlastic and synclastic deformations. These latter characteristics are generally negligible in the broader context of the surface's curvature. Notably, deviations from the monoclastic norm can largely be attributed to variations in stress levels during the deformation process. The localized occurrence of anticlastic and synclastic parts on the surface results from frustration of the material. This describes areas that exert compression and expansion by maintaining the length of the mid surface.

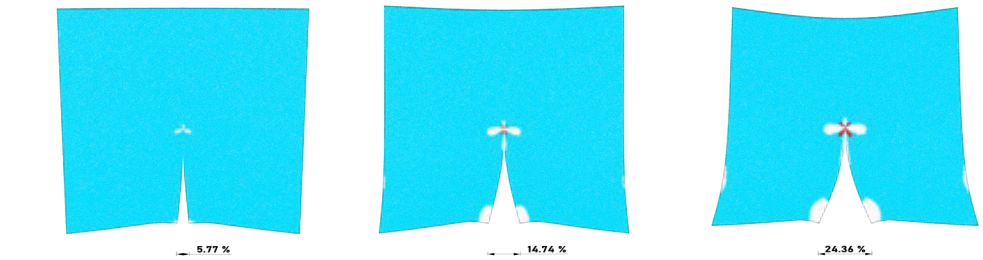

Fig.35 Curvature analysis

Fig.36 Stress distribution

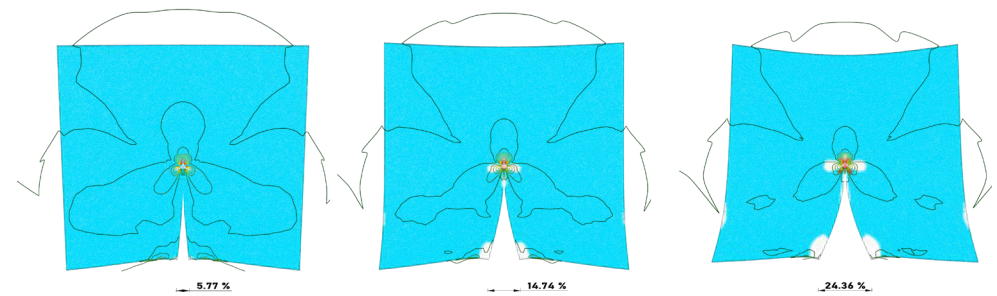

Fig.37 Curvature and stress combination

Workflow

The workflow applied is based on the integral concept. As described above, different initial geometries are subjected to targeted changes in several variants. The goal is to analyze the effects on the active bending behavior. For each initial surface, variants of 3 levels of manipulation have been added.

With the previous basic investigations on the validation of the physical experiment to the FEM simulation, a proof of concept has been created. The defined parameters serve as a framework for the FEM-simulation. By synchronizing physical and digital parameters, it is possible to evaluate the structural and geometric behavior in the form-finding process of the controlled deformation of initial planar surfaces.

This makes it possible to determine the parameters for evaluating the spatial and structural deformation properties of the planar surfaces by a linear, counter directional displacement in a plane of the points (x/x'). To evaluate the effect on surface manipulation the maximum opening is set to 25% of the side length of the surface boundary as earlier explained.

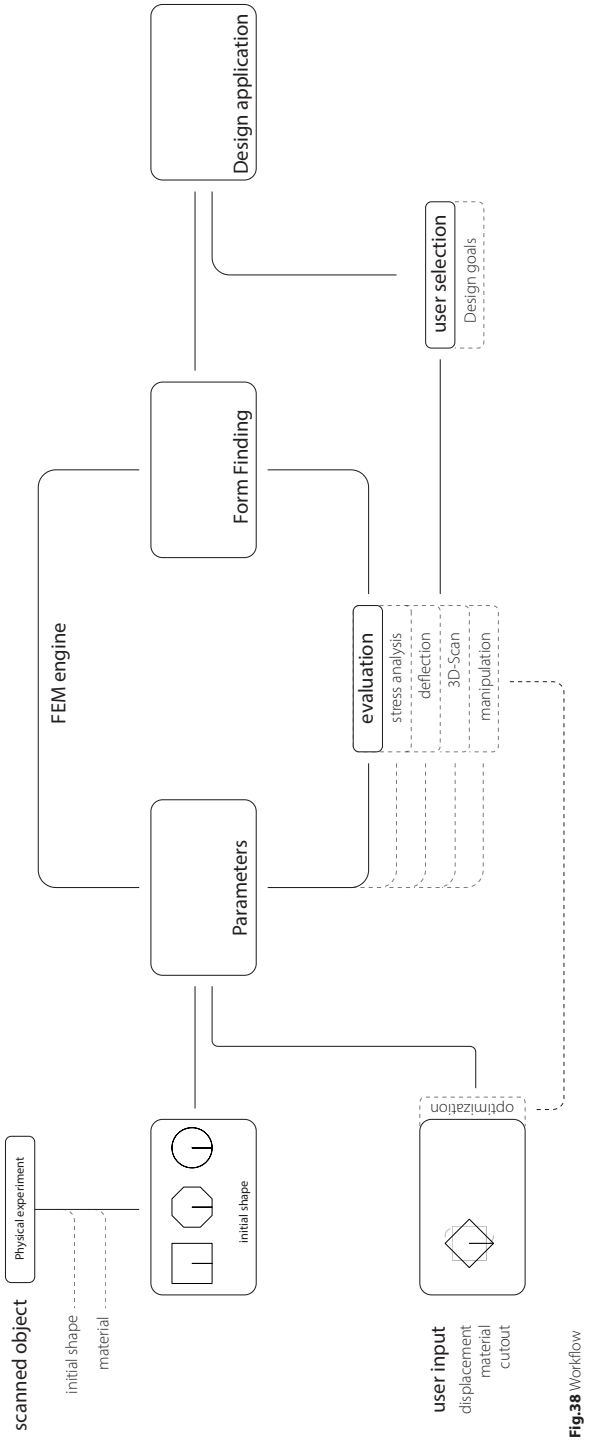

Fig.38 Workflow

Evaluation

By integrating the identified geometric boundary conditions and the material parameters, a simulation environment has been created, that ultimately allows the study of processes occurring during elastic deformation of the planar sheet material in terms of their structural and spatial properties.

In addition to the manipulation of the internal structure, the variation of the external shape and its effect on the deformation behavior is also of interest. For this purpose, the original geometry (square) was transferred to a circular shape. Starting from a square, four more edges were added to the surface and the corners were cut off by bisecting the angle. The result is an eight- and sixteen-sided polygon and finally a circular shape.

All geometries are based on the 4-sided polygonal sheet of a dimension of 200 x 200 x 0.5 mm.

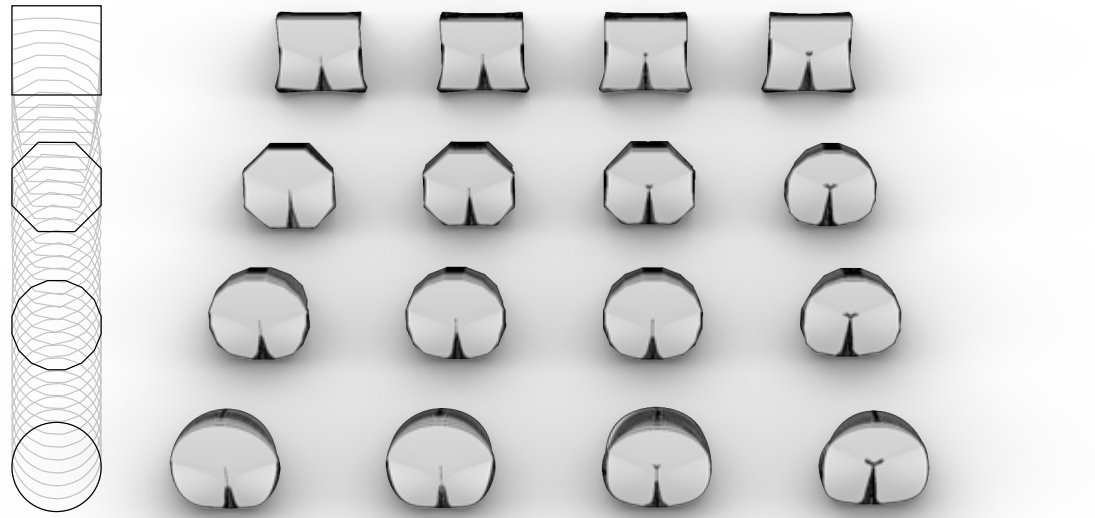

Spatial domain system

To evaluate the structural and spatial behavior ,the geometries are set in relation to their positioning in a Cartesian coordinate system, in which the x-axis represent the axis of displacement of the points (x/x'). The Spatial domains refers to the segmented areas of a structure distinguished by their spatial positioning along the Cartesian axes. These domains highlight the extents of deformation in various directions, which can be described by looking at the inclination, deflection, area domain and vertical projected boundaries of the resulting geometry of the deformed sheet material..

Reference Domain System

Width : 200 mm
Heigth : 200 mm
Depth : ± 200 mm

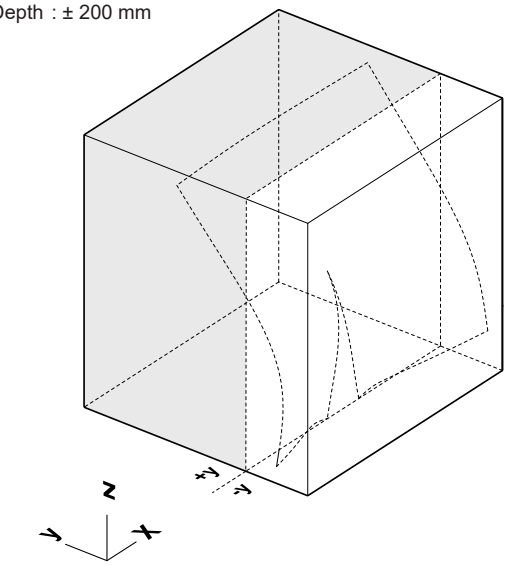

Inclination

The inclination in this context refers to the angle formed between a vertical reference plane and the point (m) of the deformed geometry. This angle quantifies how much the top of the structure deviates from its initial, flat state as a result of applied displacement of x,x'

Deflection

The deflection measures the geometry's deflection in (±y) measured from the initial plane in the x-axis, which serves as a reference in the bounds of the reference domain . The deflection quantifies the deflective performance, while bending out of plane, providing insights into the structure's response to applied forces from the top view.

Areal domain

Areal domains refer specifically to the area portions of the geometry's surface, categorized according to their displacement or deformation characteristics within a predefined coordinate system. The areal domains are quantified to understand the proportional distribution of the surface areas that extend into the +y and -y directions, providing insights into the material's response under load (displacement of x,x') its spatial and structural implications.

Area coverage

The area coverage, refers to the coverage of the deformed geometry and allows for an evaluation of the spatial impact and behavior of the structure under load. It provides data on the areal coverage as it deforms, which is crucial for understanding spatial utilization and structural efficiency.

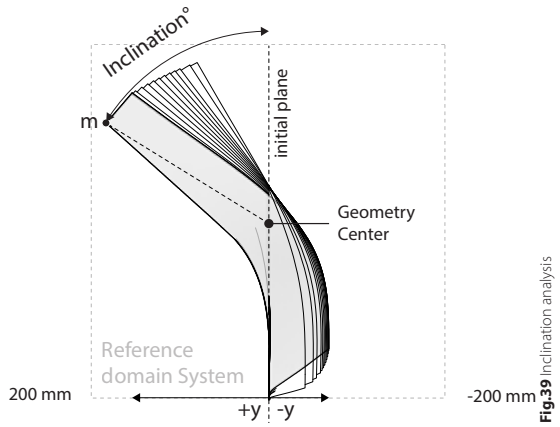

Fig.39 Inclination analysis

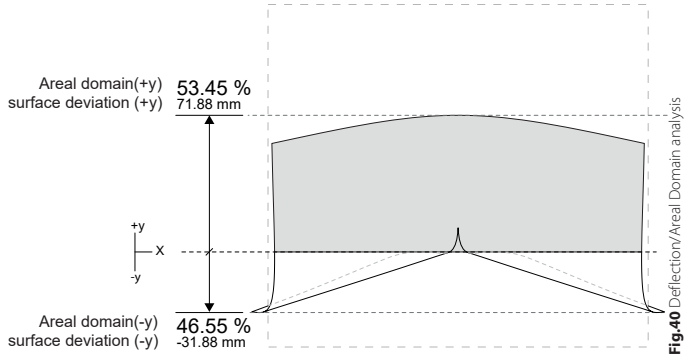

Fig.40 Deflection/Areal Domain analysis

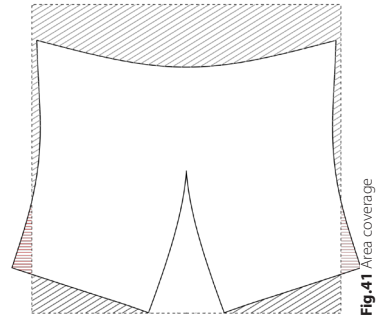

Fig.41 Area coverage

Naming scheme

The naming scheme for the various analyses is composed of an abbreviated designation of the basic geometries. The variants are then named on the second level by its cutouts and its level of variant (c1),(c2),(c3).

For the evaluation of the simulated deformations, variants (ci) and (c1) were selected; (ci) has a cut only and c1 with a single loop-like cut-out. This makes it easier to compare the effects of the optimization. The subsequent variants (c2),(c3) give a general picture of the effects of further manipulations of the section.

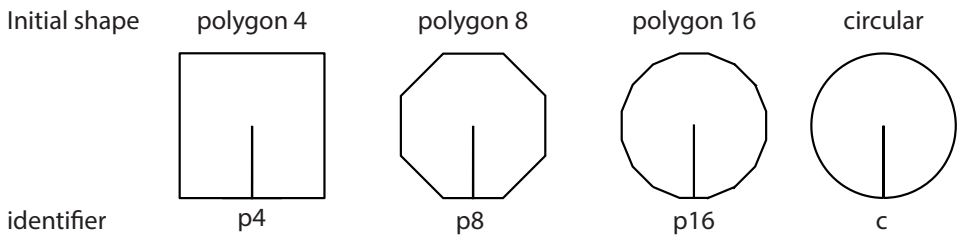

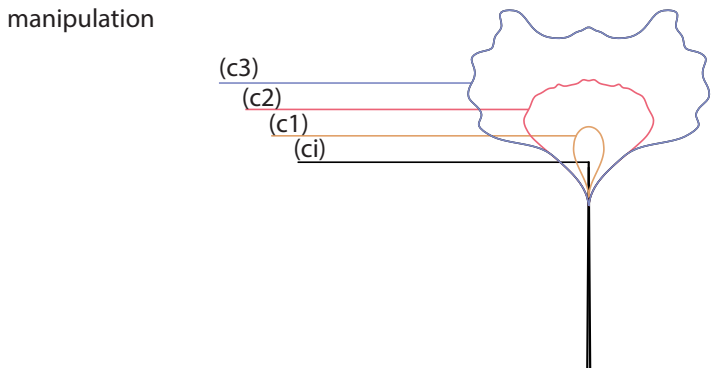

Fig.42 Naming scheme

Polygon 4

p4(ci)

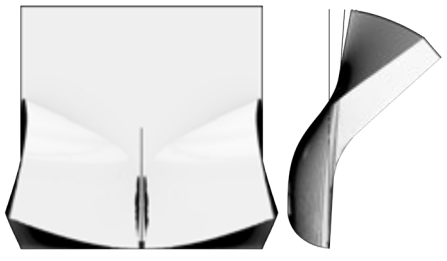

Inclination

The first simulation based on the parameters described above allows a more detailed analysis of the spatial and structural properties during the deformation process.

The angle of inclination of point (M) in relation to center of the initial flat geometry allows a general statement about the degree of deformation. In this case, with a maximum opening of (x,x'), 25%, an angle of 57.62° can be determined.

The graph for the inclination, shows a non-linear behavior at the initialization, then transitions into a almost linear progression at a value of x-displacement of 4.49% with a inclination of 21.89 °.

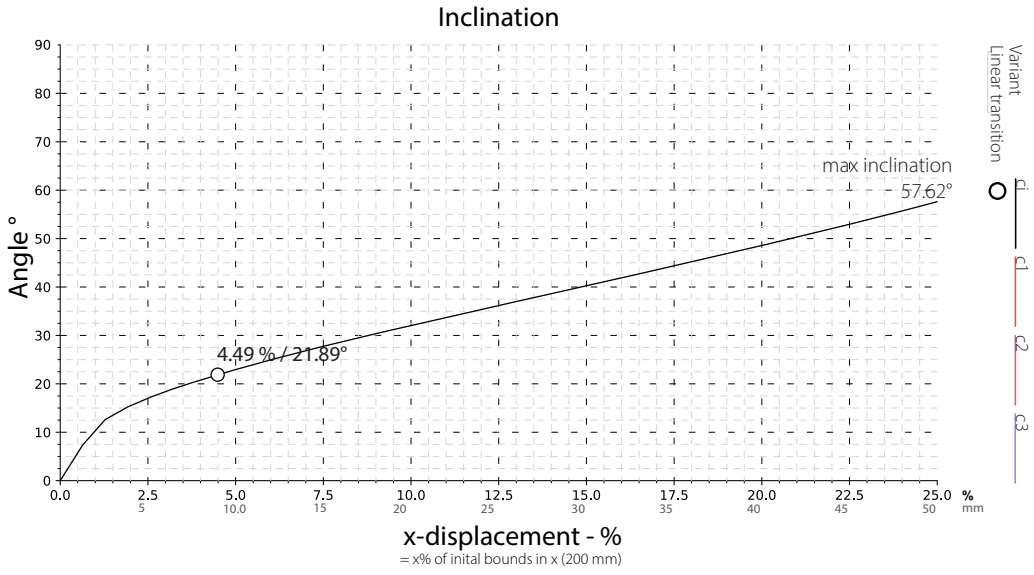

Fig.43 Graph inclination point (M)

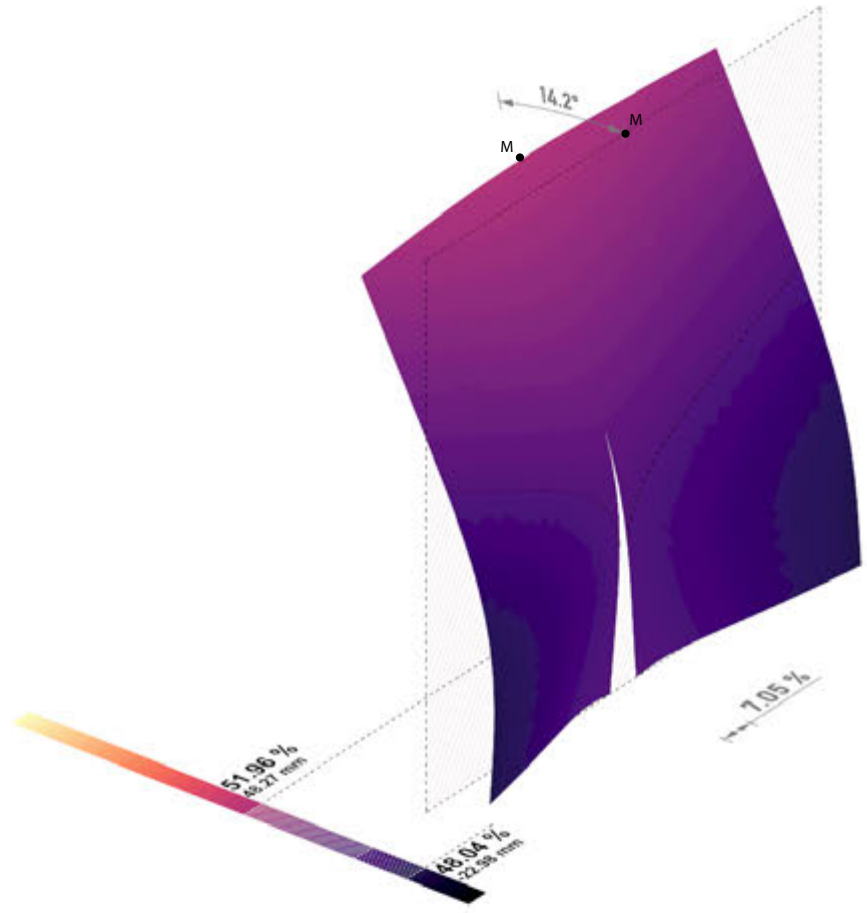

Fig.44 P4 out of plane inclination

Deflection

The analysis (figure 45) of the deflection for p4(ci) quantifies its deflective performance, while bending out of plane, providing a data of the structure's dynamic response to applied forces through the in plane counter movement of x/x' .

At a first glance, it is noticeable that the distribution of the deformation in y is asymmetric. While the deflection in +y undergoes a rapid deformation at the beginning of its initialization and starts to flatten out at a x-displacement of 4.49 % . The deformation in -y happens to be a smoother deflection. While both graphs show a non-linear behavior the deflection in -y starts to flatten out at 3.85 %.

It can be stated that the slope ratio of +y in average is about 2.30 times -y. As soon as it exhibits a linear rate of change in deflection, it indicates a stabilized state of equilibrium, resulting in a controllable, means slower, deformation.

The asymmetric deflective properties of the surfaces areas indicate different rates in deflection in ±y direction. This is explained by the different freedom of movement in the geometry's regions. Regions with a higher freedom of movement, meaning no constraints on its outer boundaries, are able to deform freely. While parts, closer to the attachment, are restricted in its freedom of deformation. The pinned support enables the geometry to translate the induced stress in a rotational manner to the upper parts of the material, which are able to move more freely in the x/y/z direction.

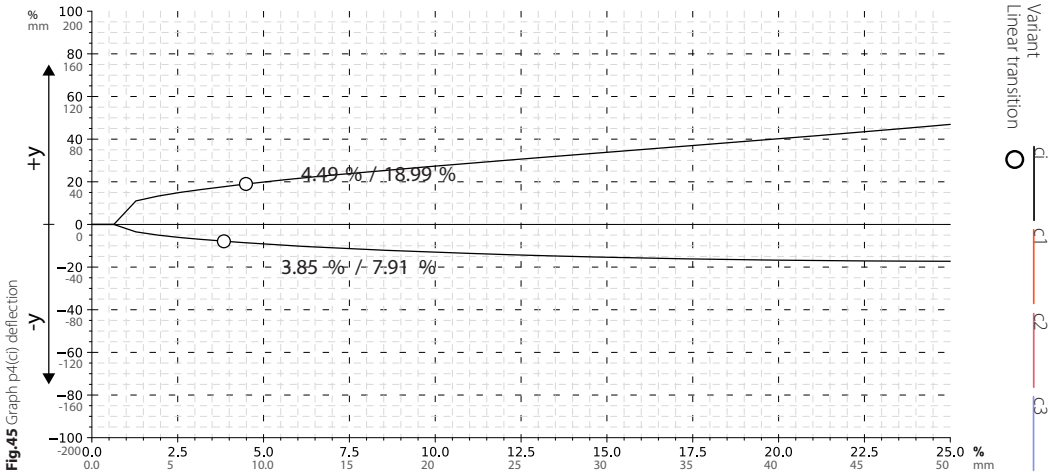

Fig.45 Graph p4(ci) deflection

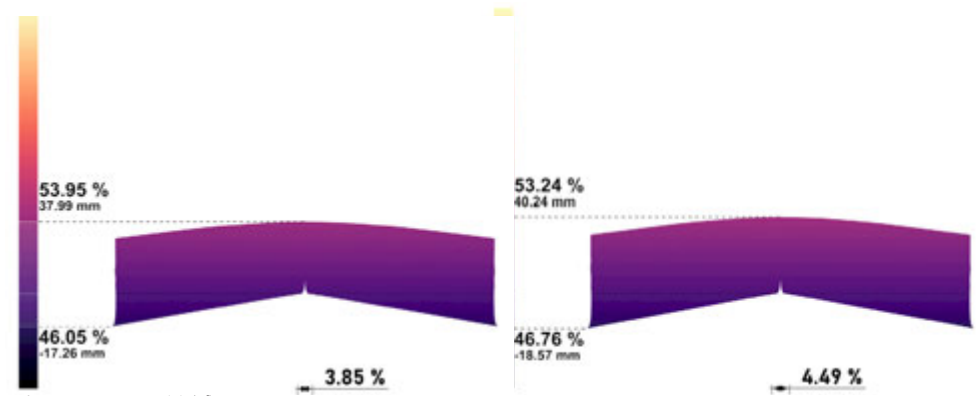

Fig.46 Comparison, p4(ci) deflection in mm

Areal Domain

While the deflective behavior of the geometry shows a strong asymmetrical performance, the area fractions allocated in the ±y parameter space, demonstrate its reflective characteristic.

At its initiation phase, a rapid change in both area fractions in ±y is observed. Compared to the deflection, the area distribution exhibits an extended non-linear performance. While in the latter described graph (Figure 45), for the deflective characteristics, the transition for the area distribution describes less a transition to a linear behavior, than a balanced distribution of the sheets ares in ±y. The analysis of the inclination and deflection shows a constant rate of change, after the phase of initialization, the area fractions behave differently. When the point of transition is reached, the change of areal distribution stays in a range of 51.96 - 58.35 % for the surface part in +y and 48.04 - 41.65 % (Figure 47).

This indicates that the geometry's deflective behavior occurs mostly due to a uniform distribution of force resulting in an almost symmetric contraction until it reaches its maximum at 7.05%. From this value on, the inherent stress distribution is dominated by the occurring stress facing towards the point (M). Conversely, stress blooms facing in the opposite direction starts to contract towards the geometry's center.

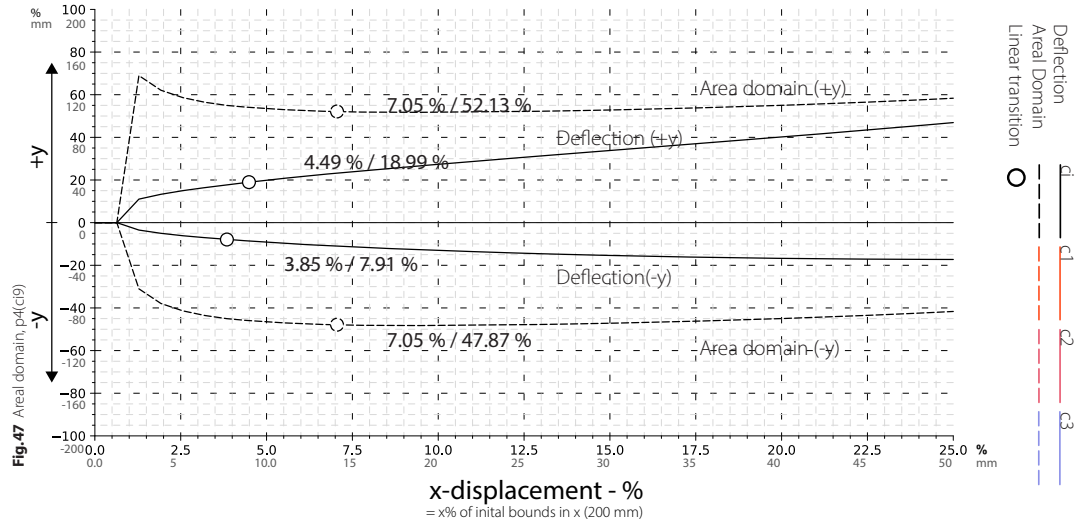

Fig.47

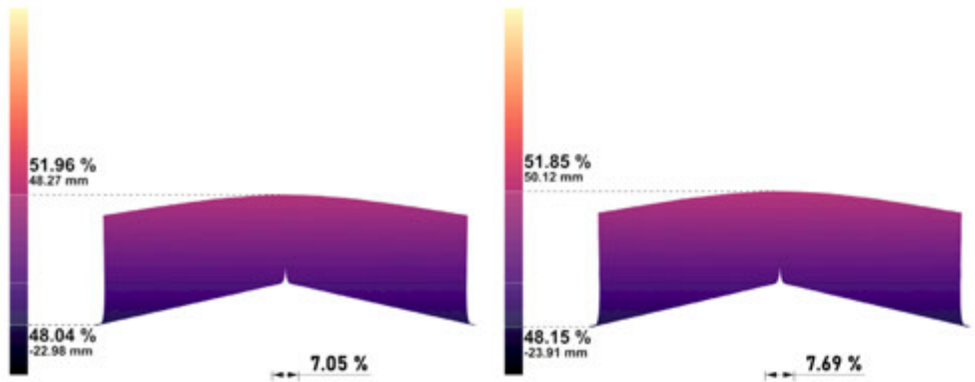

Fig.48 Comparison, p4(ci) Areal domain in %

Area Coverage

As previously stated, the bending behavior involves a complex deformation that influences the out of plane movement in 3-dimensional space, which can be observed in the aforementioned spatial investigations.

While the previous parameters mainly examine the spatial effects of the bending-active plate, the investigation of the so-called area coverage (meaning the projected surface onto a vertical plane) examines the effect of the deformation on the area coverage. This analysis allows us to quantify the effects of out-of-plane bending in relation to the x-displacement and shrinkage/expansion.

The graph (Figure 49) shows, for shrinkage as well as for expansion, an almost constant, linear behavior between coverage ratio and x-displacement. The fact that, on average, the shrinking area exceeds the expanding area by a factor of 15.76 is a clear indication of strong out-of-plane elastic deformation. This is also evident when looking at the expanding area, which, despite spreading through the x-displacement, exceeds the initial bounds at its maximum by only 1.46%.

It should be emphasized that although there is a little expansion of the area coverage due to the x-displacement, the area coverage appears to shrink to a large extent, while the surface expands into a spatial object.

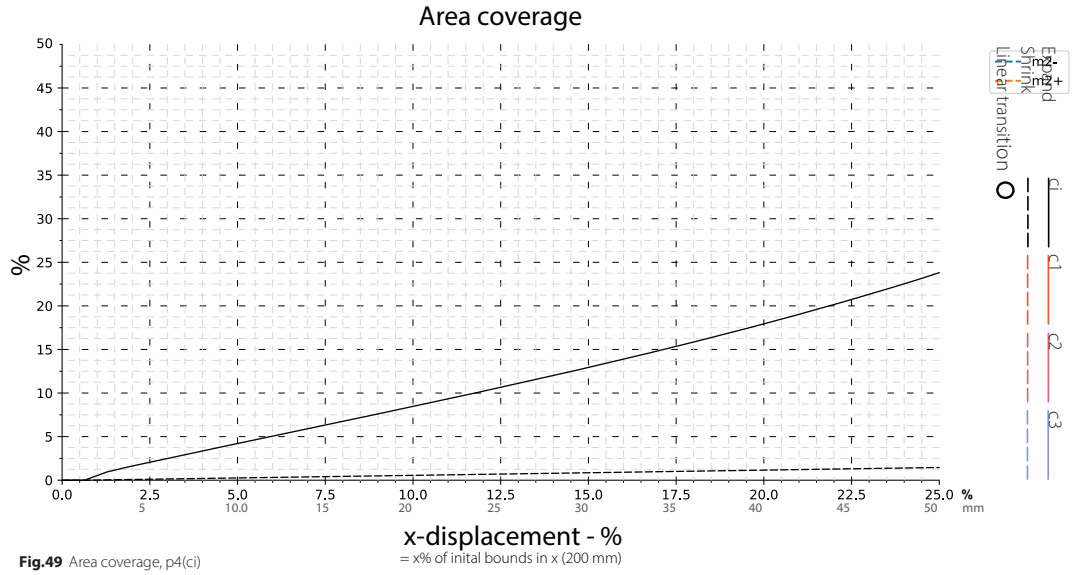

Fig.49 Area coverage, p4(ci)

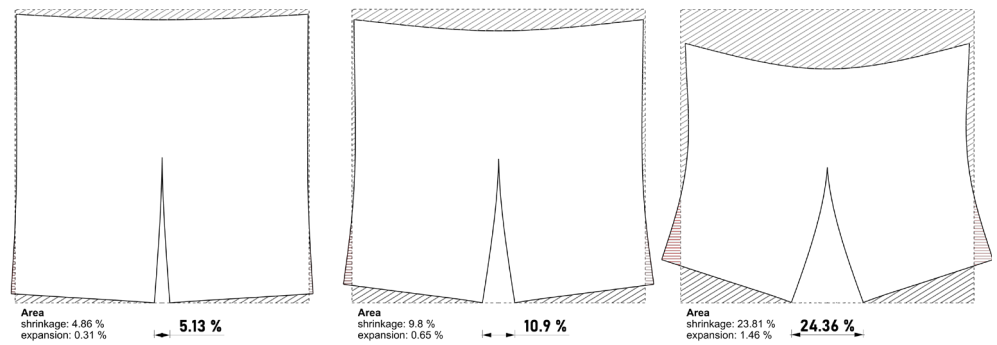

Fig.50 Area coverage, p4(ci)

Polygon 4

p4(ci)/p4(c1

The previous studies on the basic bending behavior serve as a reference for further investigations. As described earlier, the x-displacement leads to a high level of spatial deformation of the sheet material. In order to minimize the risk of material failure, the yield strength of the material must be taken into account. For this purpose, cutouts in the geometry have been created based on the van mises stress analysis in the geometry. This manipulation has an effect on the bending behavior, which ultimately also has an effect on the spatial and structural behavior of the deformed sheet.

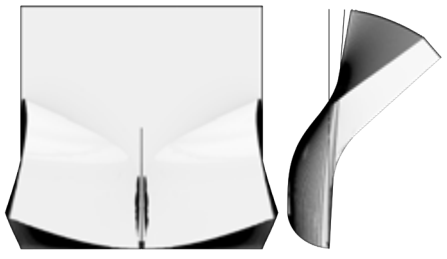

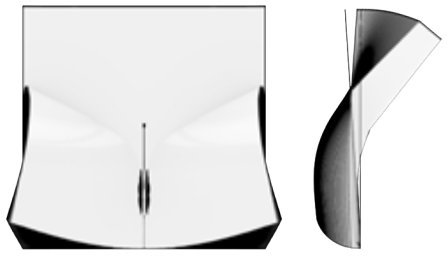

Inclination p4(ci)/p4(c1)

By comparing the inclination of p4(ci) and p4(c1), a significant difference could be observed. In contrast to the (ci), (c1) shows a smoother behavior. While (ci) shows rapid changes, especially during the initialization phase (x-displacement range 0 - 2.0 %). While the initialization for the geometry (c1) starts at 1.75% with a slower rate of inclination as seen in Figure 51. It experiences a more uniform stress distribution in the material resulting in a slower rate of inclination of point (M), indicating that the overall spatial response of the sheet material depends on an initial stress accumulation.

Thus, it can be observed that the activation of the geometry also undergoes a non-linear process, even though at a lower rate. The transition to linear behavior, which indicates the stabilization of the forces, is only marginally delayed in this case. While the transition in (ci) starts at an x-displacement of 4.49 %, (c1) starts to normalize at 5.77 %. By looking at the average difference between the variants the performance regarding to the inclination of point (M) is reduced by 33.94 %.

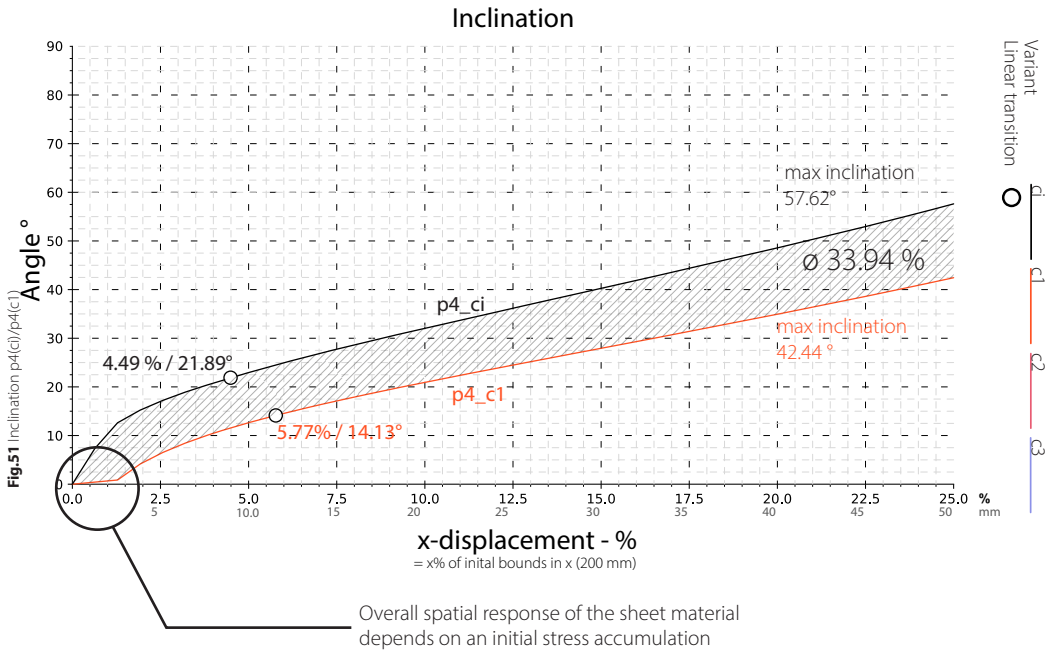

Fig.51 Inclination p4(ci)/p4(c1)

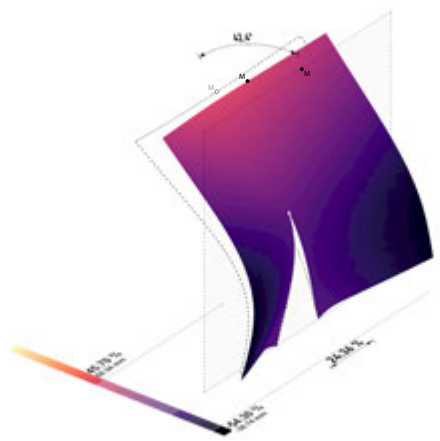

Fig.52 Comparison of the inclination of point (M), p4(ci)/p4(c1)

Deflection p4(ci)/p4(c1)

As observed in the previous analysis for the inclination of the geometries (ci) and (c1) the deflective behavior for the optimized geometry is subjected a similar behavior.

Comparing the graph for deflection (Figure 53), showing the variants p4(ci) and p4(c1), the non-linear behavior of the deflection shows a smoother deflection in +y and an offset into the linear transition. The reduction of its spatial expression in +y is reduced by 33.75 %. The surfaces deflection in -y seems to remain almost constant even an delta of 11.52% increase of the deflection in -y, while keeping its value of x-displacement for the transition into a linear distribution.

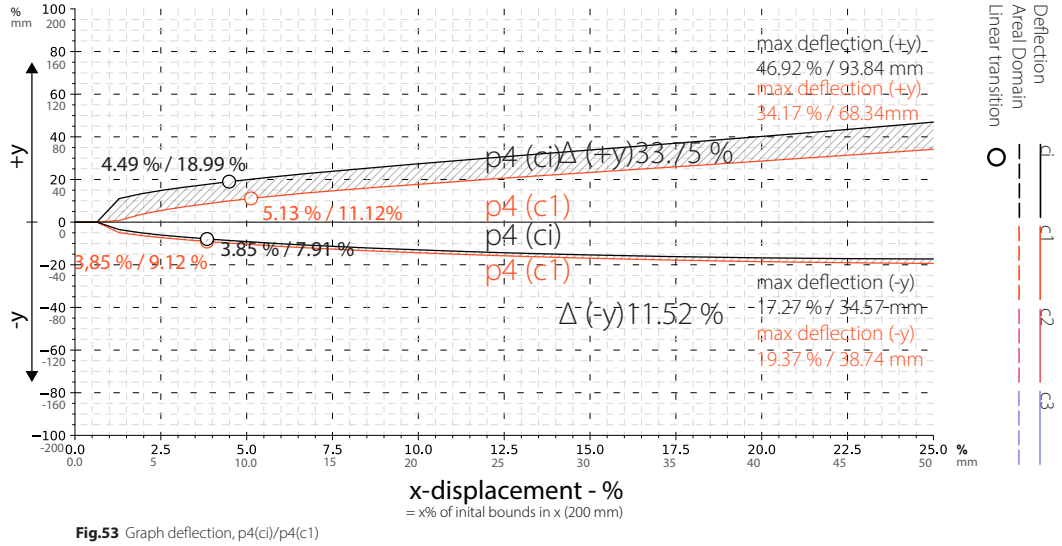

Fig.53 Graph deflection, p4(ci)/p4(c1)

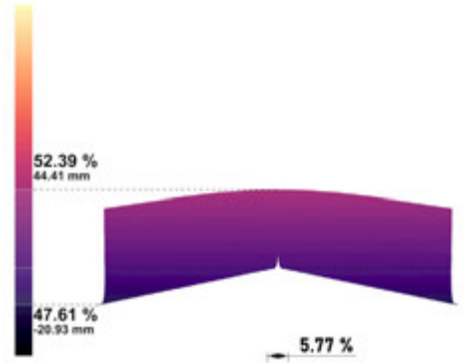

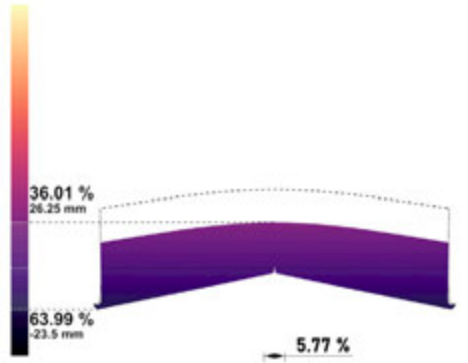

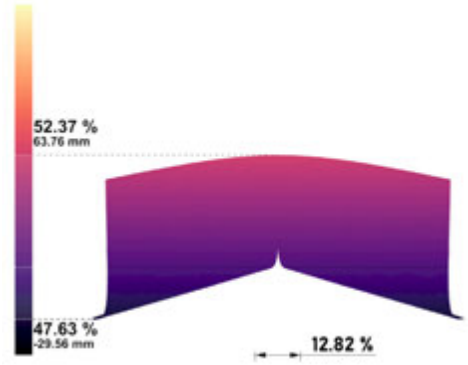

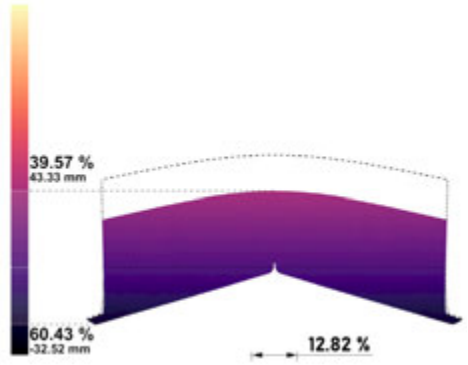

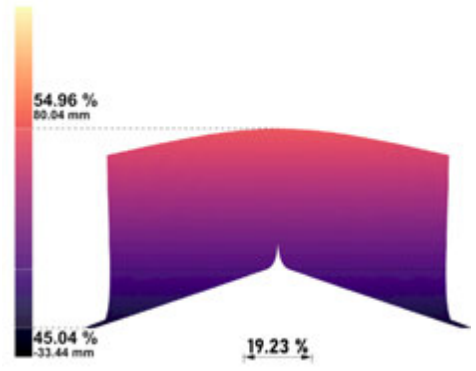

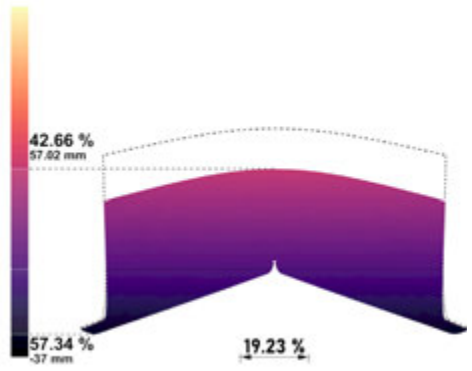

Fig.54 Deflective behavior of p4(ci), in relation of displacment of (x/x')

Fig.55 Deflective comparison of p4(ci) / p4(c1)

Areal Domain p4(ci)/p4(c1)

By analyzing the areal domain (Figure 56), which describes the parts of the deflected surface, in the ±y range, with an exception for the phase of initialization, the average change for the parts of the area which are assigned to ±y seems to shift from an mostly even distribution of the area domains towards an unbalanced distribution. Unlike observed with the deflective analysis (Figure 53), the transition into a linear distributions seems to start earlier.

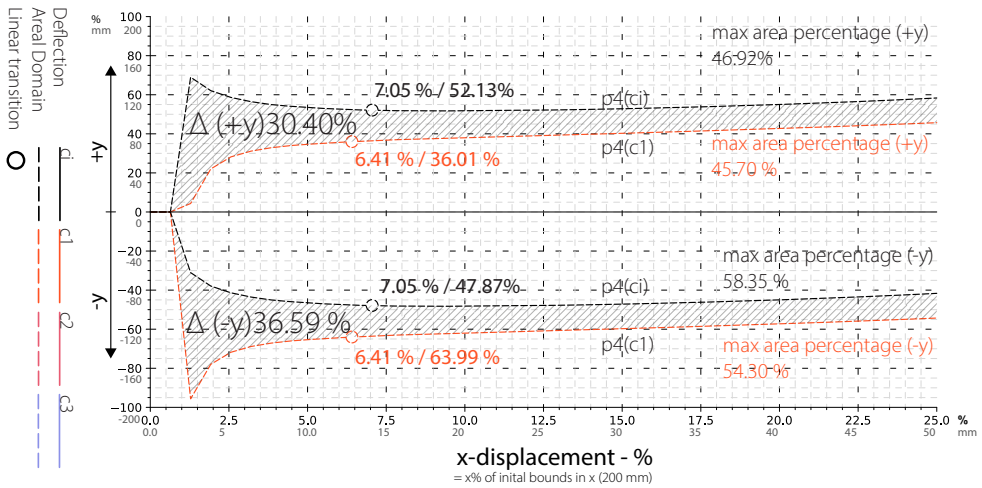

Fig.56 Areal domain, p4(ci)/p4(c1)

Area coverage p4(ci)/p4(c1)

As already noted in the initial geometry, an almost constant change in the area coverage can also be observed. It can be emphasized that the proportions of area that extend beyond the boundaries remain almost the same compared to the geometry's closed state. In comparison to the initial geometry, regarding the reduction of the area coverage (Figure 57), a significant reduction of 33.10% is shown in the coverage of the area compared to the original study to p4(c1).

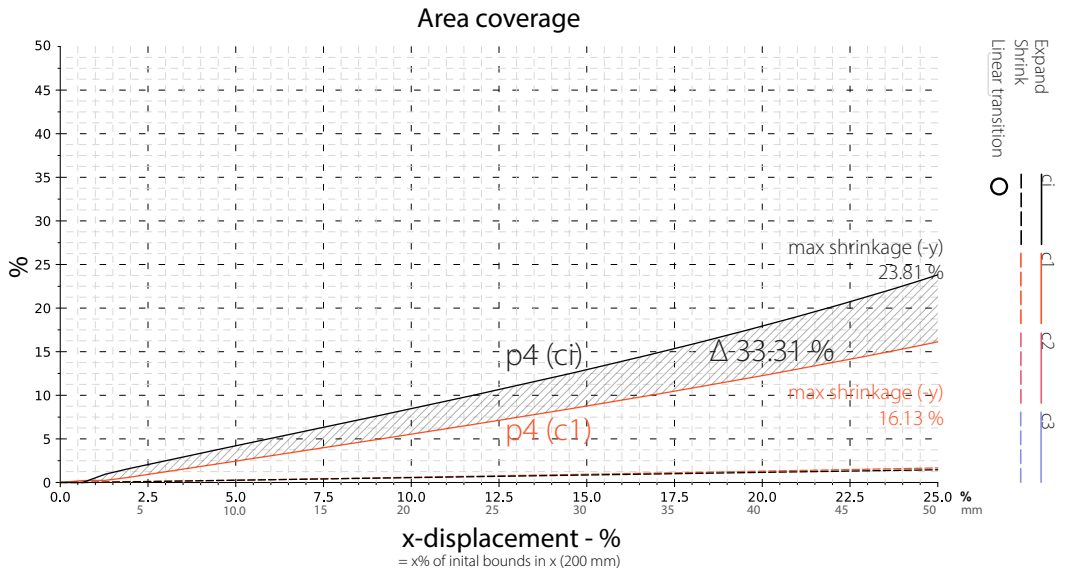

Fig.57 Graph, area coverage p4(ci)/p4(c1)

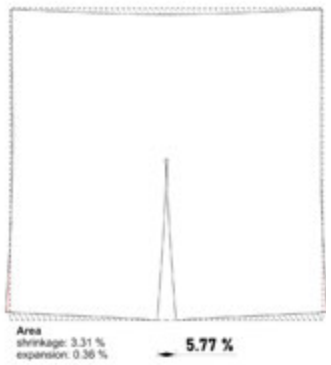

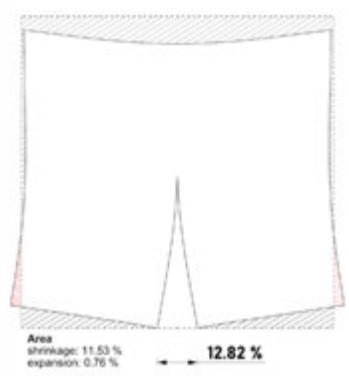

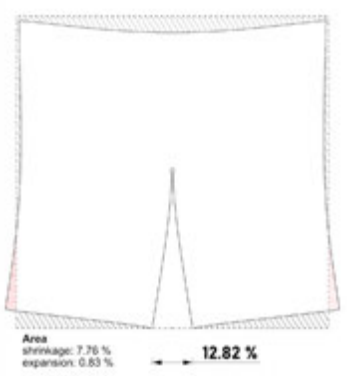

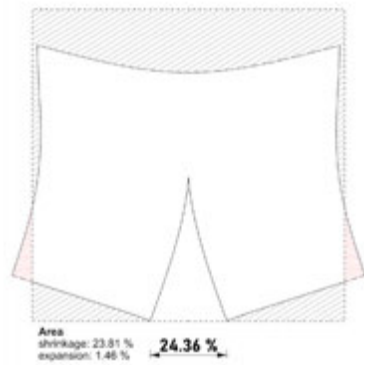

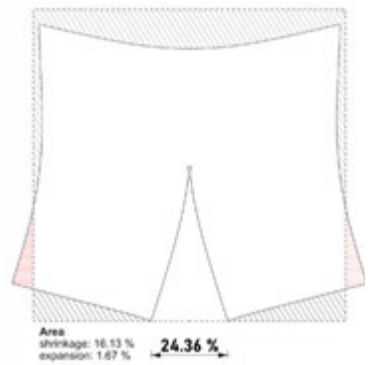

Fig.58 Area coverage, of p4(ci) in relation to (x/x')

Fig.59 Area coverage, of p4(c1) in relation to (x/x')

Circular

c(ci)/c(c1)

At the beginning of the project, for reasons of simplicity, a square was chosen for the experiments and studies of the deformation properties. The previous analyses served to better understand the process of elastic deformation both structurally and spatially.
By analyzing the graphs over the different base geometries, simpler conclusions can be drawn about the behavior. The circular shape was an interesting feature not only in terms of the graphs, but also from an aesthetic point of view.

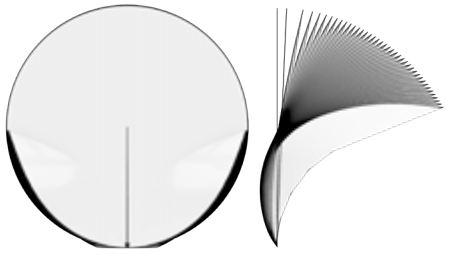

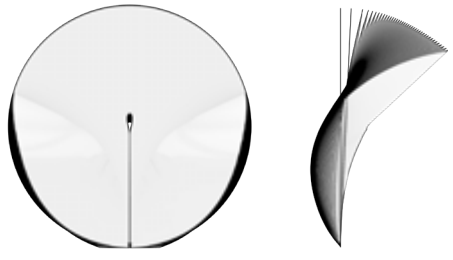

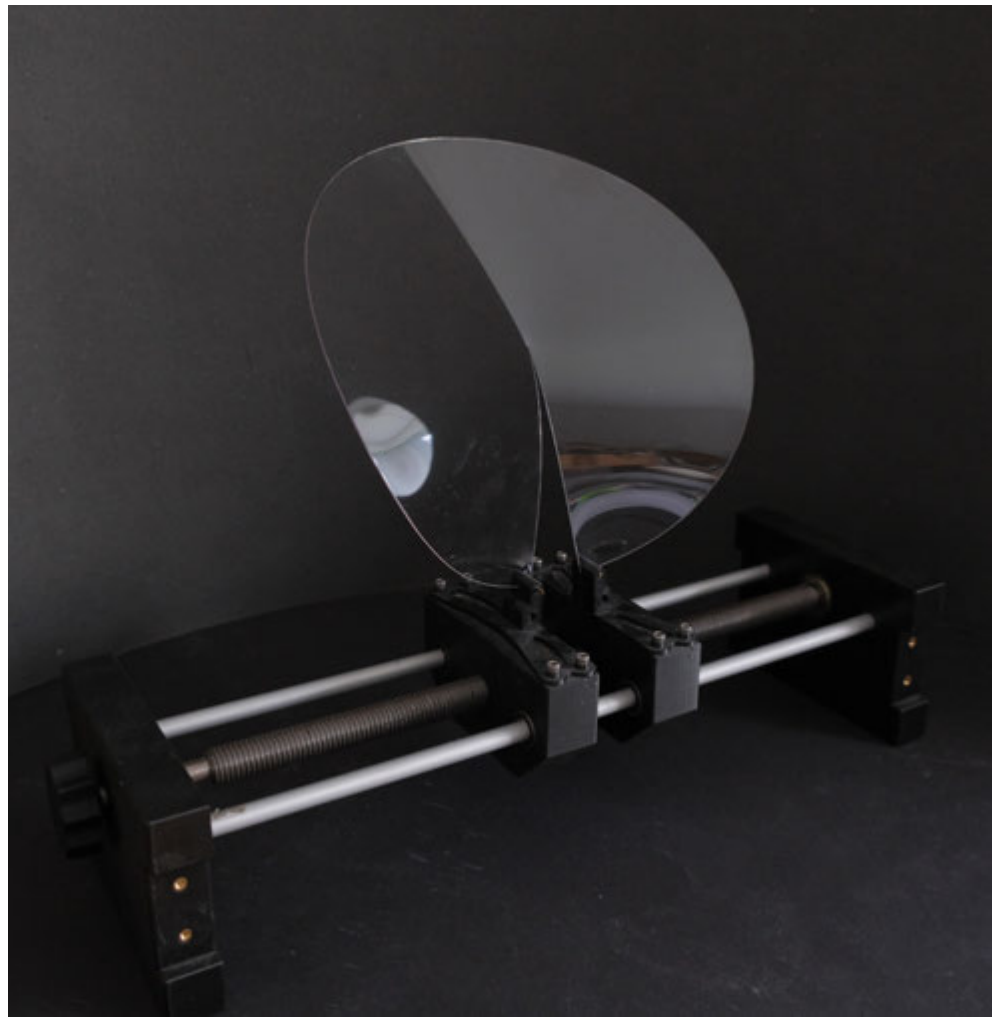

Inclination c(ci)/c(c1)

With the maximum inclination of 83.09°, the inclination of the initial shape of the circular shape shows a significantly higher inclination compared to the square sheet p4(ci).

At first glance, the graph (Figure 60) of the circular shape for the variant (c1) seems to undergo a much large reduction in the inclination of (M). At an average reduction of 36.23%. Although the angle of inclination is greatly reduced, it does not reach the value of the initial geometry of p4(ci). The graphical representation of the area of difference seems to show a much greater reduction in the inclination of point(M). On closer inspection, by setting the optimized geometry c(c1) in to context to the initial shape p4(ci), the reduction in its deflective properties seems to reach the performance of the four- sided polygon.

Comparing p4(ci) with c(c1), shows a similar behavior in terms of inclination, means similar deflection properties for c(c1) at simultaneous advantage of (c1) cutout.

The behavior of the first variant of c(c0) with respect to the angle of inclination should also be mentioned. Strictly speaking, this is not linear in the first variant, while it shows a more pronounced behavior in the second plane of the c(c1).

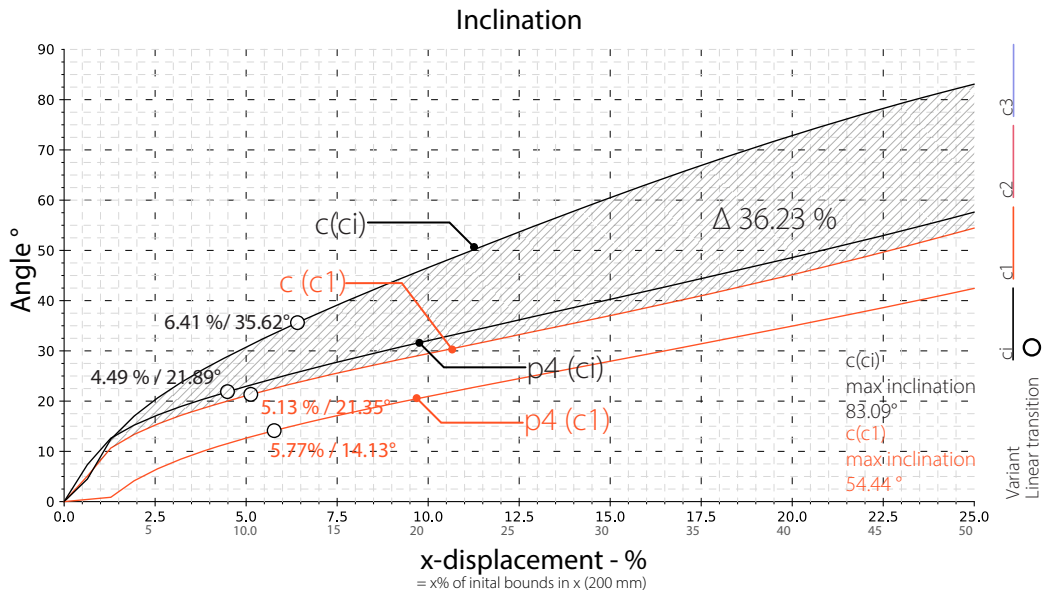

Fig.60 Inclination of point (M) for c(ci)/c(c1) and p4(ci)/p4(c1)

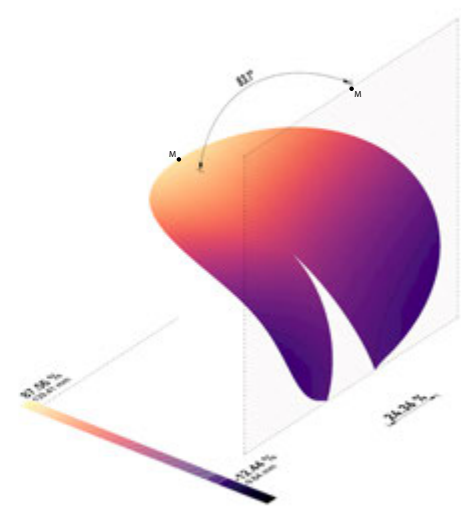

Fig.61 Inclinationof Point(M), c(ci)

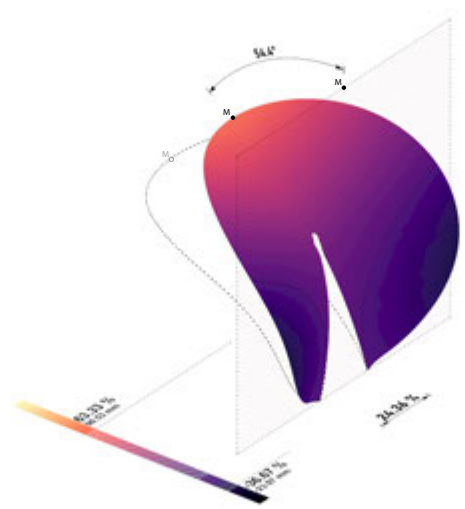

Fig.62 Inclination of Point(M), c(ci)/c(c1)

Deflection c(ci)/c(c1)

Comparing the deflection properties (Figure 63) in +y of the circular geometry with its optimized shape c(c1) and the corresponding variant p4(c1), it becomes apparent, as in the previous comparison of the tilt angle, that c(c1) has a bending behavior that corresponds to the spatial expansion of the initial geometry p4(ci).

A closer look at the deflection for the circular geometry and its deflection properties reveals a repetitive pattern similar to the spatial analysis for p4. Like the transitions of its linear behavior, which is shifting its deflection behavior towards a more balanced deflection, despite an inequality in the strength in the ±y direction.

As in the previous analysis, the average changes are in a range of about one third of the initial deflection in the +y parameter space, with a difference of 37.31%. Although the expansion in -y, with an average change of 69.51%, appears to be a large value, it is negligible in relation to the absolute numbers.

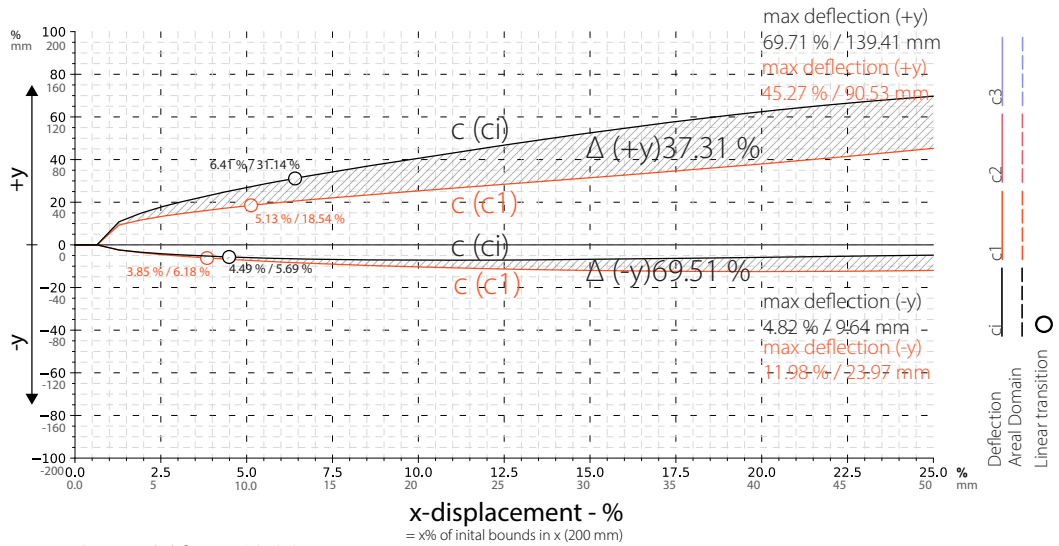

Fig.63 Graph deflection, c(ci)/c(c1)

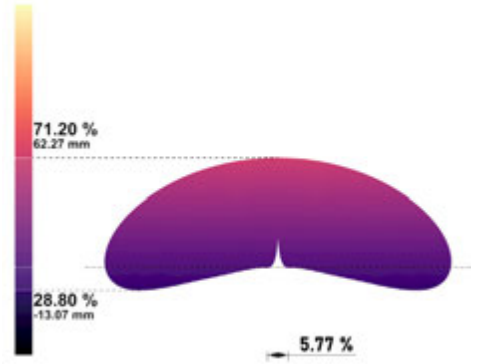

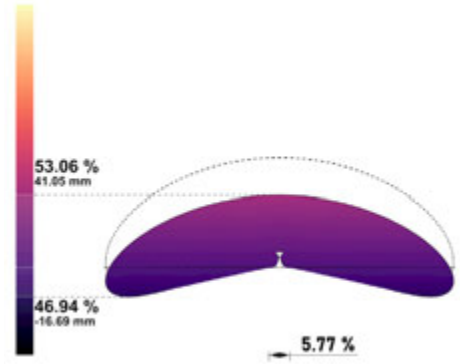

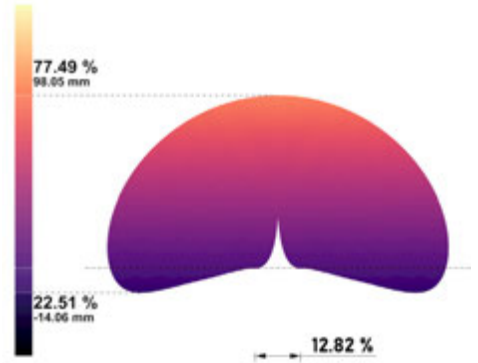

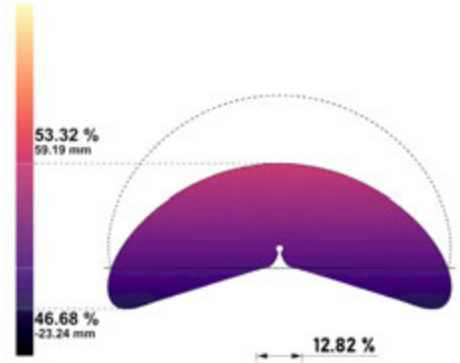

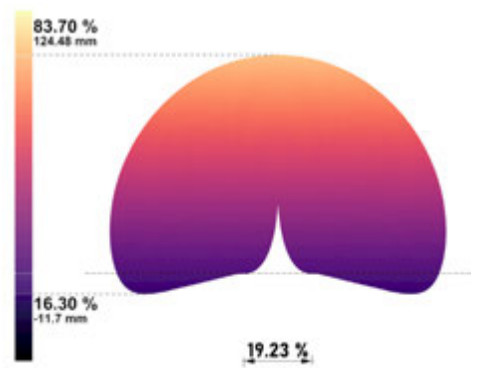

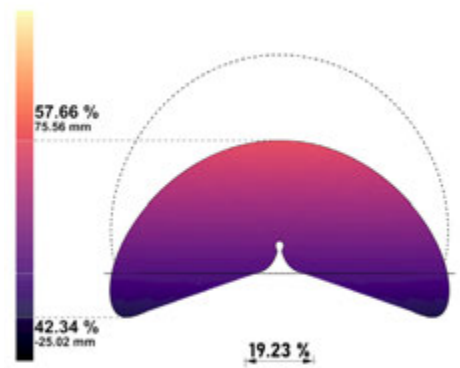

Fig.64 Deflective behavior of p4(ci), in relation of displacement of (x/x')

Fig.65 Deflective comparison of p4(ci) / p4(c1)

Areal Domain c(ci)/c(c1)

While the changes (Figure 66) in the areal domain for ±y in p4(ci) and p4(c1) range from (+y) 36.59% to (-y) 30.40%, the differences in the areal distribution tend to undergo a higher transition. The reduced flexibility in the c(c1) due to its optimization results in an average difference in +y of 27.69%, which seems to verify the trend of a performance reduction by one-third compared to its initial variant (ci).

A major divergence in the proportion of the area in -y is observed, with an average change of 96.11%, nearly doubling. This is explained by the concentration of the applied forces at the tip of the cut, which primarily manifests as a discharge in the upper part of the surface, ultimately resulting in a strong bending behavior away from the area of the attachment point. This behavior is also observed in the graph comparing the angle of inclination and its change between variants ci and c1, showing that the optimized section allows for a more even distribution of forces across the geometry. As mentioned in the latter analysis, compared to p4, the ratio of bending in c(c1) reaches the intensity level of the initial variant of p4(ci).

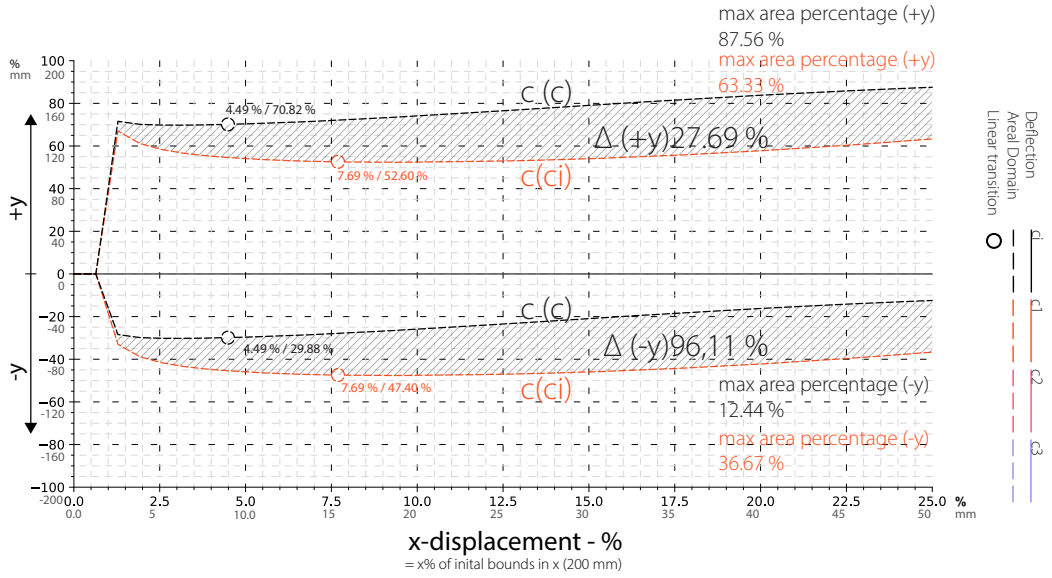

Fig.66 Areal Domain, c(ci)/c(c1)

Area coverage

The effects on the area coverage when comparing the two variants c(ci) and c(c1) are similar due to the previously analyzed parameters.

The effects on the area coverage when comparing the two variants c(ci) and c(c1) are similar due to the previously analyzed parameters (Figure 67). In the initial phase, as described earlier, the upper part of the geometry exhibits a pronounced bending behavior. However, the optimization and the resulting uniform distribution of forces have led to a significant reduction in the exposed area.(Figure 68 - 69)

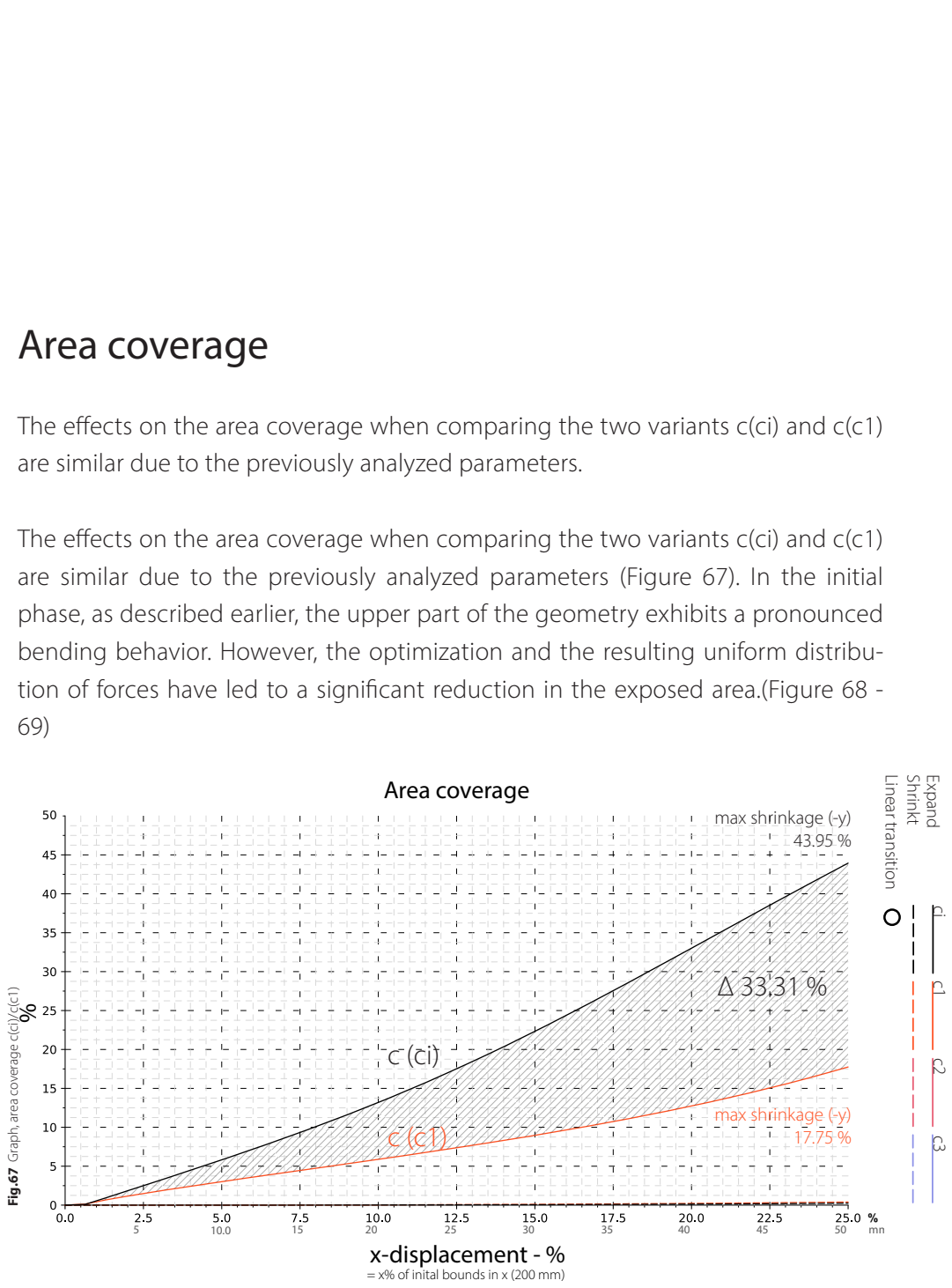

Fig.67 Graph, area coverage c(ci)/c(c1)

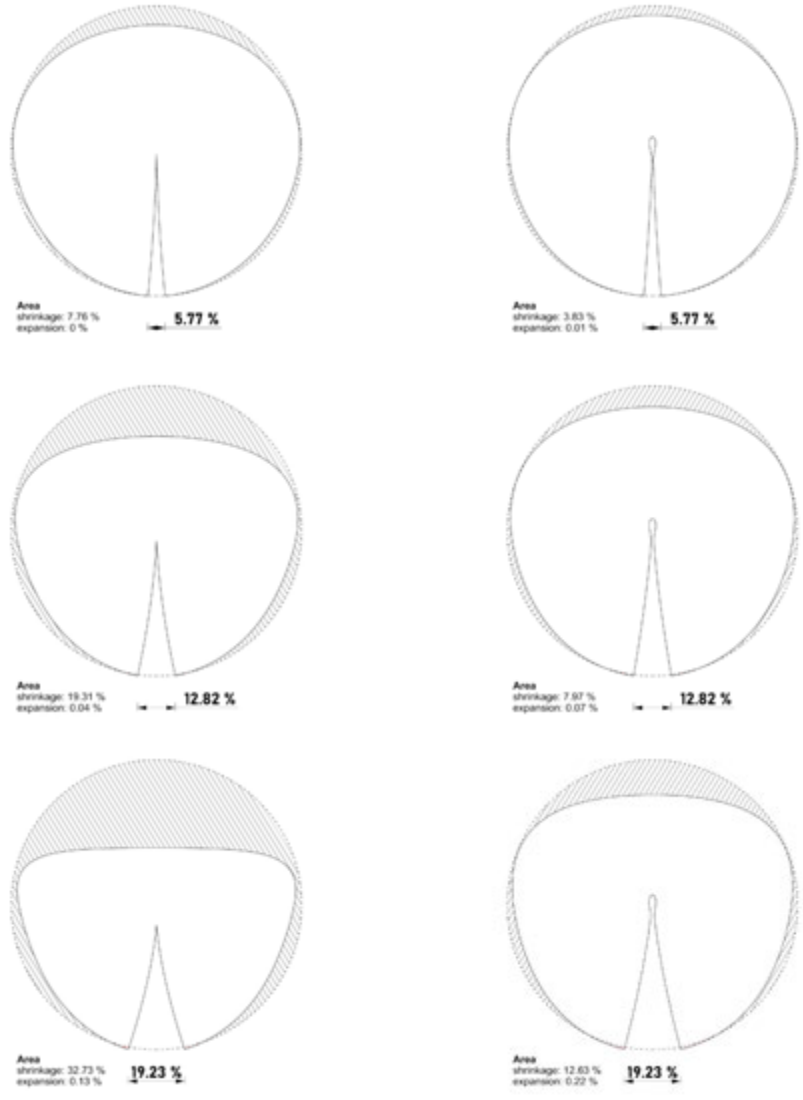

Fig.68 Area coverage, of c(ci) in relation to (x/x')

Fig.69 Area coverage, of c(c1) in relation to (x/x')

Stress/Boundary correlation

By examining different geometries, the effects on their elastic bending behavior and the resulting out of the plane buckling can be determined. It can be concluded that the overall geometrical shape, of the used planar sheet, strongly affects its geometric linearity. When transitioning from a four-sided polygon to a circular shape, the initial geometries exhibit strong non-linearity during the initialization phase, while optimized structures demonstrate smoother non-linear behavior, suggesting a more evenly distributed stresses. The transition to a linear deformation behavior occurs to set in later in relation to the x-displacement. This range extends from approx. 2.5 % (5 mm) to 6.5 % (13 mm).

For all geometries, we observed, that the frustration on the material manifests as a strong deformation in the upper part of the sheet.(Figure 70/72) This is particularly due to the characteristics of the incision and the point-like concentration of forces at its tip, which mainly leads to deformation in the top surface areas towards the point (M). As shown in Figures (71/73), it could be observed how the optimized variants (c1) distribute the stress in the material in a uniform manner, while variant (ci) has its latter described cloverleaf-like stress distribution. This leads to the assumption that variants (c1) have a higher resistance to material failure.

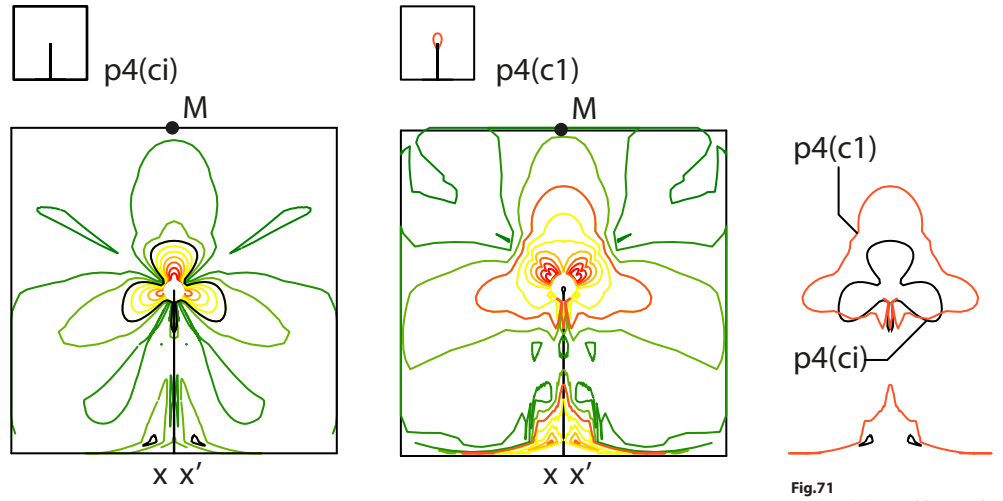

Fig.70 Stress bloom, p4(ci)/p4(c1)

Fig.71 p4(ci)/p4(c1) Stress bloom with identical displacment of (x,x')

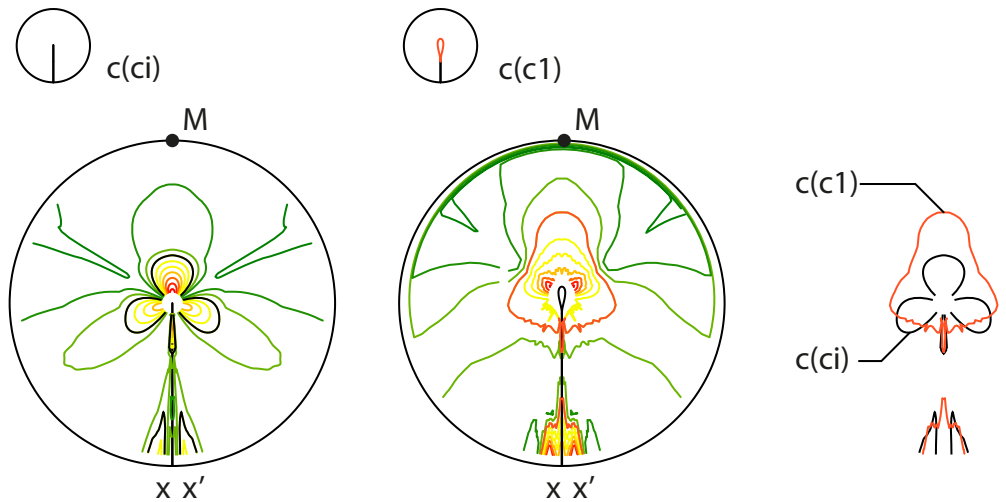

Fig.72 Stress bloom, c(ci)/c(c1)

Fig.73 c(ci)/cc1) Stress bloom with identical displacment of (x,x')

With the evaluated parameters it could be seen that mostly every optimized shape has experienced a loss in its spatial expression between 30 - 40%. While the analysis of the areal domain showed a major shift in the distribution of the areal parts from the (+y) parameter space towards (-y).

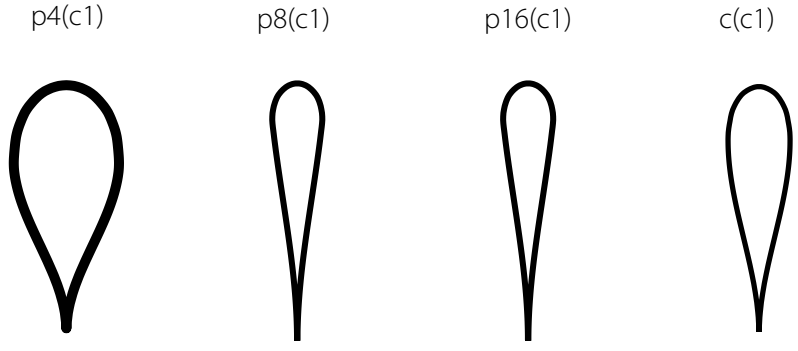

Fig.74 Cutouts, variants (c1)

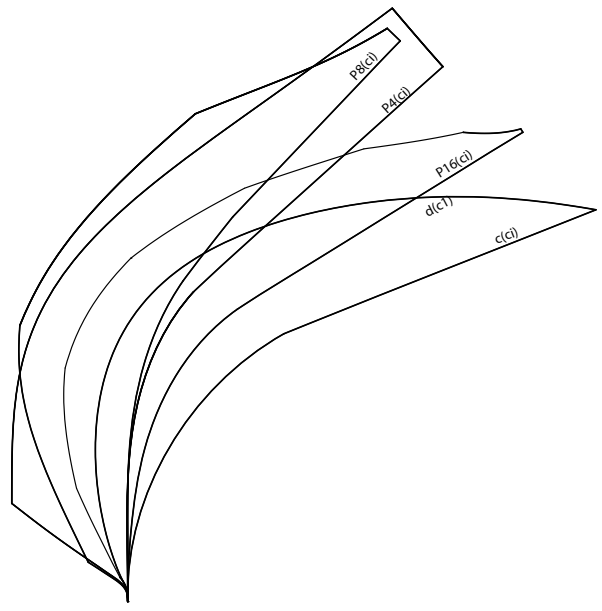

Fig.75 Initial Geometries, variant (ci)

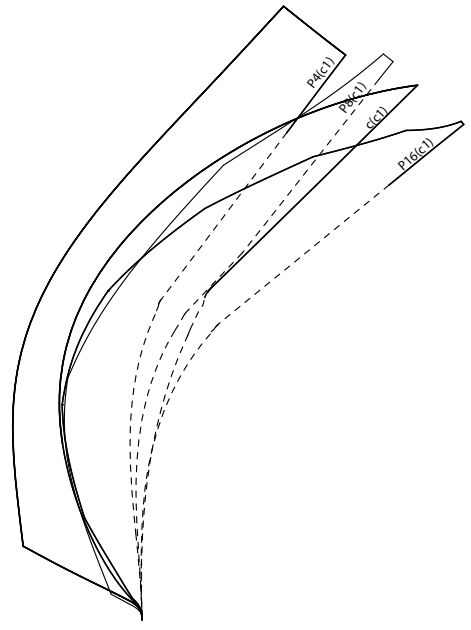

Fig.76 Optimized geometries, variant (c1)

Diamond

d(ci)/dc1)

By using a diamond shape, which is a rotated version of the four-sided polygon and the incision is oriented from one of the corners towards the geometric center of the sheet.

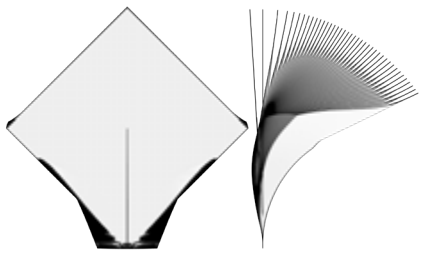

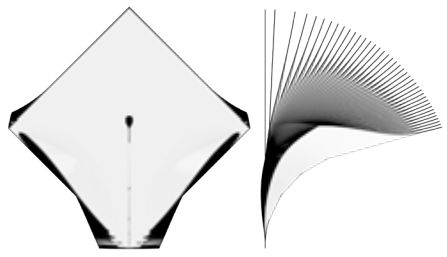

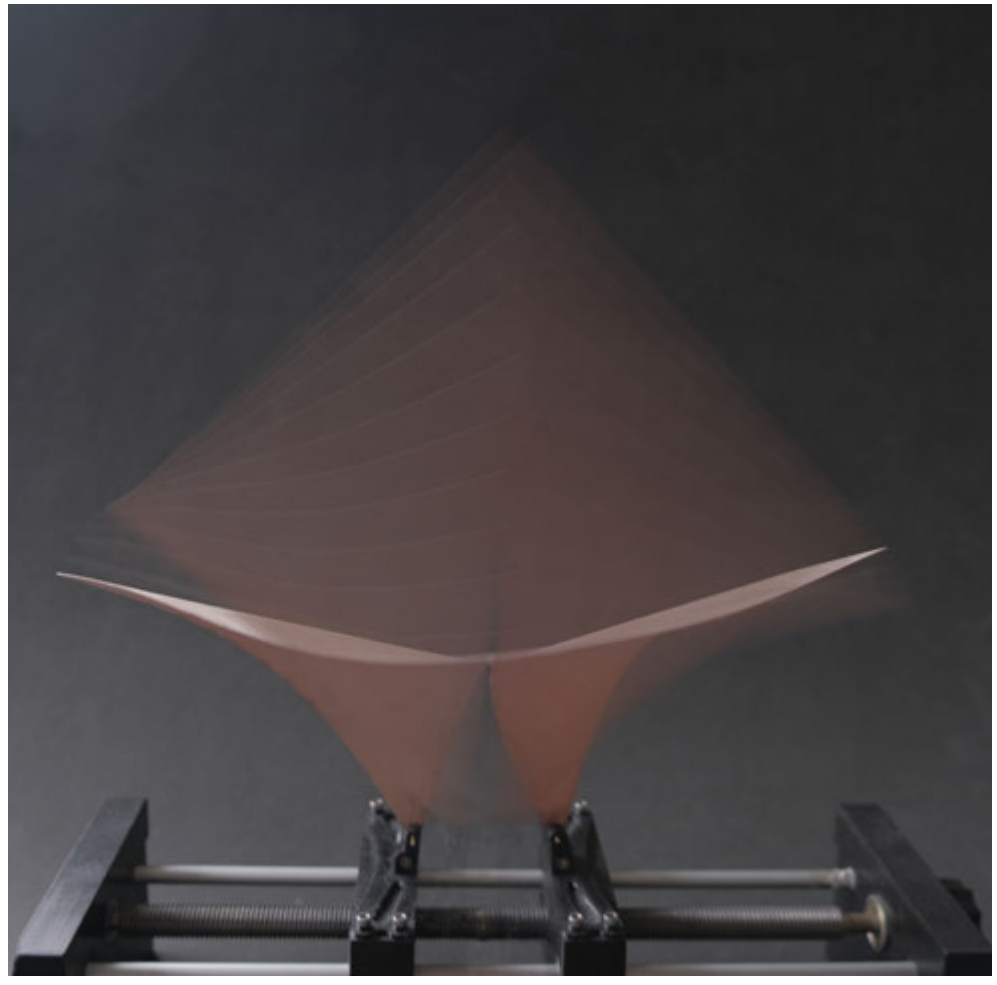

Inclination d(ci)/d(c1)

Its small surface area towards the attachment points where the geometry is constrained. The diamond shaped plate, basically a rotated square, is subject to higher frustration in the upper areas of the plate, leading to a higher rate of inclination of the point (M). While the circular shape is able to evenly distribute the applied stress in the material to its boundary, resulting in less frustration.

The inclination of the point (M), for d(ci) seems to reach almost an angle of 90°, in a non-linear matter, while the optimized geometry (c1) is at its maximum inclination of 77.1° with an average reduction of 26.46% and a transition to linear behavior. (Figure 77)

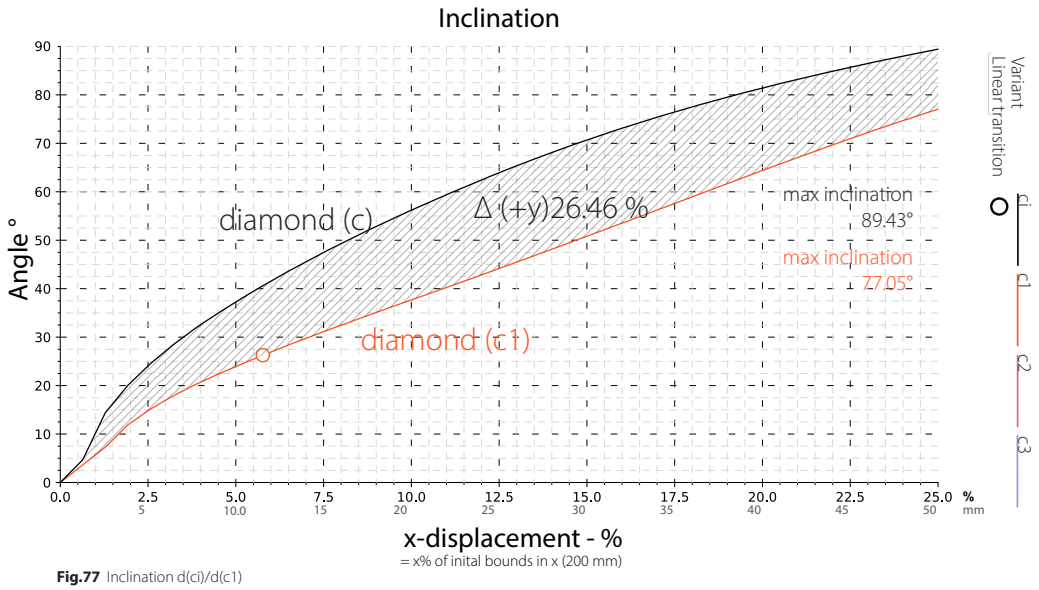

Fig.77 Inclination d(ci)/d(c1)

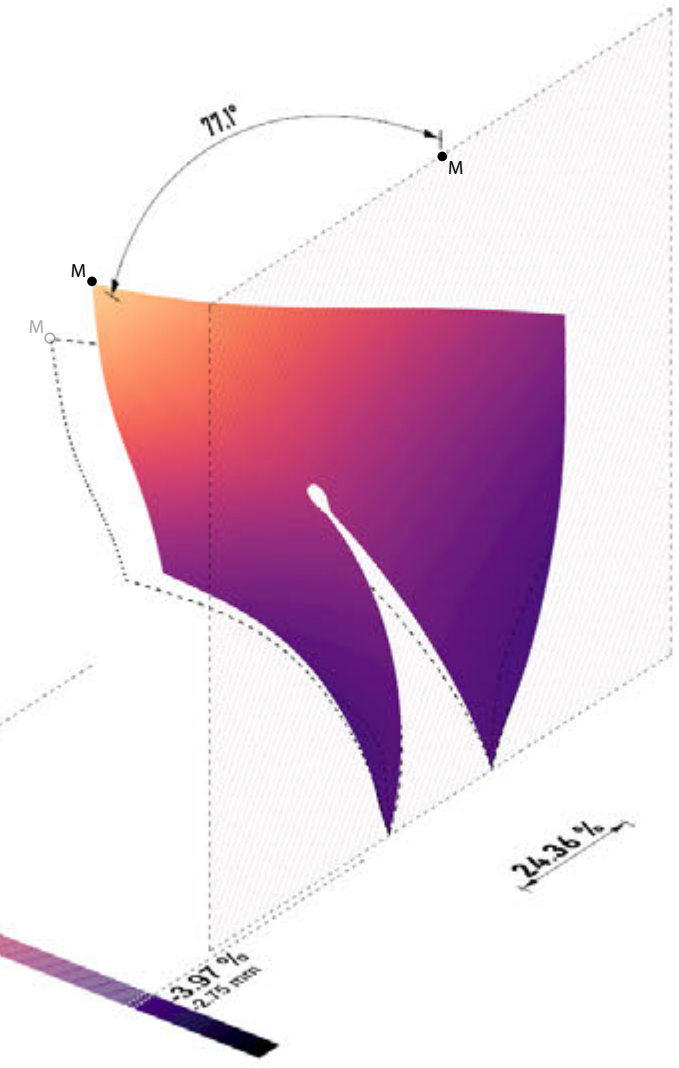

Fig.78 Perspective, inclination point (M), d(ci)/d(c1)

Deflection d(ci)/d(c1)

As with the inclination angle (Figure 79), a non-linear behavior can be observed when analyzing the deflection into the +y parameter space. In contrast, for the variant (c1), a slight deflection into the -y range can be observed. This value can be seen in the graphs with a value of 8.95 mm (4.47%) suggesting that the cutout in the middle applies a more even distribution of stresses in the material, leading to a more balanced strain over the geometries surfaces.

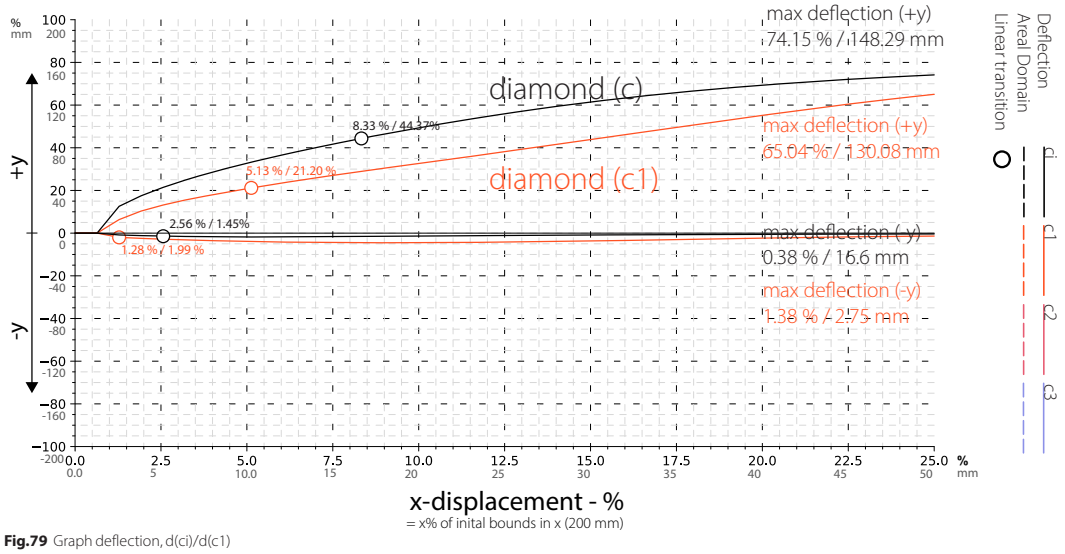

Fig.79 Graph deflection, d(ci)/d(c1)

Areal Domain d(ci)/d(c1)

For the distribution of the area parts (Figure 80) on the ±y, as for most of the investigated geometries, the distribution of the areal parts can be described as linear. The diamond shape seems to have an offset, in the areal distribution, between d(ci) and d(c1) similar to the latter investigated shapes, after its transition it converges with an increasing x-displacement to a value of the initial variant d(ci).

This also can be seen by looking at the average delta of both variants (ci) and (c1) with about 16.34% for the parts in (+y).

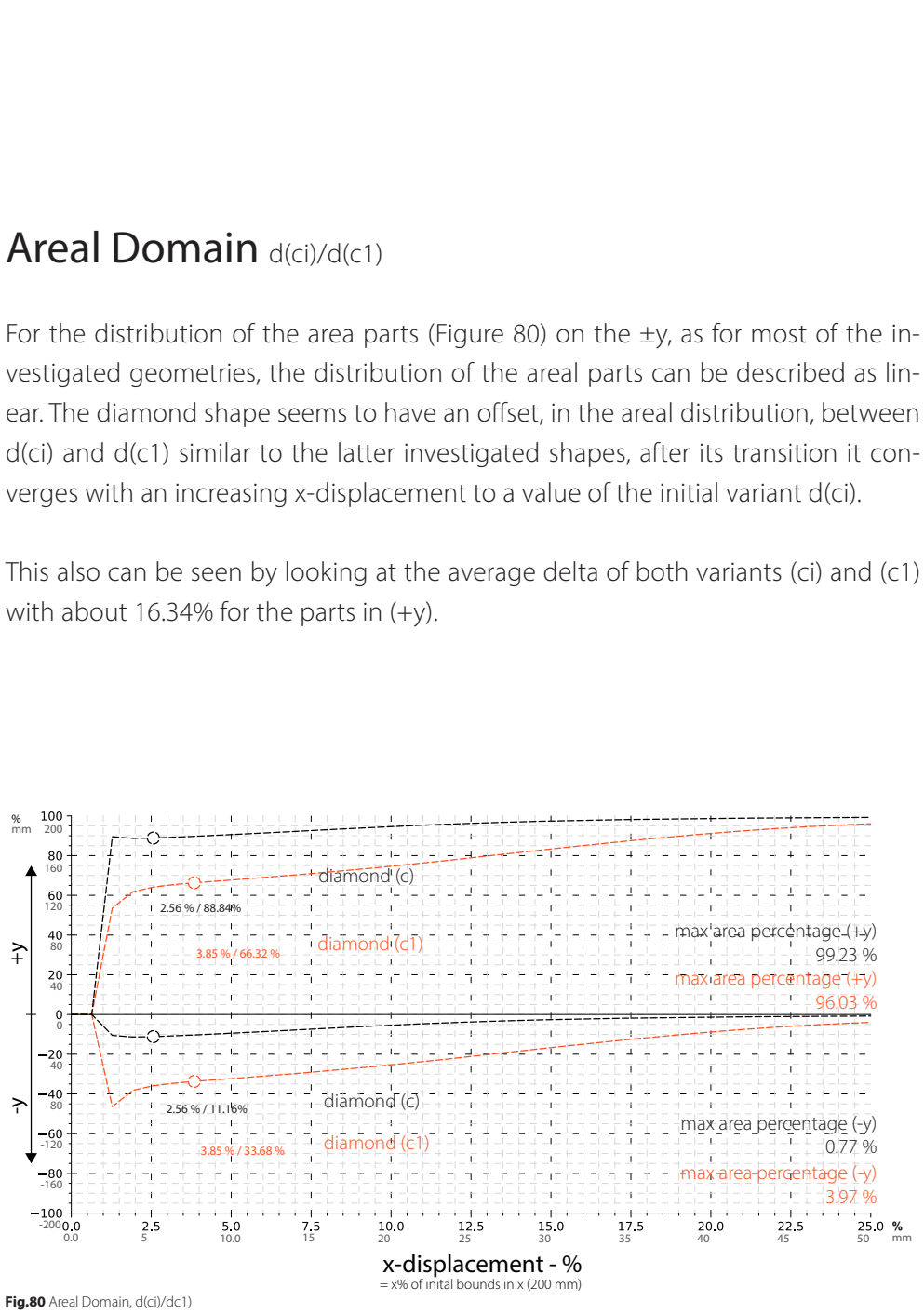

Fig.80 Areal Domain, d(ci)/dc1)

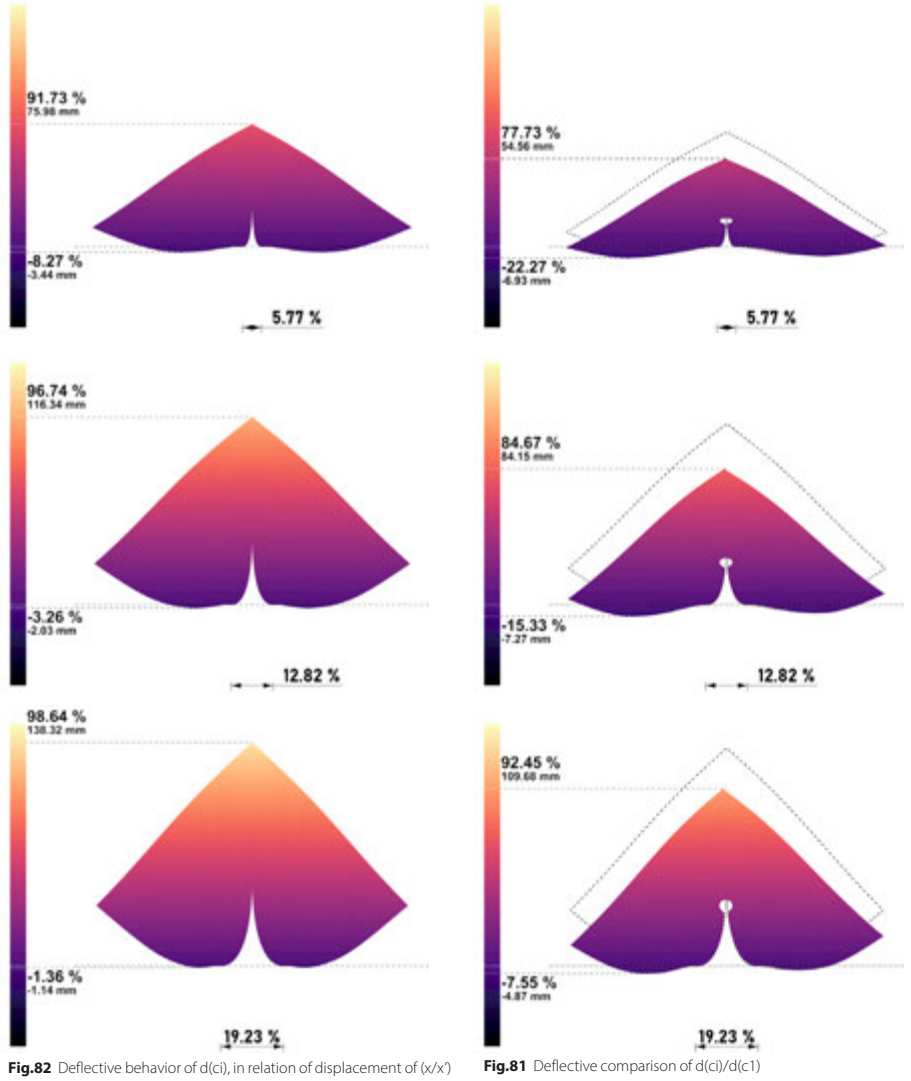

Fig.82 Deflective behavior of d(ci), in relation of displacement of (x/x')

Fig.81 Deflective comparison of d(ci)/d(c1)

Area coverage d(ci)/d(c1)

As previously stated, the diamond shows a strong spatial expansion, which becomes apparent when looking at the area coverage. While mainly the part in the area of the points x to be moved naturally exceeds the original limits, the void in the area coverage compared to its flat state shows a remarkable change, suggesting a high deflective behavior. This follows the empirical values that have been shown in previous simulations and experiments.

The optimized shape shows a significant reduction in its vertically, projected surface coverage, compared to its initial shape, d(ci). The absolute numbers of the area coverages shrinkage reaches a value of 39.81% in reduction between the variants d(c1) and d(c1) (Figure 85).

Another striking feature of the variant d(c1) is its non-linear behavior from the middle towards the end. While the original variant behaves as expected, the change in area coverage appears to be non-linear and more closely approximates the value of d(ci).

In comparison of the variants (ci)/(c1) between the diamond and circular shapes, the optimized variant d(c1) reaches almost the values of the initial variant of the circular shape c(ci).

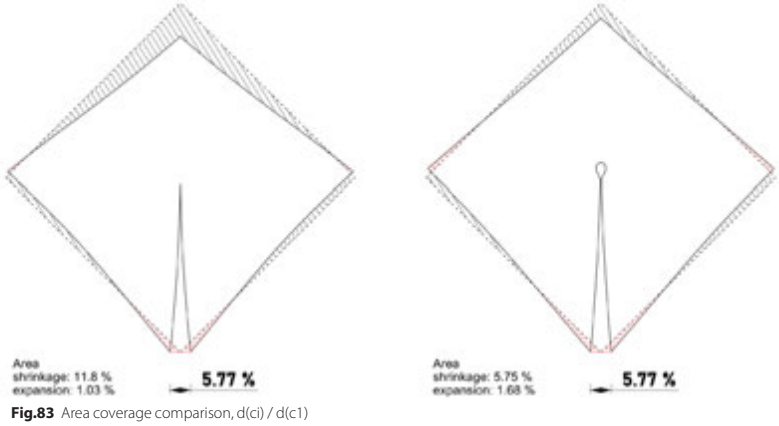

Fig.83 Area coverage comparison, d(ci) / d(c1)

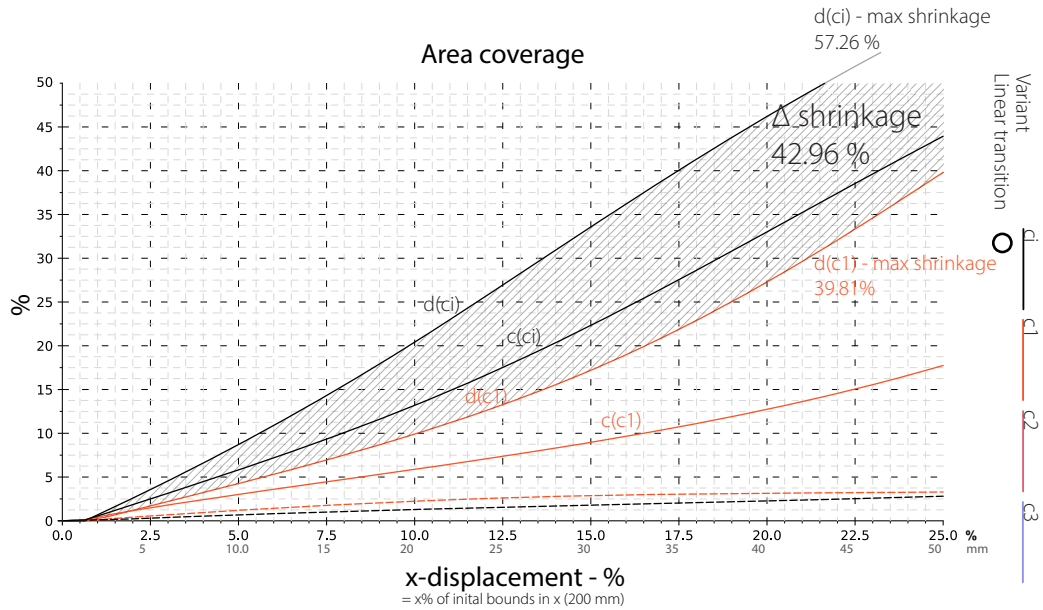

Fig.85 Graph, area coverage d(ci)/d(c1) and c(ci)/c(c1)

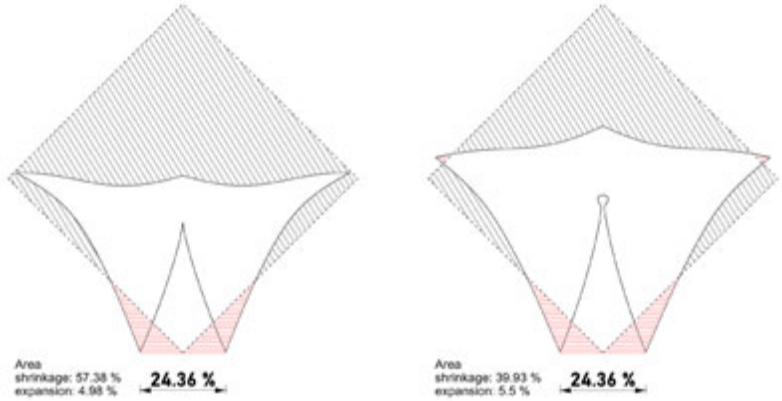

Fig.84 Area coverage comparison, d(ci) / d(c1)

Application

Displacement mechanics

The previous investigation of the bending behavior of the elements provided important insights about its bending behavior and in relation to its angle of opening.

To ensure a controlled deformation, it must also be ensured that the points of attachment can rotate freely at the same time it must be constrained to its axis of displacement, meaning the points of attachment are not able move perpendicular to its axis of movement.

The existing mechanism for moving the points (x,x') in the opposite direction is mainly driven by a threaded rod with a counter-rotating thread in the moving axis. Since the drive is located next to the sheet, in the axis of displacement, it expands the overall width of the sheet. In a scenario where the sheets are placed over an area, which can be a challenge for a large area application

Therefore the displacement is being translated into a circular system in which the driver for the mechanics is placed in the back of the mechanism.

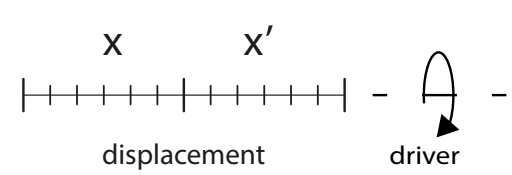

Fig.86 existing mechanism

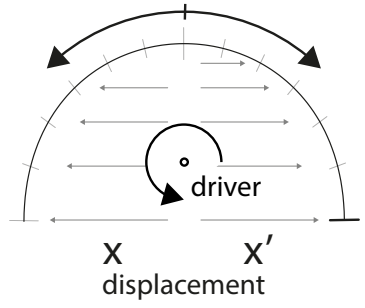

Fig.87 Translated mechanism

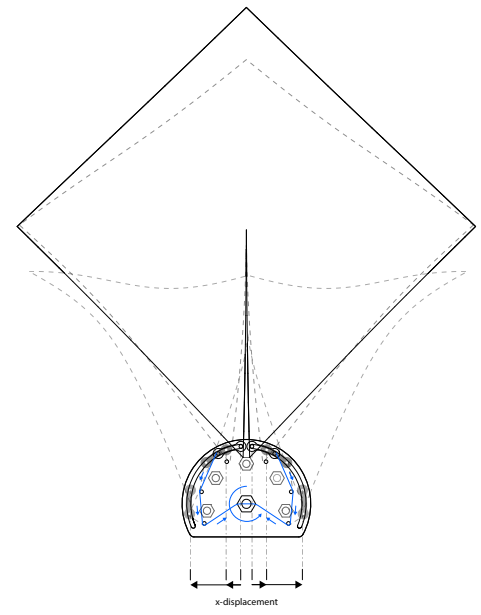

Fig.88 Front view mechanism

The points of attachment are in a guided rail on which a slider connected to the element is being pulled by a cable mechanism. It provides a continuous, equal distribution. Since the object is mounted in between two plates the objects freedom of movement is restricted to the direction of displacement.

Since the Plate in its stressed state acts like a spring, the energy for closing of the element is stored in the deflected plate,this system enables a closing mechanism which is operated solely by releasing the cable, without a need for great force.

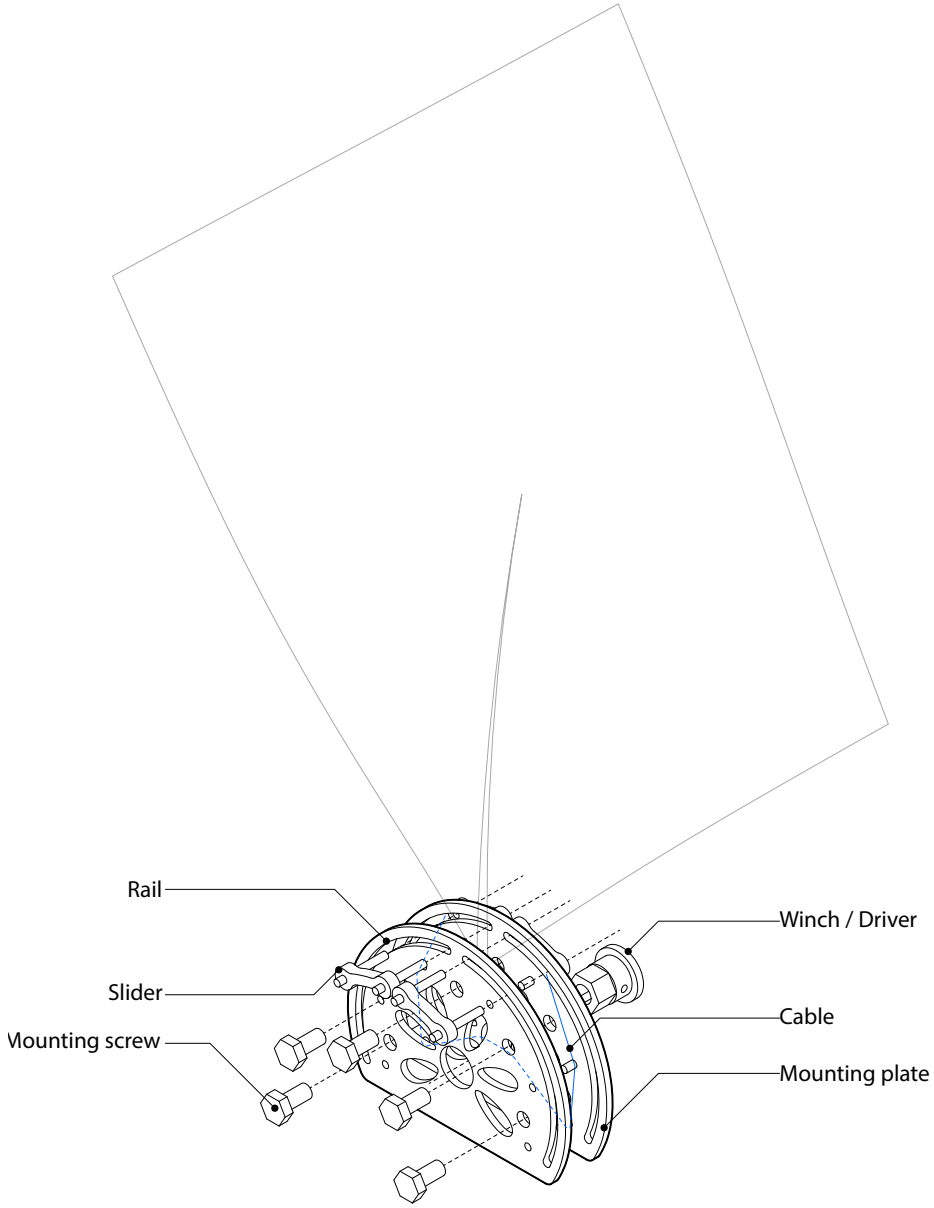

Fig.89 Exploded view mechanism

Adaptive System

The deformation of the geometry is expressed in its dynamic change and the kinematic behavior during its deformation. Both can have a wide range of applications in architecture, where different effects on its spatial and aesthetic properties can be achieved depending on the field of application.

Therefore, an environmentally aware system is designed to act as an adaptive solar shading system by populating building facades with a diamond shaped geometry. The system blocks, depending on the intensity of the sun, where the geometry is in a relaxed state with its maximum area coverage, while at the same time leaving areas that are not exposed to increased solar radiation in an open state, providing a view to the outside.

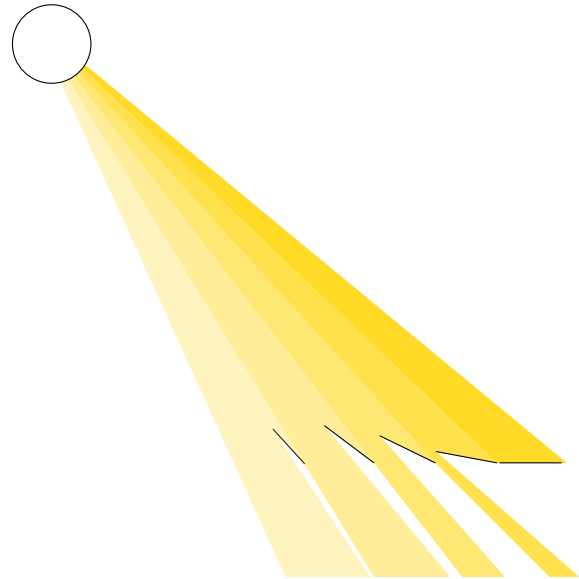

Facade

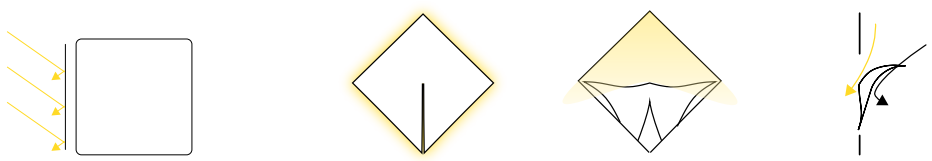

To test the performance of the geometry, an office prototype is used to evaluate the solar shading performance. The facade system is placed in front of the window openings. The system responds to the intensity of the sun and maximizes its area coverage when inside the hot spot area. The radiation analysis shows a significant shading effect on the areas with the highest radiation intensity, suggesting a cooling effect on the office space.

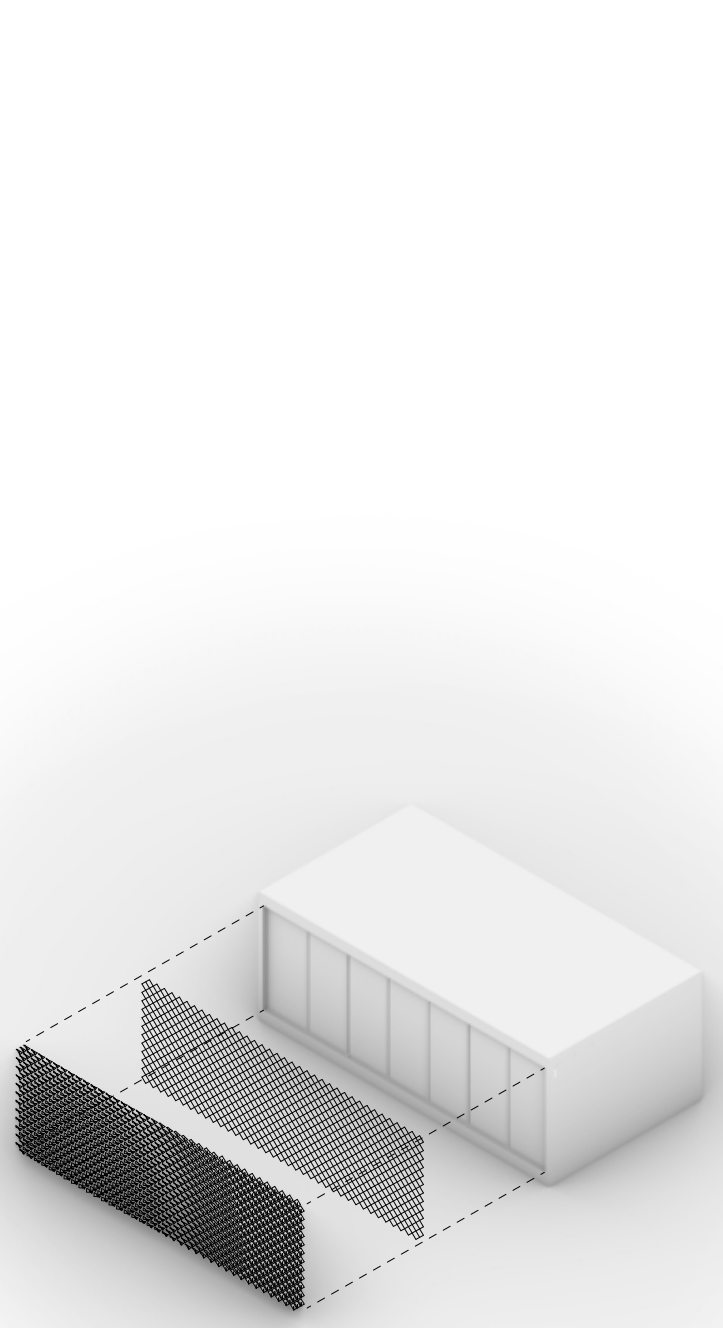

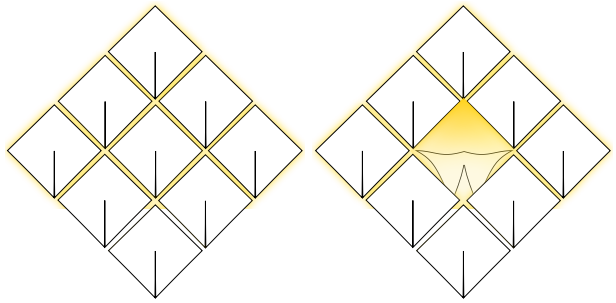

Fig.90 Diagrid configuration

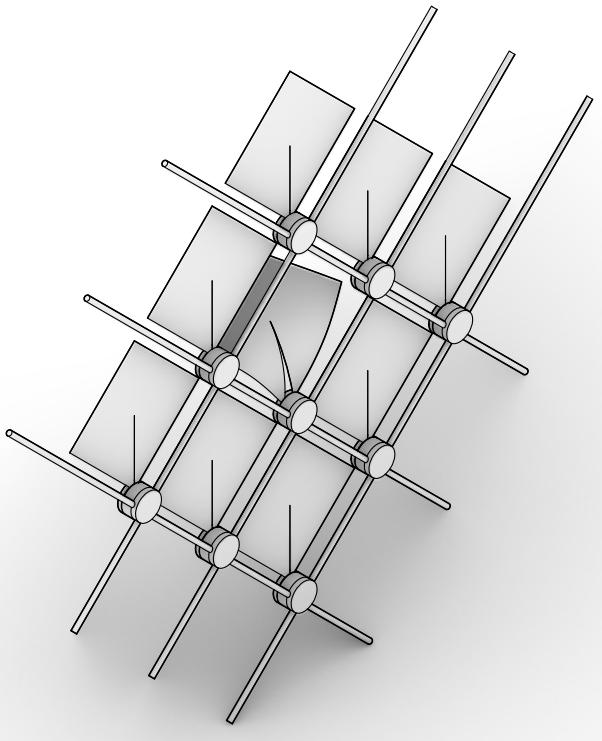

Fig.91 Diagrid substructure

The diamond shaped sheets has been selected to demonstrate the application possibilities in a real-world scenario (Figure 91). For the application, a diagrid configuration applied in front of a windowed is created. The diagrid substructure is made out of a rod system to attach the individual elements (Figure 92).

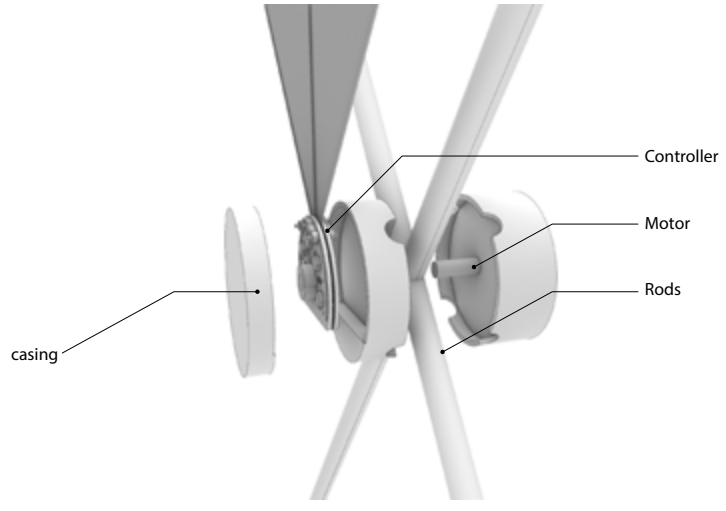

Fig.92 Mounting system of the sheet elements

Radiation analysis___frontview

Morning

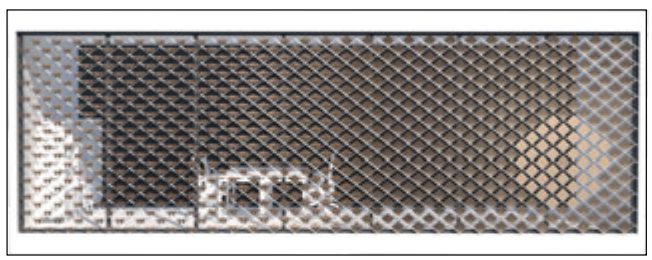

Noon

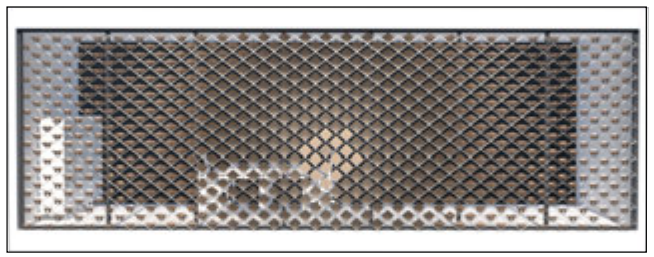

Evening

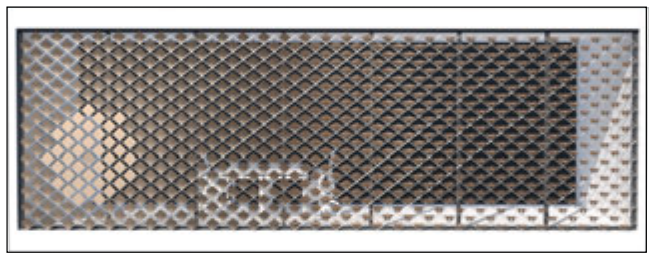

Radiation analysis___floorplan

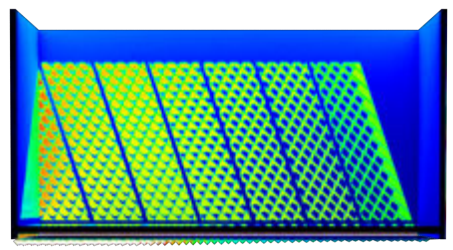

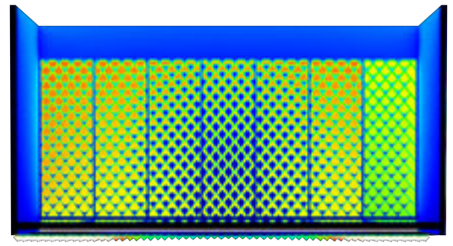

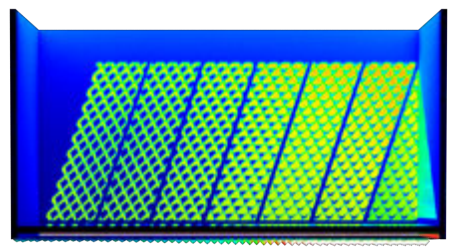

Pattern

The analysis shows not only changes in the physical nature of the building, but also in the design aspect. The facade becomes an extended design surface that creates a direct connection to nature. It acts as an intermediary between the built and natural spaces. The pattern, such as opening and closing in response to sunlight, can also be deliberately controlled by the user. Either detached from the environmental conditions or in combination to achieve various visual effects on the buildings facade.

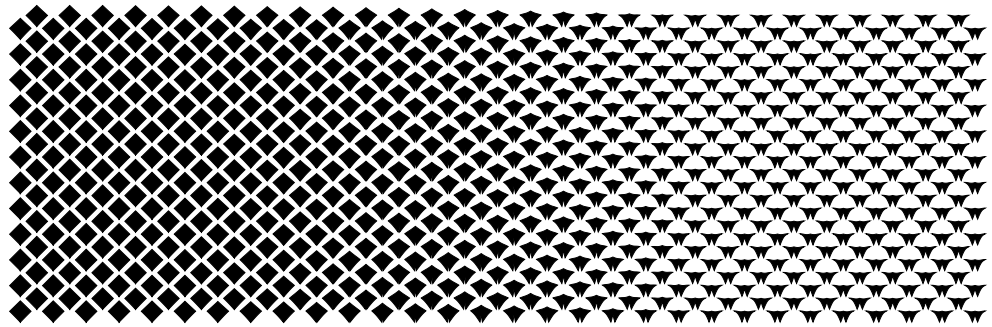

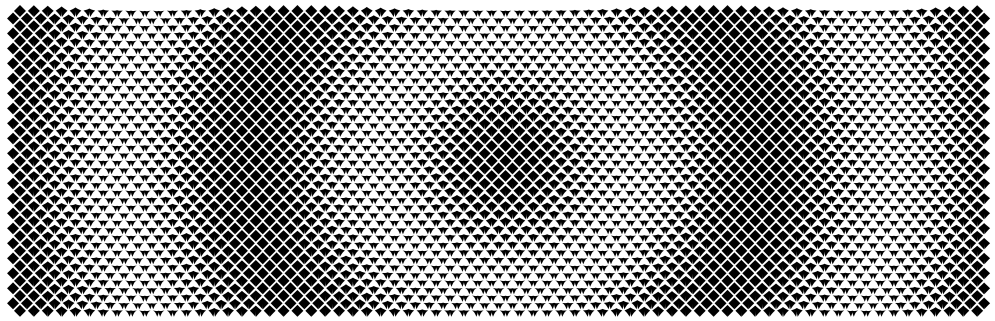

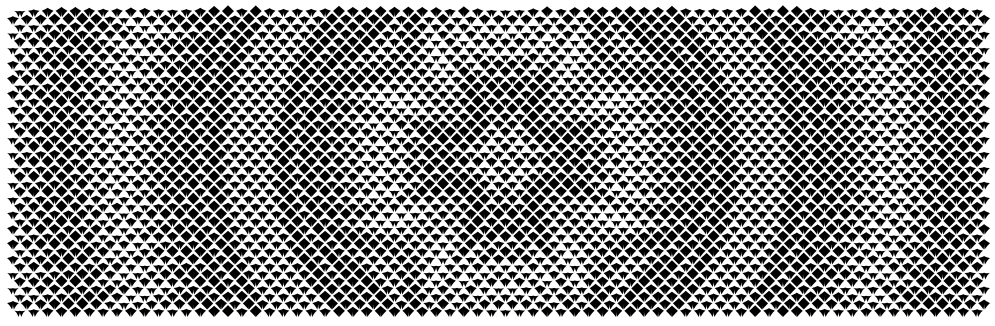

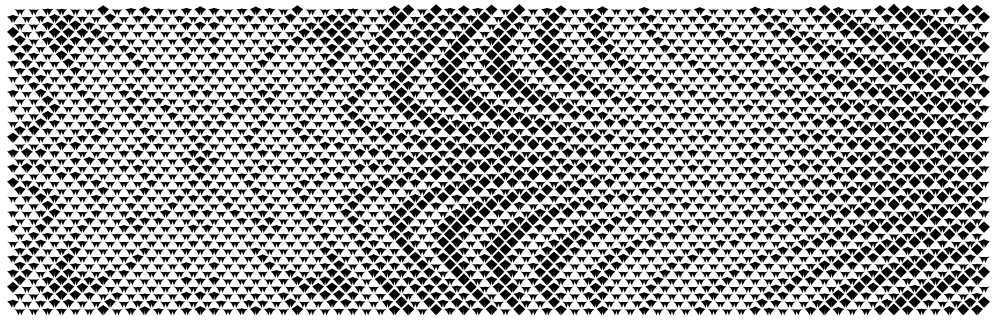

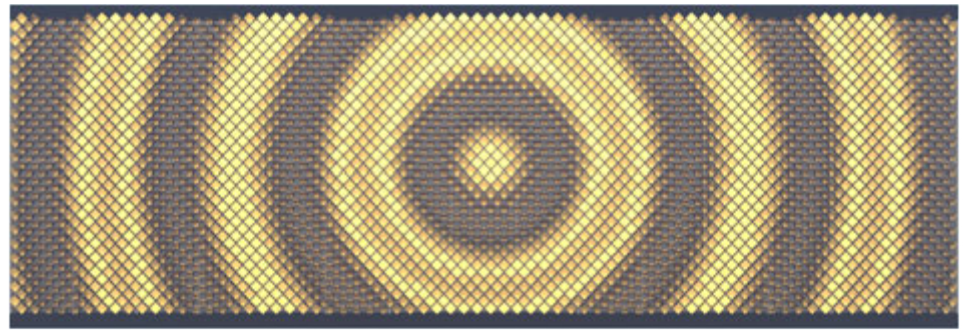

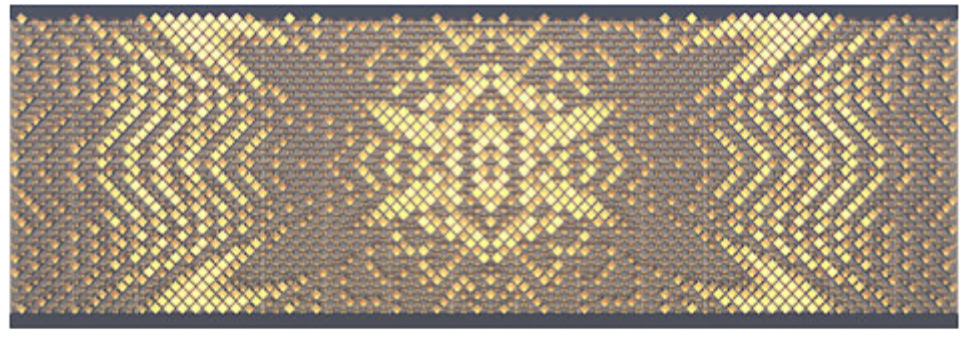

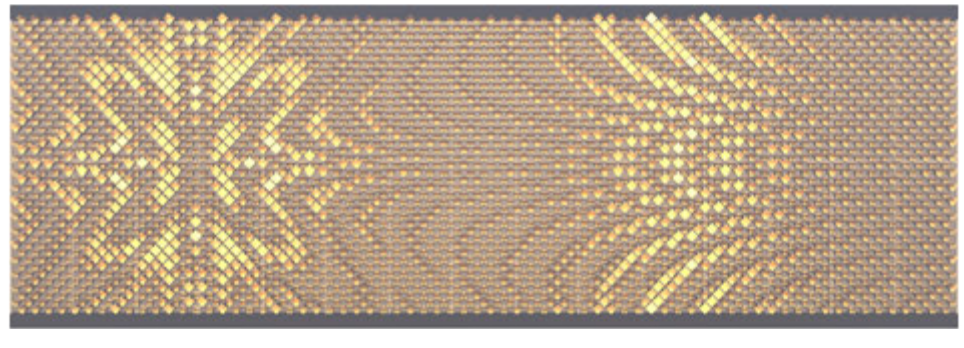

Loop

While the latter described project is an additive system that is essential to the buildings functionality. This concept demonstrates how a horizontal use case application of the adaptive geometries are part of the structures functionality.

By shingling the elements onto a canopy like free form, it demonstrates how it is possible to provide an aesthetically pleasing structure combined with a protective layer in which the adaptive elements are able to respond to different environmental conditions.

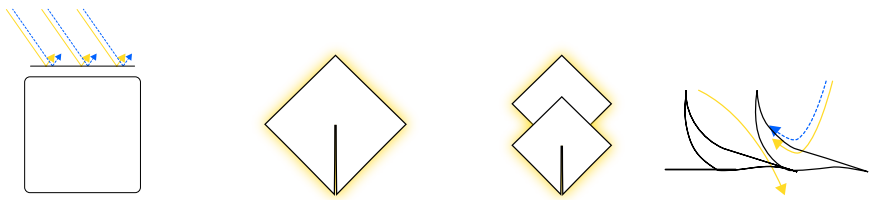

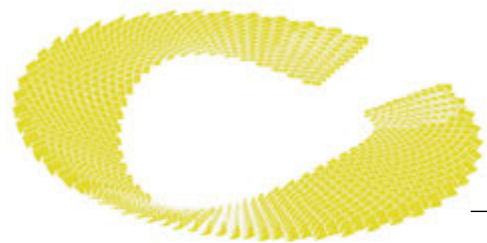

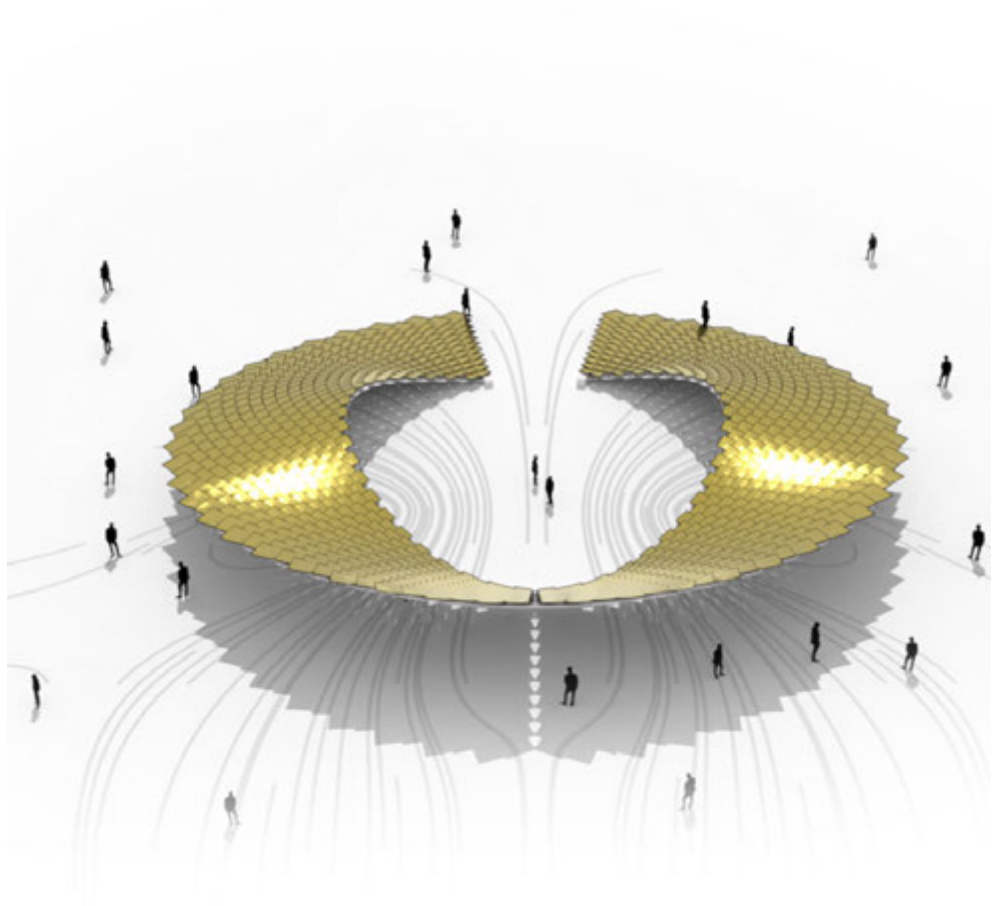

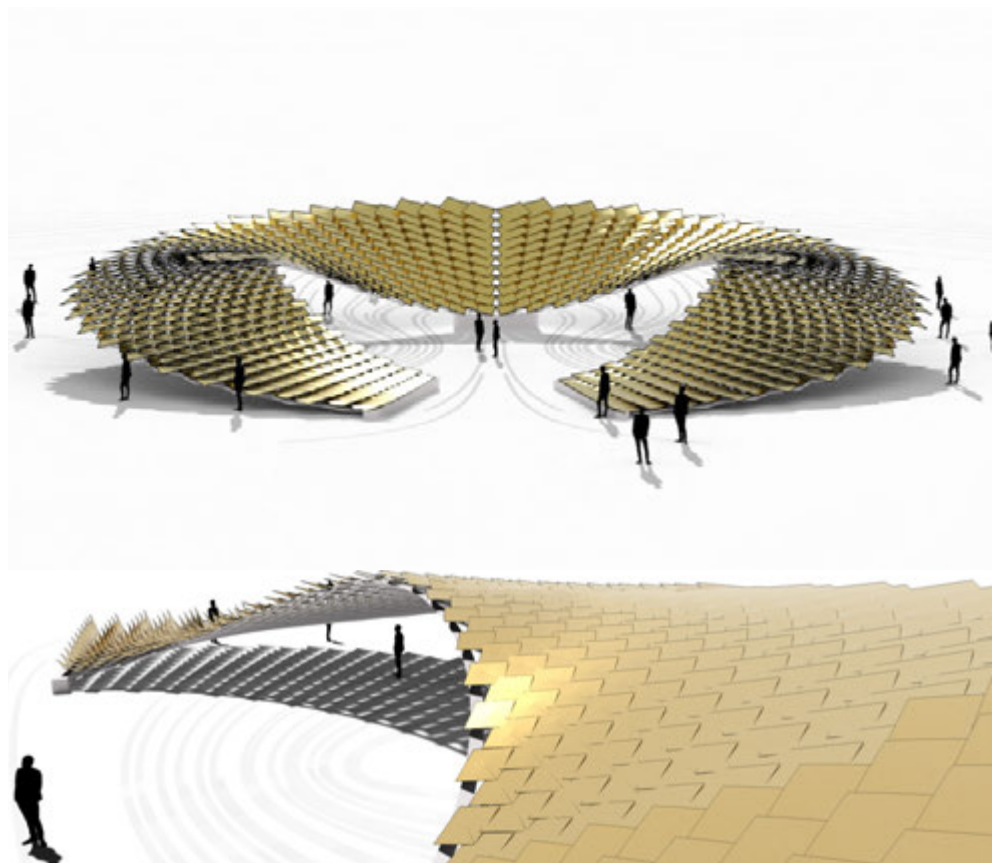

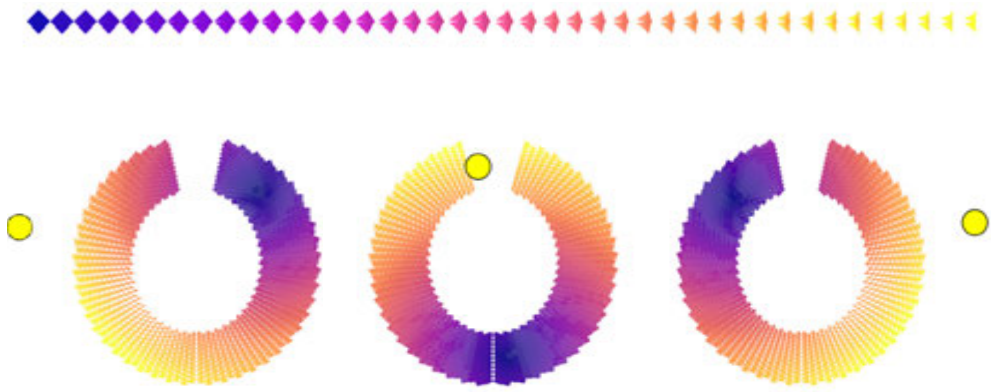

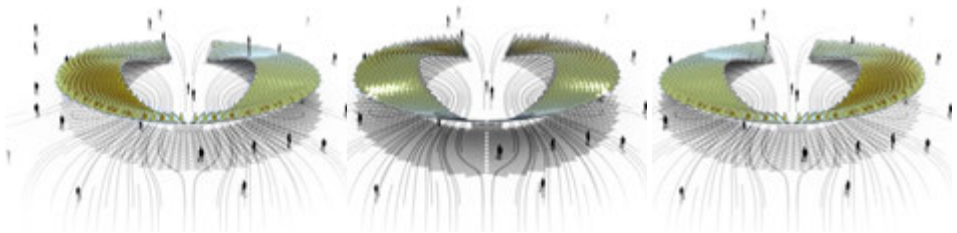

Spiral

This concept is based on the idea of showing the adaptability of the deflected geometries on various structures. This spiral-like installation should demonstrate its interactive features. Since the lattter described projects are focused on the adaptibiliy to environmentel conditions, with this approach the user is in the center of interest.

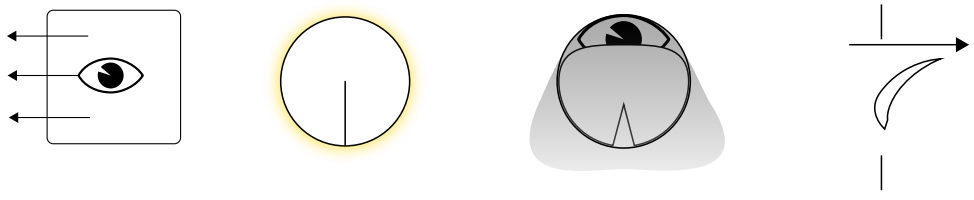

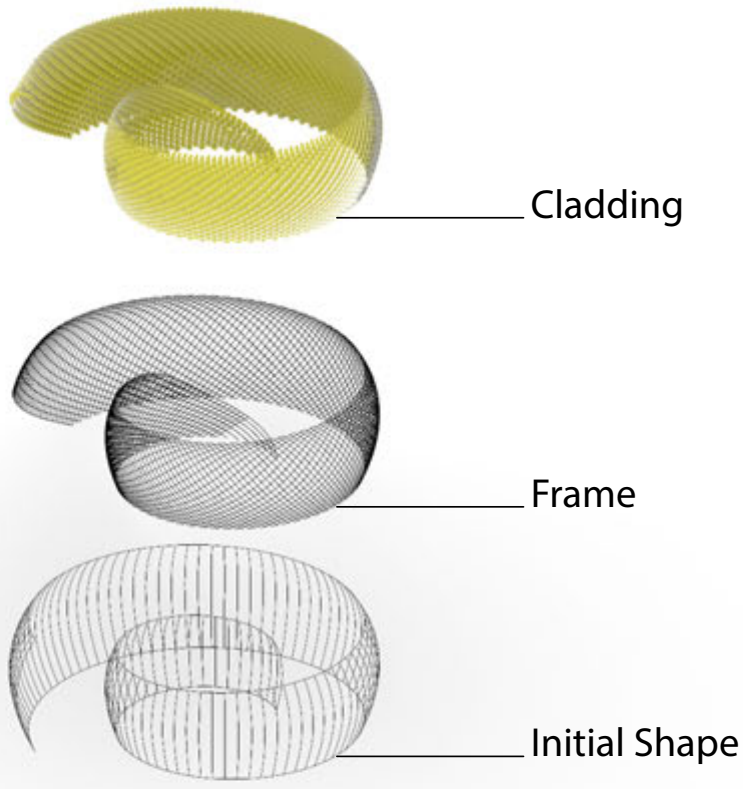

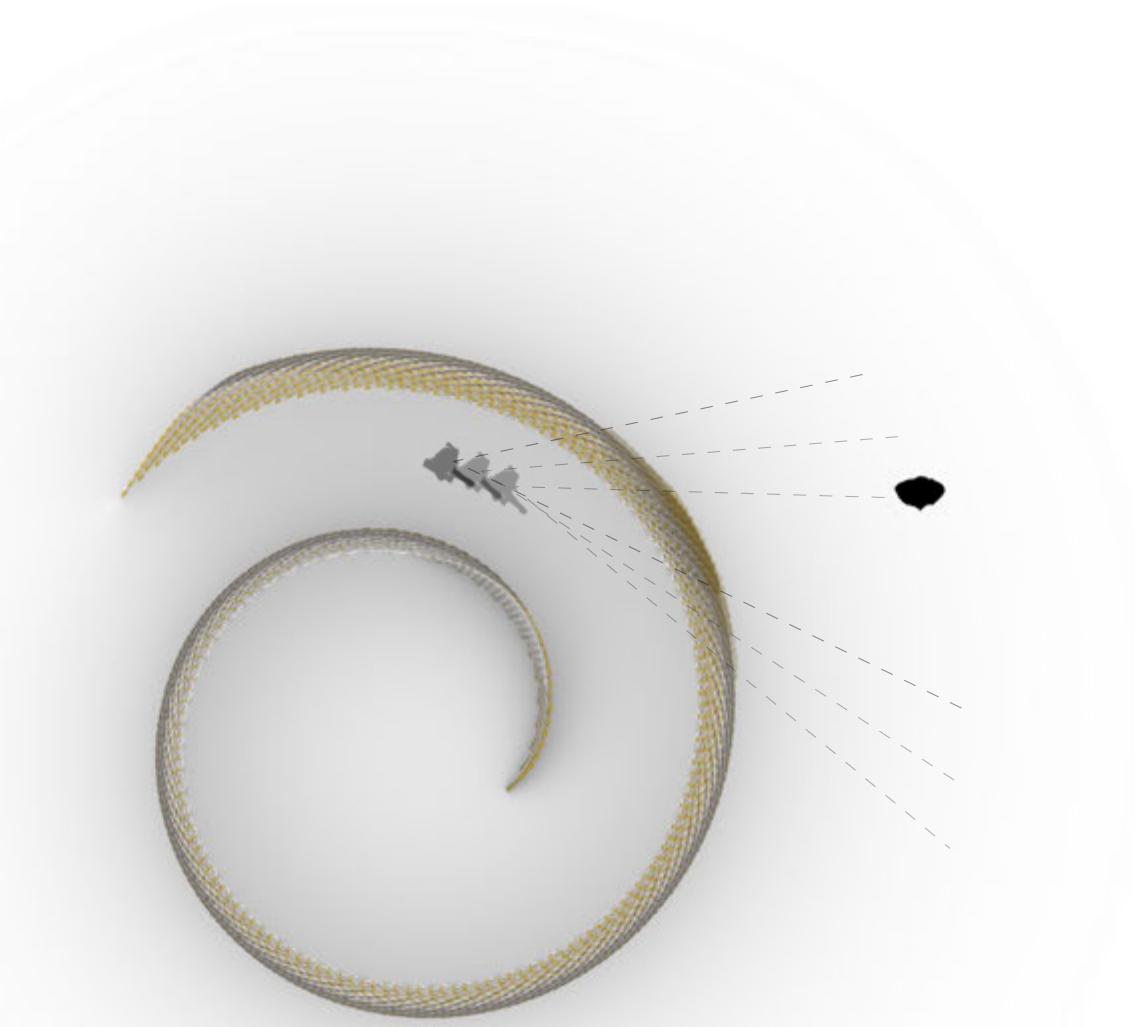

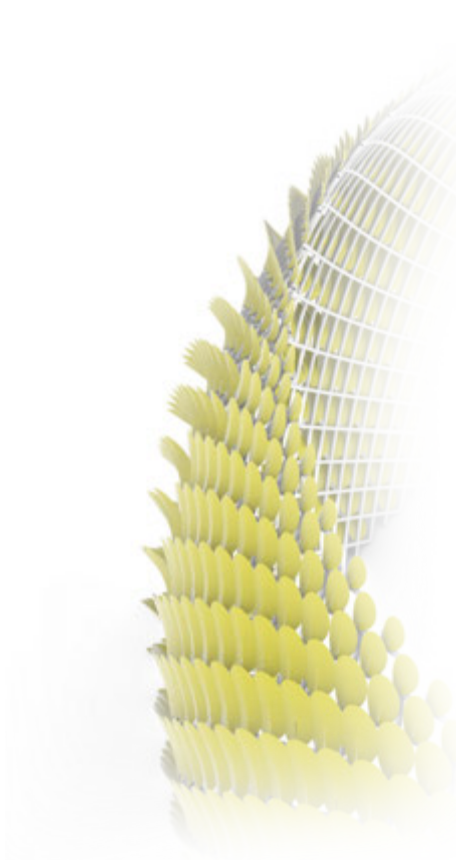

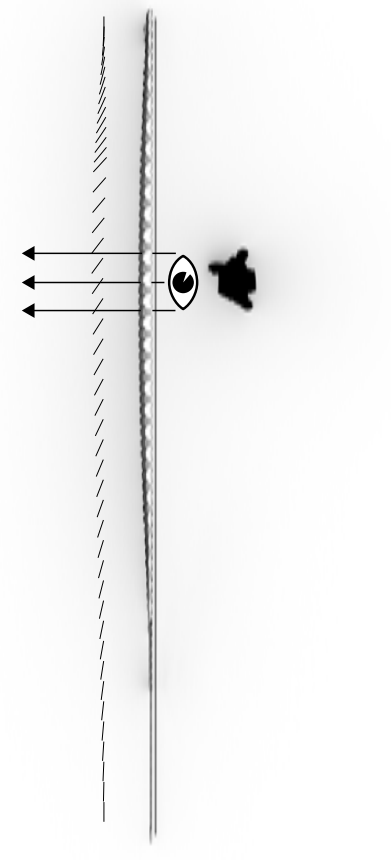

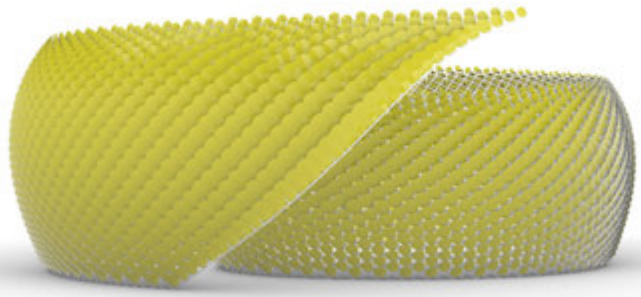

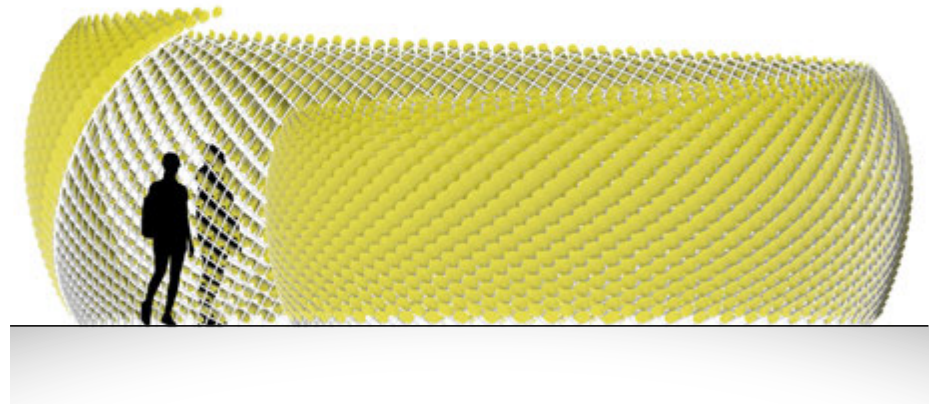

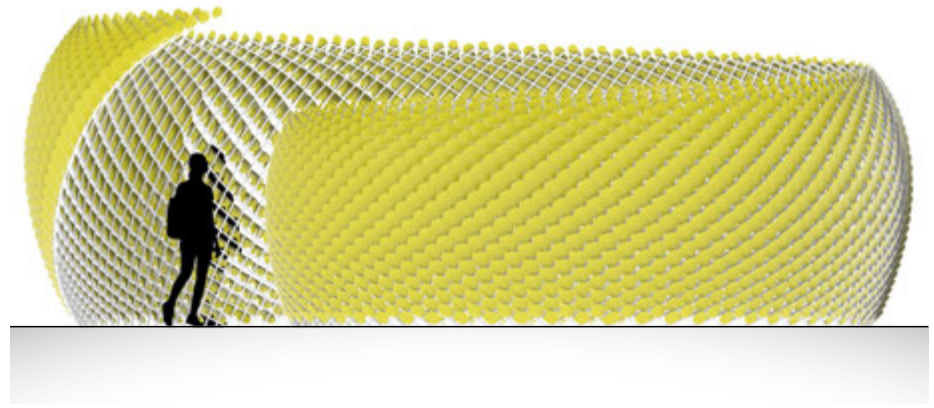

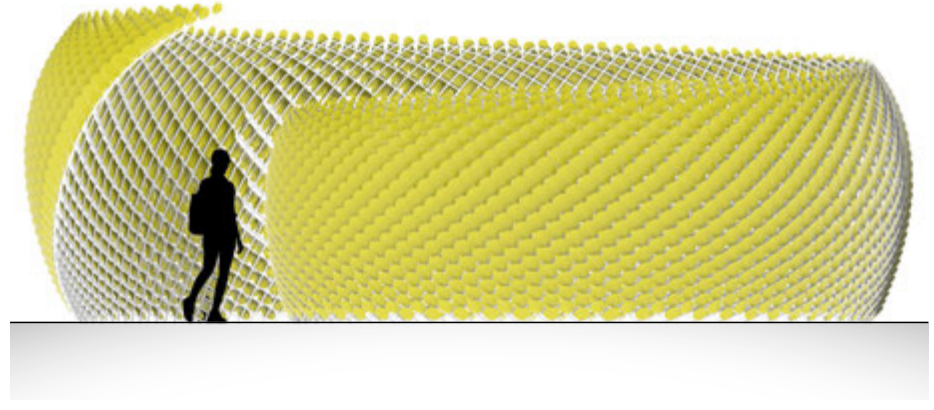

Showcases

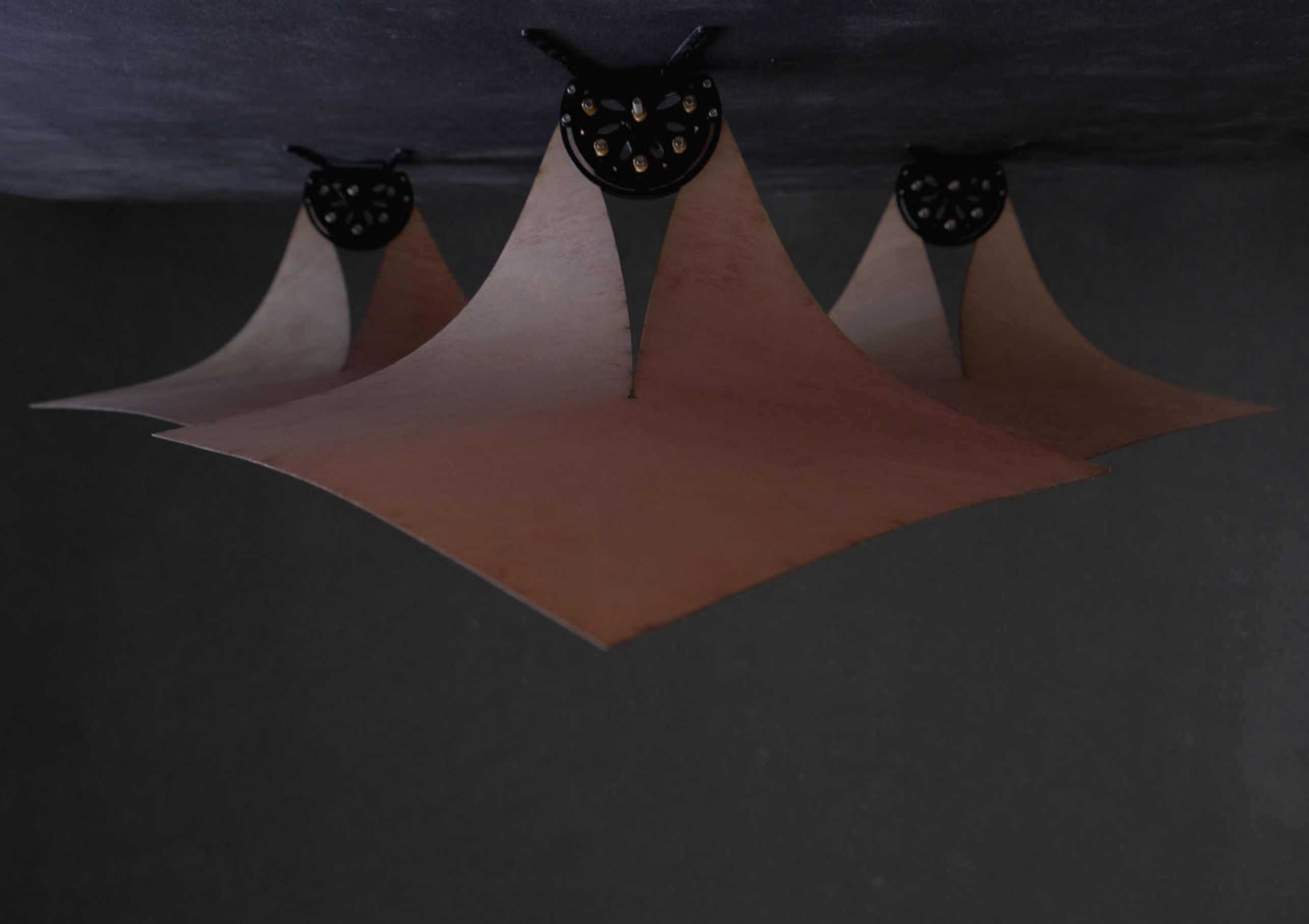

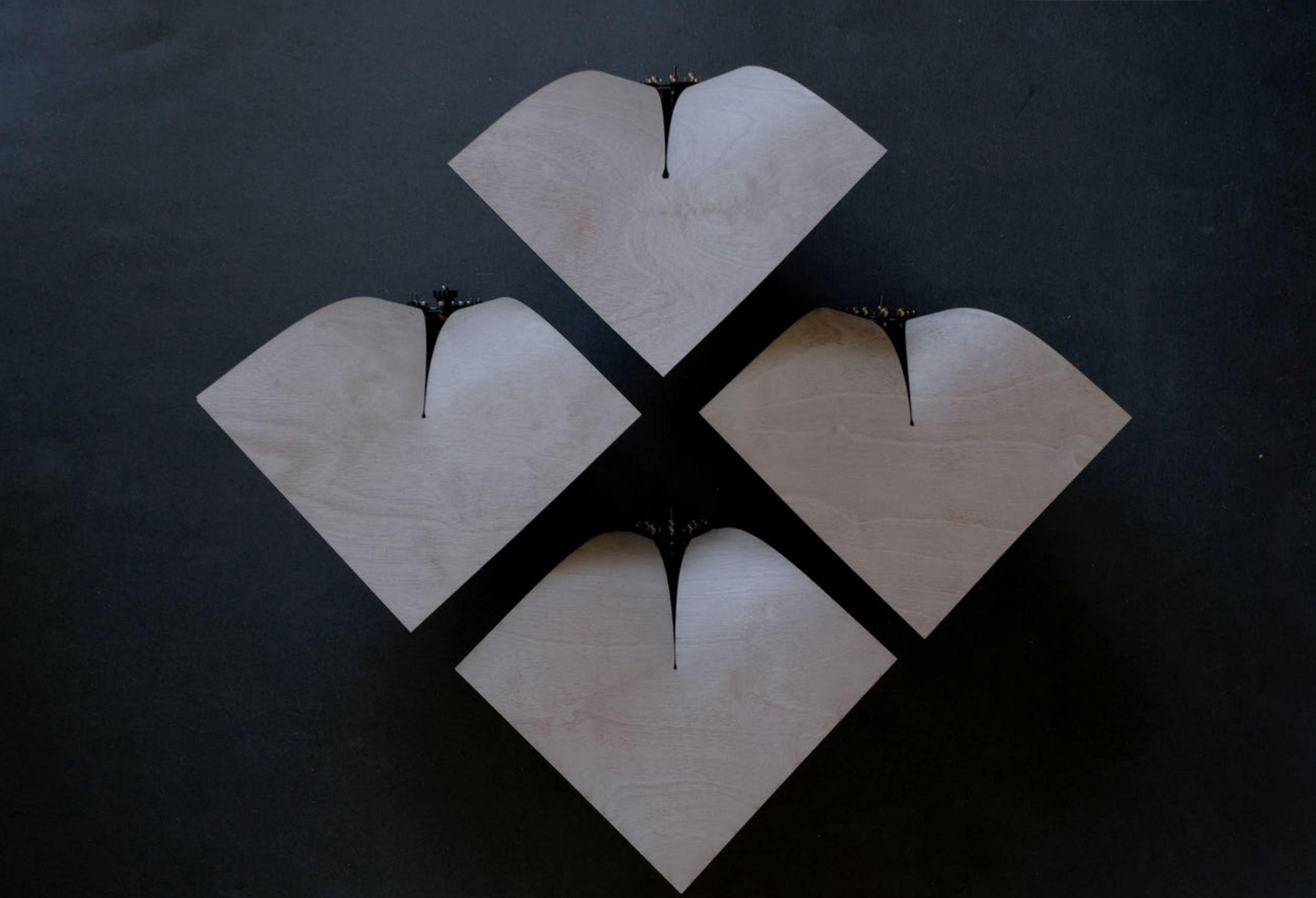

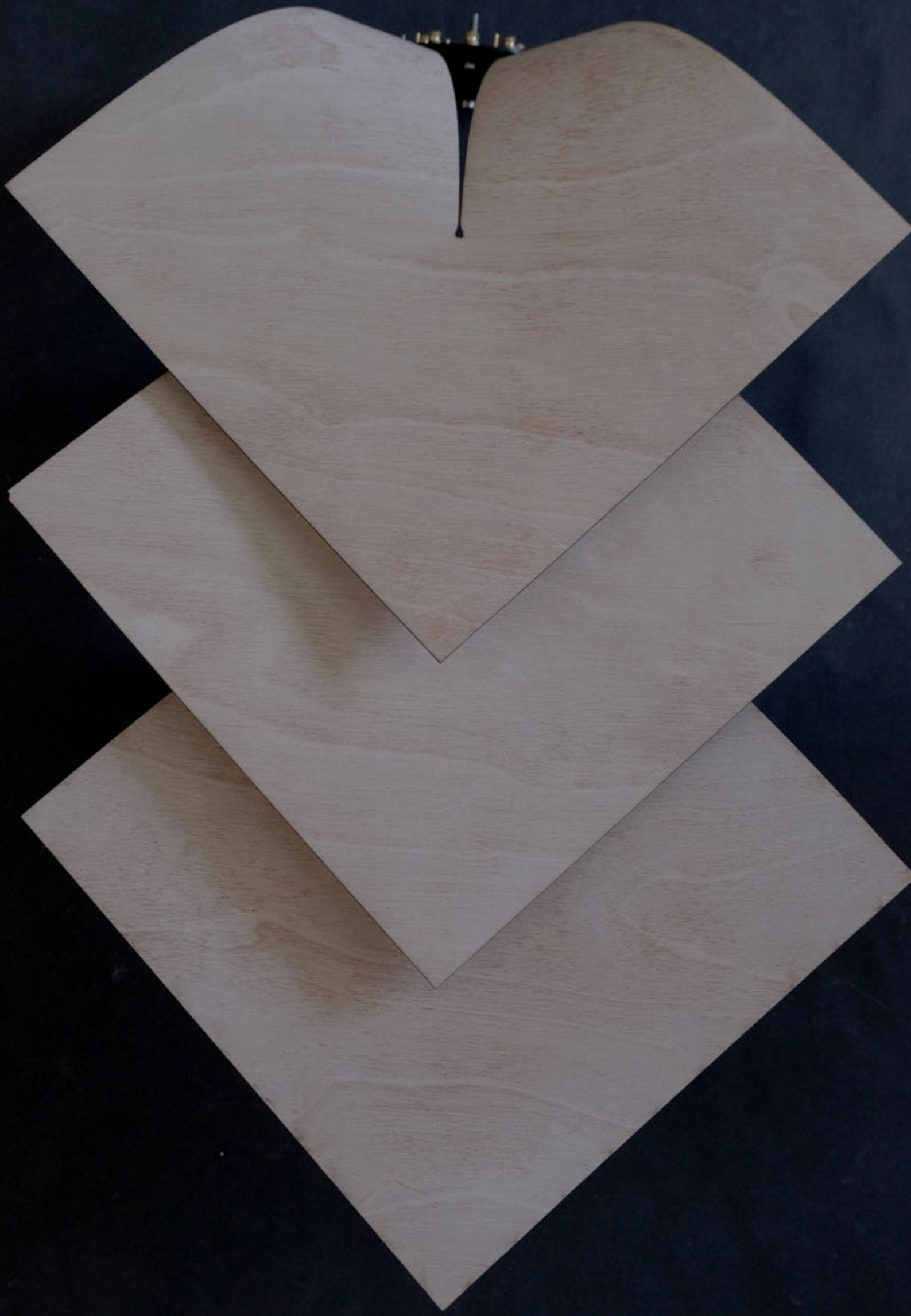

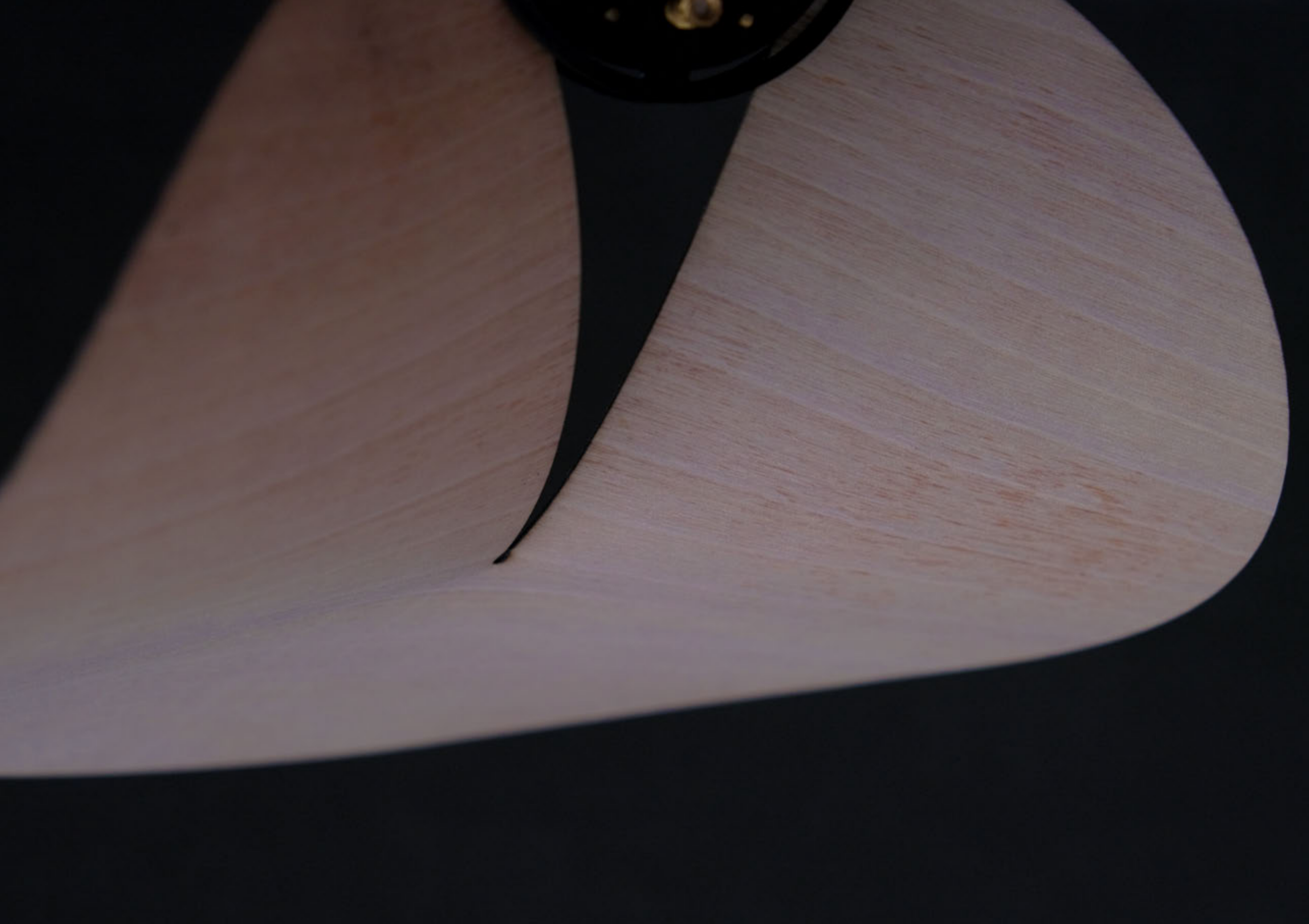

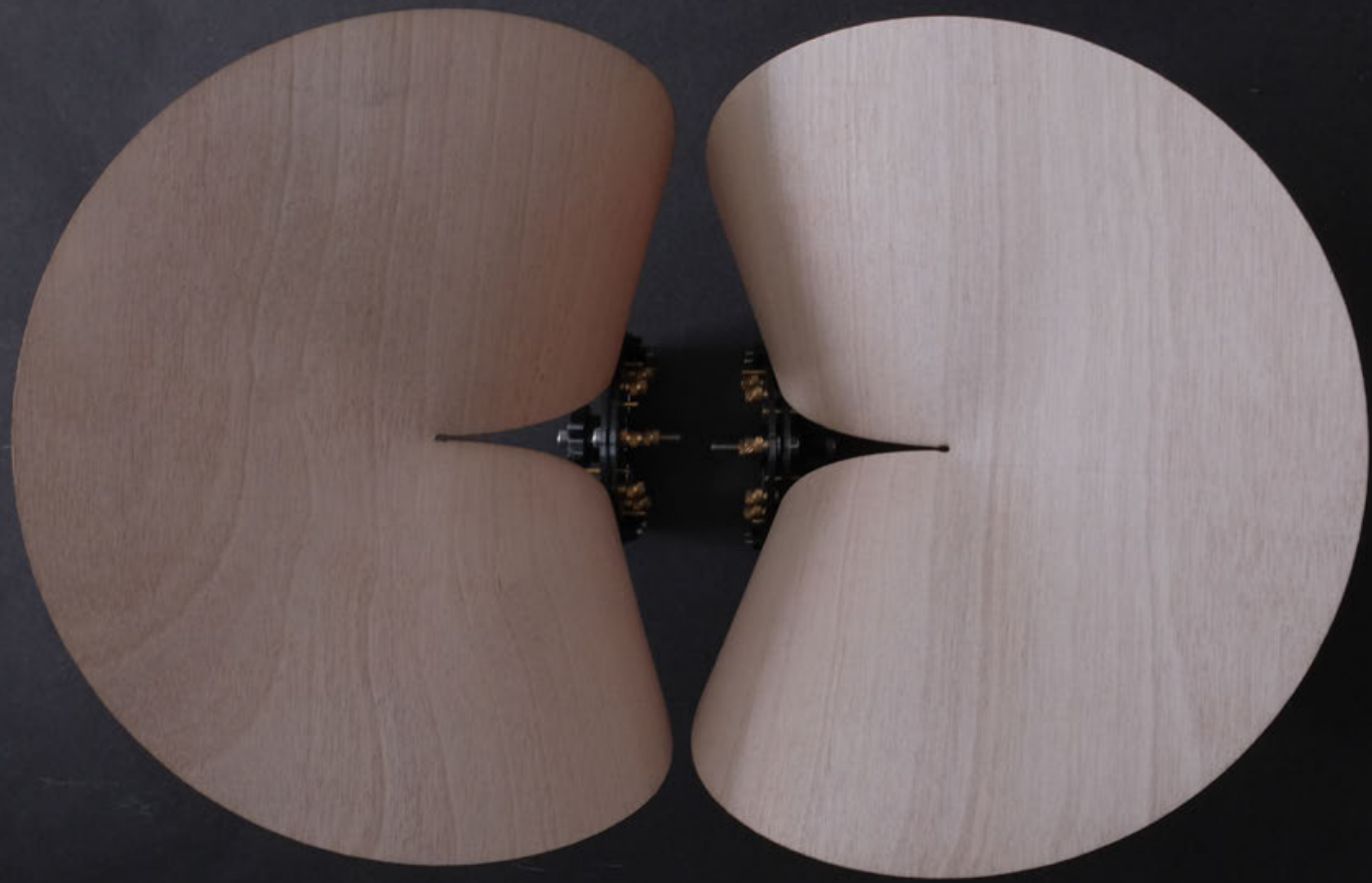

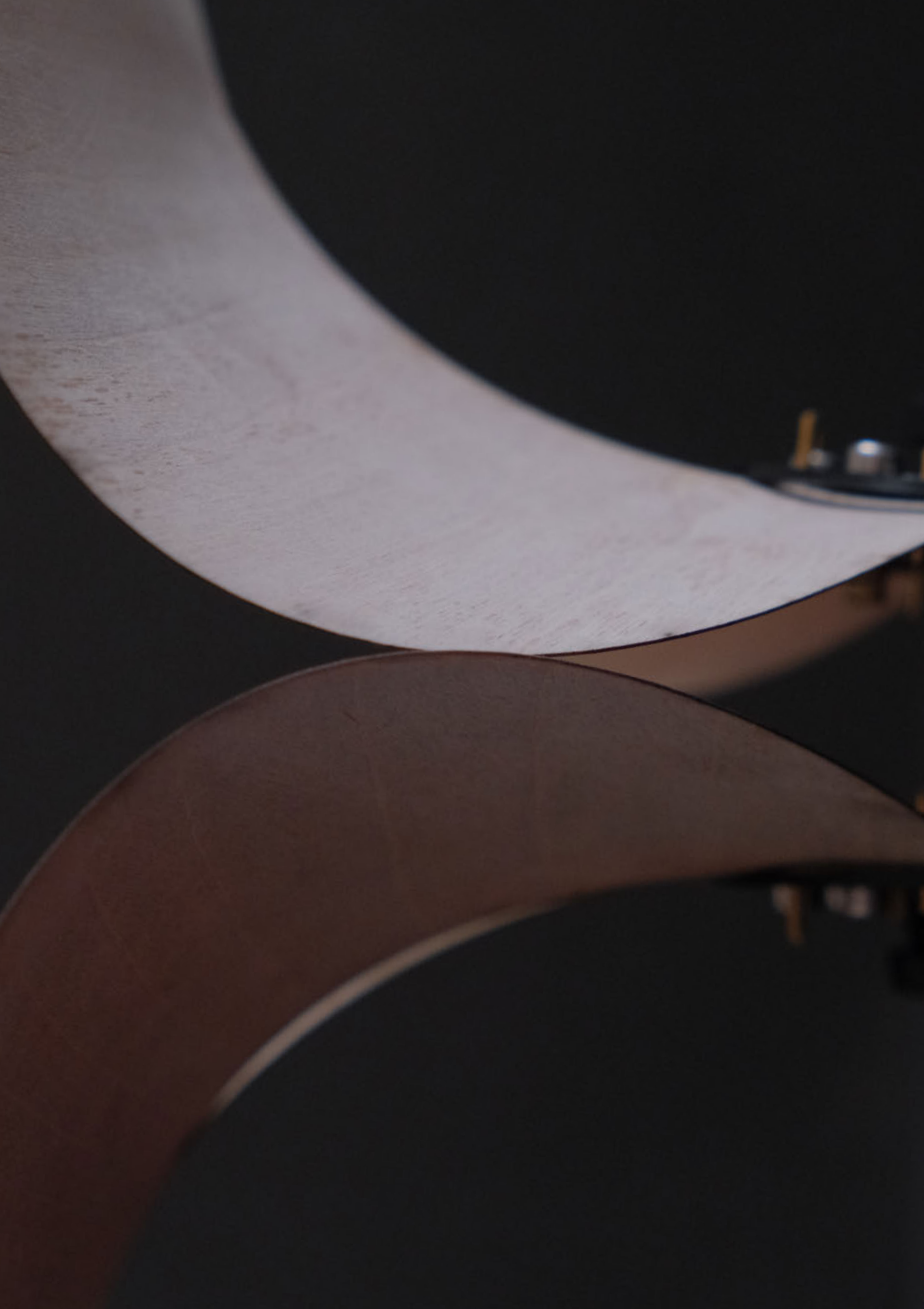

Data

polygon 4

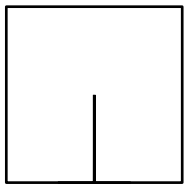

p4

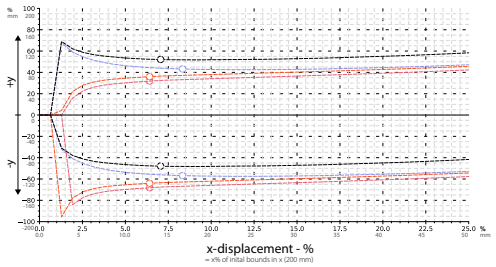

Deflection ci c1 c2 c3
Areal Domain
Linear transition

Area coverage

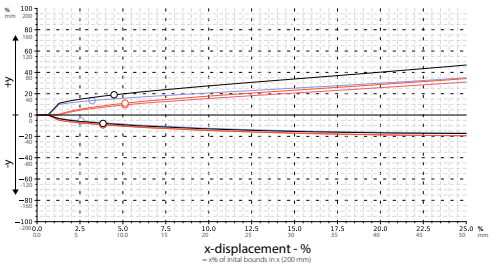

Deflection ci c1 c2 c3
Areal Domain
Linear transition

Inclination

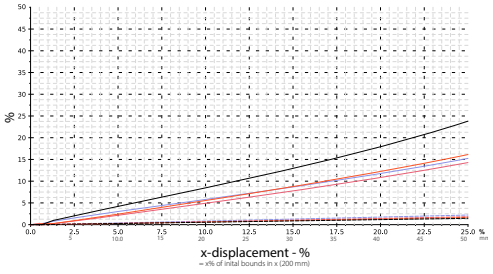

Expand ci c1 c2 c3
Shrink
Linear transition

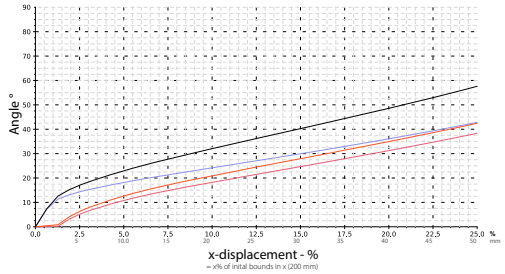

Variant ci c1 c2 c3
Linear transition

polygon 8

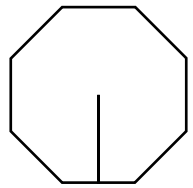

p8

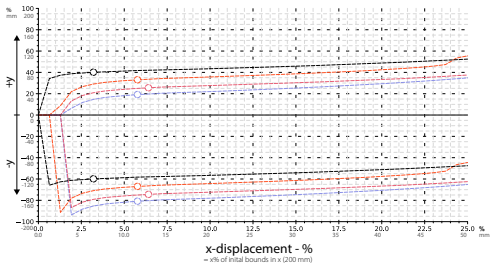

Deflection ci c1 c2 c3
Areal Domain
Linear transition

Area coverage

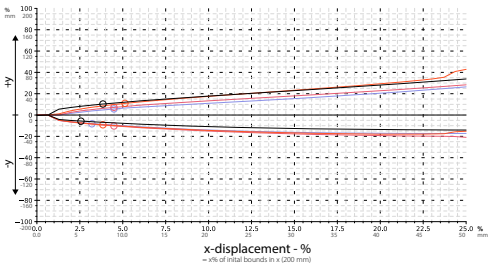

Deflection ci c1 c2 c3
Areal Domain
Linear transition

Inclination

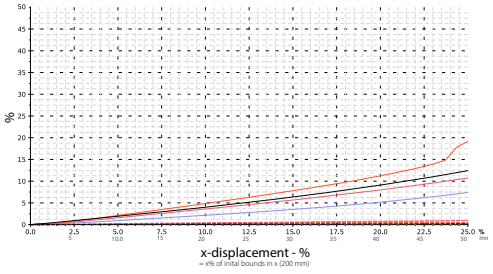

Expand ci c1 c2 c3
Shrink
Linear transition

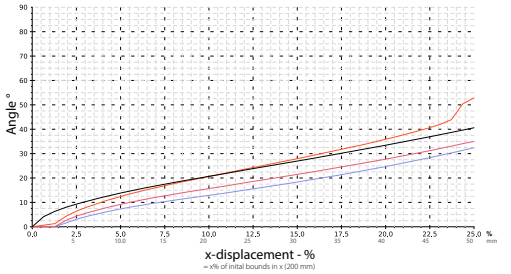

Variant ci c1 c2 c3
Linear transition

polygon 16

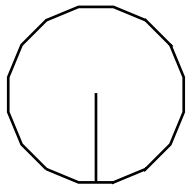

p16

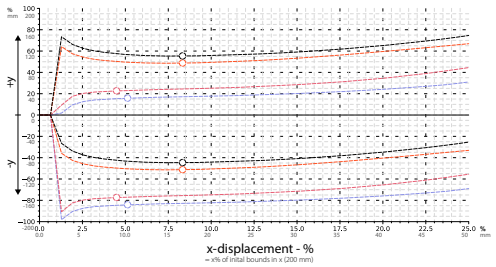

Deflection ci c1 c2 c3
Areal Domain
Linear transition

Area coverage

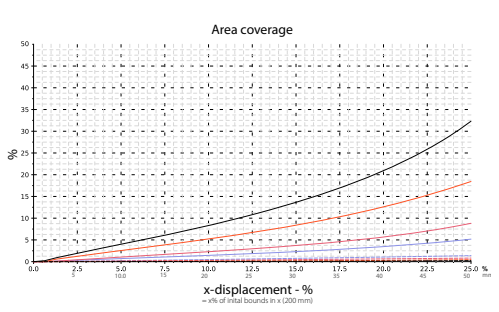

Expand ci c1 c2 c3
Shrink
Linear transition

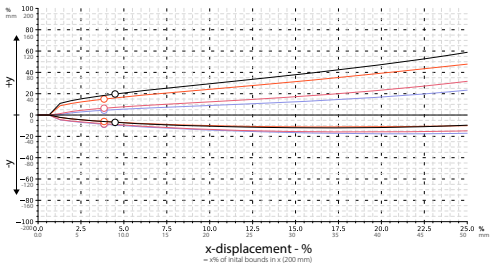

Deflection ci c1 c2 c3
Areal Domain
Linear transition

Inclination

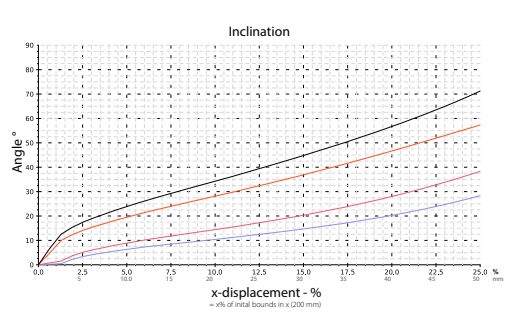

Variant ci c1 c2 c3
Linear transition

circular

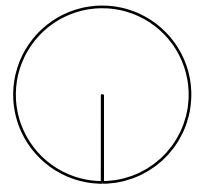

c

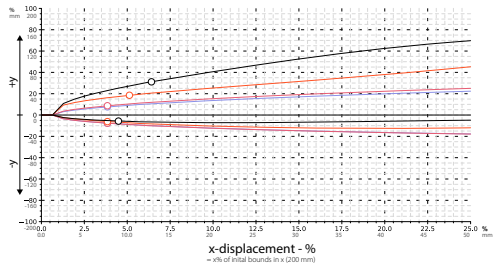

Deflection ci c1 c2 c3
Areal Domain
Linear transition

Area coverage

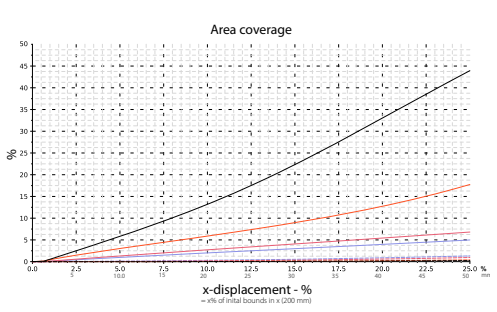

Expand ci c1 c2 c3
Shrink
Linear transition

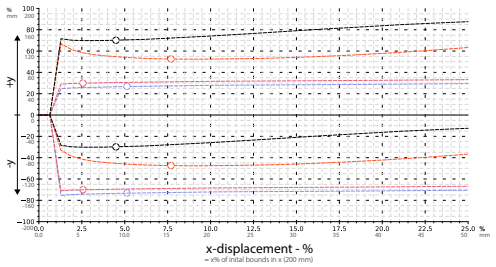

Deflection ci c1 c2 c3
Areal Domain
Linear transition

Inclination

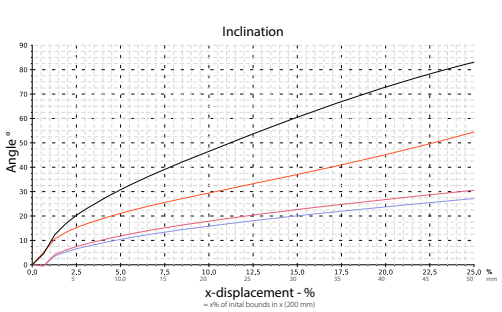

Variant ci c1 c2 c3
Linear transition

diamond

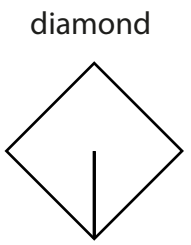

d

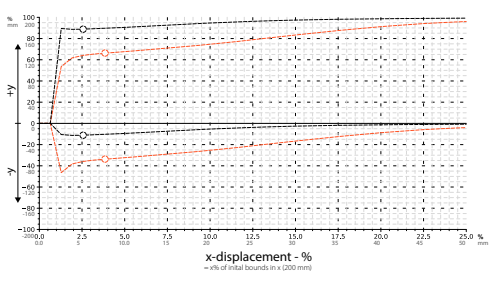

Deflection ci c1 c2 c3
Areal Domain
Linear transition

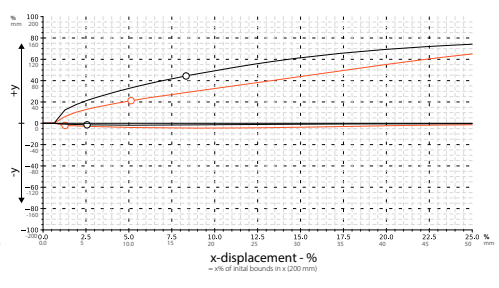

Deflection ci c1 c2 c3
Areal Domain
Linear transition

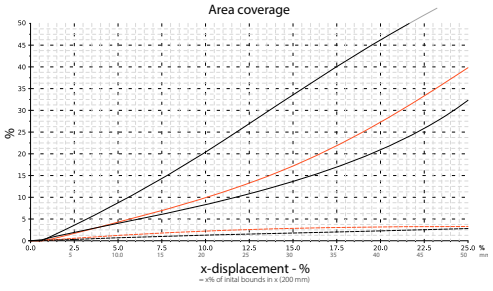

Expand ci c1 c2 c3
Shrink
Linear transition

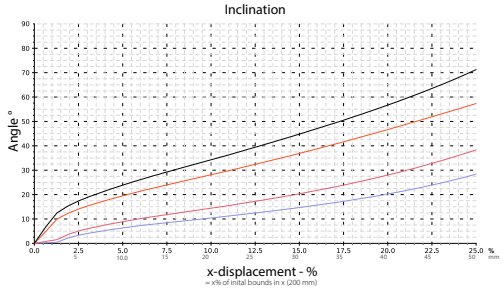

Variant ci c1 c2 c3
Linear transition

Appendix

List of references

1 Lienhard, J. (2014) Bending-active structures: Form-finding Strategies Using Elastic Deformation in Static and Kinetic Systems and the Structural Potentials Therein. , pp 10-13

2 Lienhard, J. et al. (2013) 'Active Bending, a Review on Structures where Bending is Used as a Self-Formation Process,' International Journal of Space Structures, 28(3–4), pp. 187–196. https://doi.org/10.1260/0266-3511.28.3-4.187, p. 2

3 Lienhard, J. (2014) Bending-active structures: Form-finding Strategies Using Elastic Deformation in Static and Kinetic Systems and the Structural Potentials Therein, pp.104

4 Lienhard, J. (2014) Bending-active structures: Form-finding Strategies Using Elastic Deformation in Static and Kinetic Systems and the Structural Potentials Therein, pp.104

5 Adriaenssens, S. (2014) Shell structures for architecture: Form Finding and Optimization. , p.46

6 Lienhard, J. (2014) Bending-active structures: Form-finding Strategies Using Elastic Deformation in Static and Kinetic Systems and the Structural Potentials Therein. , pp. 50

7 Filz, Günther H./Stefan Kainzwaldner (2014): Between Folding and Bending - buckling from plane to object by 3 predefined points, in: ResearchGate, [online] https://www.researchgate.net/publication/286071539_Between_Folding_and_Bending_-_buckling_from_plane_to_object_by_3_predefined_points.

8 Filz, Günther H./Ines Kumric (2017): Z-Snap Pavilion – advanced fabrication and assembly of self-locking, bending active modules into a..., in: ResearchGate, [online] https://www.researchgate.net/publication/322663890_Z-Snap_Pavilion_-_advanced_fabrication_and_assembly_of_self-locking_bending_active_modules_into_a_semi-double-layer_shell-like_structure.

9 Maleczek, Rupert Werner/Günther H. Filz/Christian Scheiber/Clemens Preisinger (2016): curved folded cone assemblies, in: ResearchGate, [online] https://www.researchgate.net/publication/326678025_curved_folded_cone_assemblies.

10 Chair of Structural Analysis, Technical University of Munich, str.ucture GmbH, Kiwi!3D BETA 0.6.0

11 Robert McNeel & Associates, Rhino Version 8 SR6 (8.6.24101.5001, 2024-04-10)

12 Nerfstudio: A Modular Framework for Neural Radiance Field Development, v.034, https://github.com/nerfstudio-project/nerfstudio

13 Robert McNeel & Associates, Rhino Version 8 SR6 (8.6.24101.5001, 2024-04-10),

14 La Magna, R. (2017) Bending-Active plates: Strategies for the Induction of Curvature Through the Means of Elastic Bending of Plate-based Structures. , pp:44-45,

15 La Magna, R. (2017) Bending-Active plates: Strategies for the Induction of Curvature Through the Means of Elastic Bending of Plate-based Structures., p:49

16 La Magna, R. (2017) Bending-Active plates: Strategies for the Induction of Curvature Through the Means of Elastic Bending of Plate-based Structures., pp:45,

List of Figures

All external figures and images included in this work have been listed. Any figures not mentioned in this section are created and copyrighted by the author.

Figure 1 Historical order of bending active structures. Retrieved from: (2014) Bending-active structures: Form-finding Strategies Using Elastic Deformation in Static and Kinetic Systems and the Structural Potentials Therein. , p. 51 (08.12.2023)

Figure 2 Yomut Iran housing, Retrieved from: https://www.researchgate.net/profile/Julian-Lienhard/publication/261596411/figure/fig1/AS:296823706144769@1447779694273/Mudhif-B1-8-Atabay-Yomut-11_W640.jpg (20.01.2024)

Figure 3 Mudhif Houses, Iraq Retrieved from: https://www.researchgate.net/profile/Julian-Lienhard/publication/261596411/figure/fig1/AS:296823706144769@1447779694273/Mudhif-B1-8-Atabay-Yomut-11_W640.jpg (20.01.2024)

Figure 4 The Loop" (Howeler ,Yoon, 2013), "elastic habitat" (Santini,Taddei, 2006) Retrieved from: https://www.researchgate.net/profile/Julian-Lienhard/publication/261596411/figure/fig3/AS:667782328889360@1536223122541/Loop-New-York-2006-14-and-Elastic-habitat-Saint-Etienne-2006-15_W640.jpg (10.11.2023)

Figure 5 Hanging model multihalle mannheim, Retrieved from: https://mannheim-multihalle.de/wp-content/uploads/2018/12/multihalle_architektur_gitterschalenmodell_frei-otto.jpg (05.04.2024)

Figure 6 Multihalle Mannheim, Retrieved from: https://mannheim-multihalle.de/wp-content/uploads/2017/09/mh_projekt_slider_aufgang-1_daniel-lukac.jpg (10.12.2023)

Figure 7 Plydome, Buckminster Fuller in 1959, Retrieved from: https://www.researchgate.net/profile/Arshita-Ravindranathan/publication/374589448/figure/fig11/AS:11431281205186355@1700141247625/Construction-of-Plydome-and-patented-by-Buckminster-Fuller-in-1959_W640.jpg (08.12.2023)

Figure 8 ICD research pavilion, 2010 Retrieved from: https://www.icd.uni-stuttgart.de/img/wp-content/gallery/icd_research_pavilion_2010/pavilion_image_07.jpg?__scale=w:1000,h:1000,q:100,t:3 (05.04.2024)

Figure 9 Bending stress test, Retrieved from: https://www.icd.uni-stuttgart.de/img/wp-content/gallery/icd_research_pavilion_2010/pavilion_image_21.jpg?__scale=w:1000,h:1000,q:100,t:3 (05.04.2024)

Figure 10 Computational model , Retrieved from: https://www.icd.uni-stuttgart.de/img/wp-content/gallery/icd_research_pavilion_2010/pavilion_image_17.jpg?__scale=w:1000,h:1000,q:100,t:3 (05.04.2024)

Figure 11 Computational Workflow , Retrieved from: https://www.researchgate.net/profile/Riccardo-La-Magna/publication/308112796/figure/fig11/AS:420643242823681@1477300572548/a-Base-geometry-b-Mesh-approximation-c-Double-layer-offset-d-Conversion-to-bent_W640.jpg (03.02.2024)

Figure 12 Bend9 case study , Retrieved from: https://www.researchgate.net/profile/Riccardo-La-Magna/publication/308112796/figure/fig13/AS:420648317931521@1477301783114/View-of-the-Bend9-structure_W640.jpg (03.02.2024)